DEVELOPMENT OF A KINETIC MODEL FOR LOOP-FREE COLONOSCOPY TECHNOLOGY

A Thesis Submitted to the College of

Graduate Studies and Research

In Partial Fulfillment of the Requirements

For the Degree of Doctor of Philosophy

In the Division of Biomedical Engineering

University of Saskatchewan

Saskatoon

By

WUBIN CHENG

PERMISSION TO USE

In presenting this thesis in partial fulfilment of the requirements for a Postgraduate degree from the University of Saskatchewan, I agree that the Libraries of this University may make it freely available for inspection. I further agree that permission for copying of this thesis in any manner, in whole or in part, for scholarly purposes may be granted by the professor or professors who supervised my thesis work or, in their absence, by the Chair of the Division or the Dean of the College in which my thesis work was done. It is understood that any copying or publication or use of this thesis or parts thereof for financial gain shall not be allowed without my written permission. It is also understood that due recognition shall be given to me and to the University of Saskatchewan in any scholarly use which may be made of any material in my thesis.

Requests for permission to copy or to make other use of material in this thesis in whole or part should be addressed to:

Chair of the Division of Biomedical Engineering

University of Saskatchewan

Saskatoon, Saskatchewan CANADA S7N 5A9

ABSTRACT

The colonoscope is an important tool in diagnosis and management of diseases of the colon. One of the ongoing challenges with this device is that the colonoscope may form a loop together with the colon during the procedure. The result of the loop is that further insertion of the scope in the colon may not be possible. The loop may also cause risks of perforation of the colon and pain in the patient. There are currently several existing devices to overcome loop formation in colonoscopy, some of which have been introduced in clinical work. However, empirical assessment shows that these devices do not work very well. This is the motivation for the research presented in this thesis.

In this thesis, a new paradigm of thinking, "doctor-assisted colonoscopy," is proposed to overcome loop formation. In this new approach, the physician's role is enhanced with new information that is acquired by sensors outside the human body and inferred from the mathematical model. It is referred to as a kinetic model due to the fact that this model describes the kinetic behaviour of the scope. This thesis is devoted to development of this kinetic model. In this study, the model of the colonoscope and the model of the colon are developed based on the Timoshenko beam theory, and parameters in both models are determined by the experiments. The following conclusions then are made: (1) self-locking of the colonoscope is the most basic cause for a loop to occur, while structural instability of the colonsocope is dependent on the self-locking; (2) both the scope and the colon can be well represented with the Timoshenko beam elements and the Linear Complementary Problem (LCP) formulation derived from Signorini's law, and Coulom's law for representation of interactions between the colon and scope is

adequate; (3) there are effects from the location, looping, and tip deflection of the scope on flexural rigidity of the scope. Approximately, the flexural rigidity of the CF-Q160L colonoscope ranges from 300 to 650 $N \cdot cm^2$, and its accuracy is proven by a good agreement between the model predicted result and experimental result; (4) Rayleigh damping for the CF-Q160L colonoscope depends more on the mass matrix [M] of the colonoscope than the stiffness matrix [K], which is evident by the large coefficient value of "alpha" (0.3864) and the small coefficient value of "beta" (0.0164).

The contributions of this thesis are: (1) the finding that the main cause of the loop is not structural instability of the colonoscope but rather self-locking of the colonoscope, which could lead to design of a "new-generation" colonoscope to avoid the loop; (2) a systematic evaluation of the existing colonoscopy technologies based on the well-proven Axiomatic Design Theory (ADT), which will serve as a guideline for the development of future new colonoscopes in future; (3) an approach to developing a kinetic model of the colonoscope useful to modeling similar objects such as a catheter guide-wire; (4) a novel ex-vivo colonoscopy test-bed with the kinetic and kinematic measurements useful for validation of new designs in colonoscopy technology and also useful for training physicians who perform the colonoscopy procedure; and (5) a new paradigm of thinking for colonoscopy called "doctor-assisted colonoscopy," which has potential applications to other medical procedures such as catheter-based procedures.

ACKNOWLEDGMENTS

I would like to take this opportunity to express my sincere gratitude to my supervisor, Professor W. J. (Chris) Zhang, whose encouragement, support, expertise, and guidance led me to complete this thesis. His enthusiasm for and dedication to his own work has influenced and inspirited me greatly. I appreciate him for all of what he has given me.

I would like particularly to thank one member of my advisory committee, Dr. Michael Moser, who gave me guidance and advice for the experimental set-up, and especially for his participation in the experiments. He also helped me to prepare several manuscripts for publication, and for this I will always be grateful to him.

I also would like to give thanks to the other members of my advisory committee: Professor James D. Johnston, Professor Fangxiang Wu, and Professor Mohamed Boulfiza. Their valuable advice and constructive suggestions have greatly improved the present work.

I would like to extend my appreciation to Dr. Christian Duriez for his technical programming support.

I am grateful also to Dr. Sivaruban Kanagaratnam, who has helped me develop a working relationship with other institutions and given me guidance and valuable suggestion for this research.

I would like to thank Dr. Louis Korman and Dr. Noune Sarvayzan, Artann Laboratories, who provided me with one of the most important instruments in this thesis research, the Colonoscopy Force Monitor.

My thanks extend to include Mr. Doug Bitner and Mr. Louis Roth, for their technical assistance during mechanical experiments. Special thanks are given to my friends Jialei Huang and Xiaohua Hu for their help during the experiments.

Finally, I wish to thank the China Council Scholarship (CSC) for partial financial support for my PhD study; the Shanghai Science and Technology Foundation for international collaborative research funding (Funding No.: 12410709900), and the Natural Science and Engineering Research Council of Canada (NSERC) for a Discovery Grant to Professor W. J. (Chris) Zhang that provided partial financial support for my PhD work.

DEDICATED TO

My wife Yunyun

My parents Yumei Gui and Wanli Cheng

My sisters Guili Cheng and Guifeng Cheng

Thank you for your love and continuous support.

TABLE OF CONTENTS

LIST OF FIGURES

LIST OF TABLES

Table Page

ACRONYMS

ADT: Axiomatic Design Theory

BMI: Body Mass Index

CFM: Colonoscopy force monitor

CR: Constraint requirement

CT: Computer tomography

DMS: Dynamic material spline

DP: Design parameter

DOF: Degrees of freedom

FR: Functional requirement

FEM: Finite element method

FBEM: Finite beam element model

FEA: Finite element analysis

LCP: Linear complementarity problem

MEI: Magnetic endoscopic imaging

MSM: Mass spring model

NES: NeoGuide Endoscopy System

RCT: Randomized controlled trial

RMSE: Root mean square error

SAC: Standard adult colonoscopy

SMA: Shape memory alloy

VSC: Variable stiffness colonoscope

CHAPTER 1

INTRODUCTION

1.1 Research Background and Motivation

Colonoscopy is the most effective way to examine the colon and rectum for diseases such as colorectal cancer. Not only is it a useful screening and diagnostic tool, but it also provides the possibility of removing premalignant polyps [1-2]. However, its failure rate today is still about 10% [3]. Failure is due primarily to loop formation in the colonoscopy procedure. Loop formation can be responsible for incomplete procedure, bowel perforation, and bleeding from mesenteric tear [4-5].

1.1.1 Anatomy of the Colon

The colon is a long flexible organ constrained by muscles and by mesentery within the abdomen. The colon consists of rectum, sigmoid colon, descending colon, splenic flexure, transverse colon, heptic flexure, ascending colon, and cecum, as shown in Figure 1.1. The rectum, ascending colon and descending colon are fixed to the retroperitoneum, and they are almost completely immobile and unstretchable; however, the sigmoid colon is entirely surrounded by the peritoneum which

forms a mesentery (also called the sigmoid mesocolon). Thus, the sigmoid colon is quite mobile in the abdominal cavity [6].

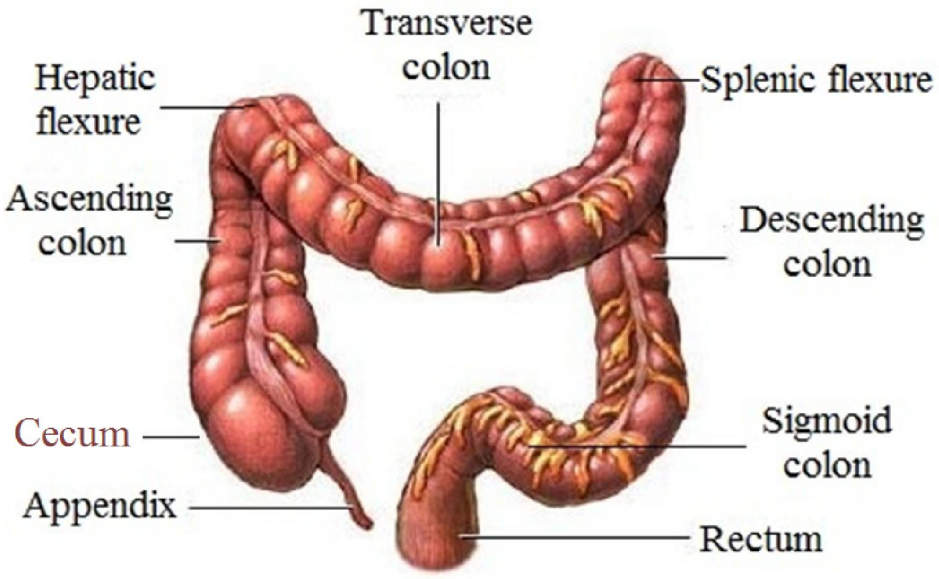

Figure 1.1 Anatomy of the colon

(Adapted from http://www.umm.edu/imagepages/8832.htm)

1.1.2 Colonoscope

The colonoscope comprises (1) the hand control unit with two valves for air insufflation and suction and two knobs for controlling the bend section at the tip and (2) an insertion tube carrying the light guide; the camera; and the water, air, and biopsy channels, as shown in Figure 1.2 and in Figure 1.3. An umbilical (or so-called universal cord) connects the colonoscope to the light source, processor, air supply, and suction as shown in Figure 1.2.

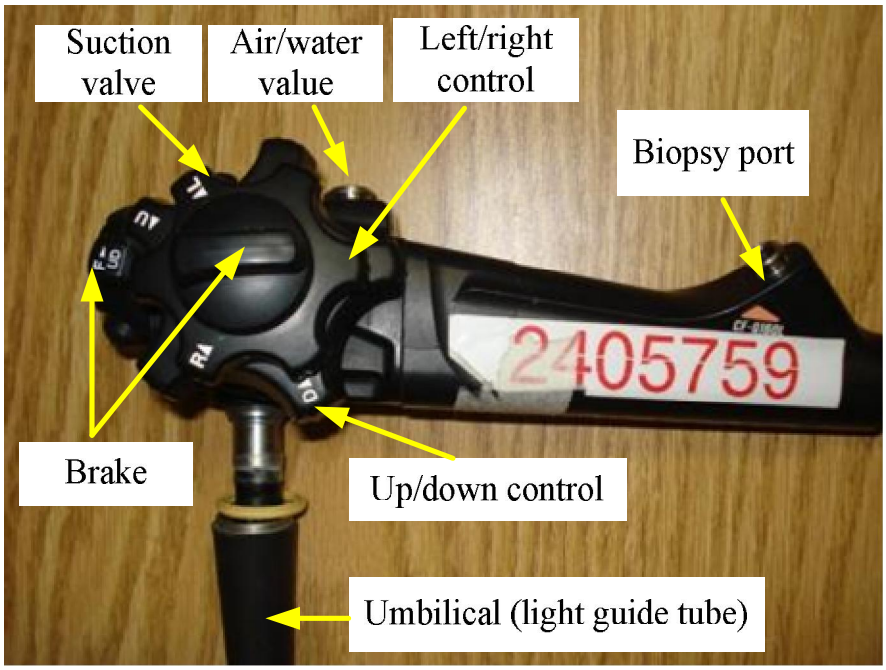

Figure 1.2 Hand control unit of colonoscope

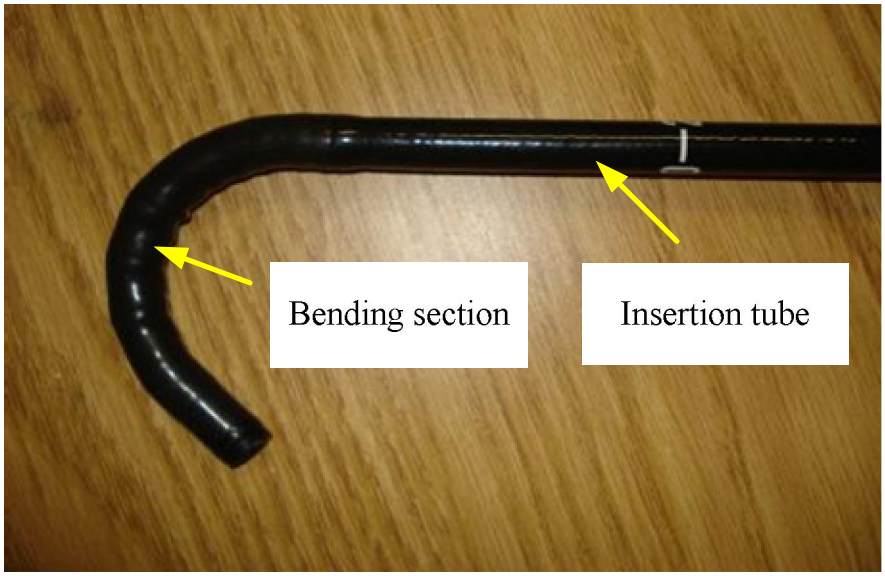

Figure 1.3 Bending section of colonoscope

The bending section 10 cm (see Figure 1.3) of the colonoscope can be deflected along the up/down plane and the along right/left plane. The tip of the colonoscope can bend up to 180^0 or more. Control of the bending section depends upon pulling wires that connect the tip of the colonoscope to the two angulation control knobs (for up/down and right/left movements) at the hand control unit, as shown in Figure 1.2. The two knobs use a braking system; thus, the tip of the scope can be kept fixed in any desired position. The insertion tube is torque-stable, i.e., the rotating movement applied to the proximal end is transmitted to the tip of the scope [7].

The colonoscope has a complex internal structure. The insertion tube of the scope incorporates the biopsy, suction, air, and water channels originating at the entry "biopsy port" and ending at the opposite end of the scope [8].

1.1.3 Colonoscopy Procedure

The procedure of colonoscopy involves the intubation of a colonoscope from the anus through the colon to the cecum [7]. During a complete colonoscopy procedure, the insertion shaft is inserted into the anus then pushed through the rectum, sigmoid colon, descending colon, transverse colon, and ascending colon through to the cecum.

There are two methods for performing colonoscopy: two-person and one-person. In the one-person colonoscopy, the physician performs the examination alone, managing the angulation controls and valves with one hand and inserting or twisting the shaft with the other hand. In one-person colonoscopy, the physician uses the right hand to insert the scope and controls the

orientation of the distal end of the scope with the left hand. Thus, the one-person method typically creates a better coordination of the two operations during the procedure.

In the two-person colonoscopy, a physician and an assistant perform the two-person colonoscopy, i.e., the physician controls the orientation of the scope, and the assistant pulls and pushes the colonoscope according to the physician's command. By contrast, in the two-person method, an assistant pushes or pulls the scope while the physician controls the scope orientation. In the latter method, good coordination often is hard to achieve. As a result, the two-person method often creates more procedure-induced abdominal pains than does the one-person method [8-11].

1.1.4 Loop Formation in Colonoscopy

Despite the wide availability and use of colonoscopy in the world today, the failure rate (incomplete colonoscopy) continues to remain as high as 10%, i.e., failure to reach to the cecum occurs in more than 1 in 10 procedures [12]. The main reason for this failure is loop formation [13].

In colonoscopy, the most difficult site for advancing the colonoscope is at the sigmoid-descending junction (see Figure 1.1), especially in an acute angle. At this place, the scope can get stuck in the colon, then go either upwards or downwards, forming an alpha loop or "N" loop from a lateral view as shown in Figure 1.4. Other sites for potential loop formation are the junction of the descending colon to transverse colon and the junction of the transverse colon to ascending colon. Furthermore, individual colon attachments are unusually mobile, which may

result in types of atypical loops such as the reverse splenic flexure loop (3% of all loops), reverse alpha loop (5% of all loops), reverse sigmoid spiral (1% of all loops), transverse gamma loop (1% of all loops) when the scope reaches the transverse colon [12].

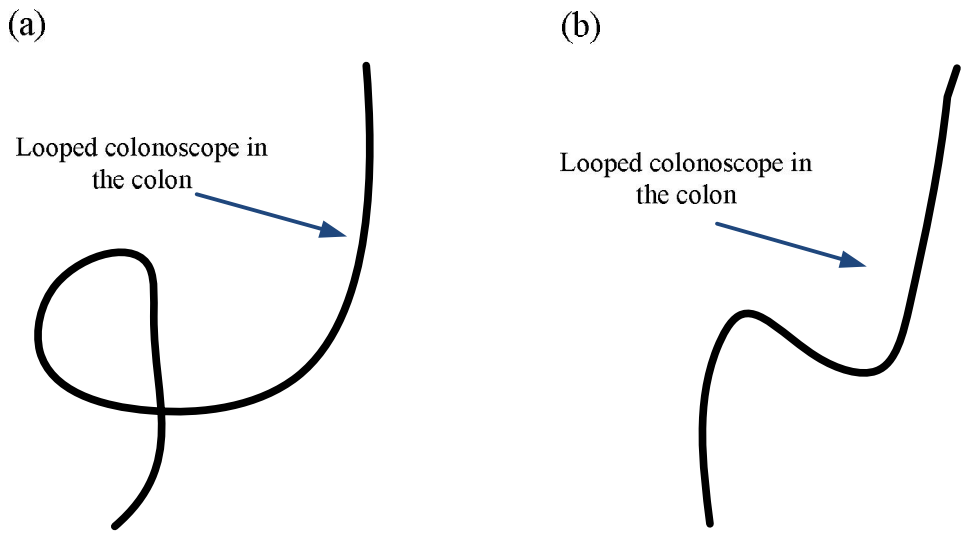

Figure 1.4 (a) a large sigmoid alpha loop; (b) a sigmoid spiral "N" loop

Learning effective maneuvers for preventing/controlling loop formation is the most important part of the physician's specialized training in colonoscopy. For a short sigmoid colon, the physician may achieve almost "direct" passage from the sigmoid colon to the descending colon without a large loop formation. For a redundant sigmoid colon, the physician repeatedly may pull the scope back or withdraw, and twist the scope in order to straighten the scope at the sigmoid-descending junction (see Figure 1.5) [15]. Although the colonoscope may pass through the descending colon smoothly after the physician straightens the scope, a loop can reform in the sigmoid colon when the colonoscope passes the splenic flexure as well as at the hepatic flexure, which also offers an obstacle to advancing of the scope.

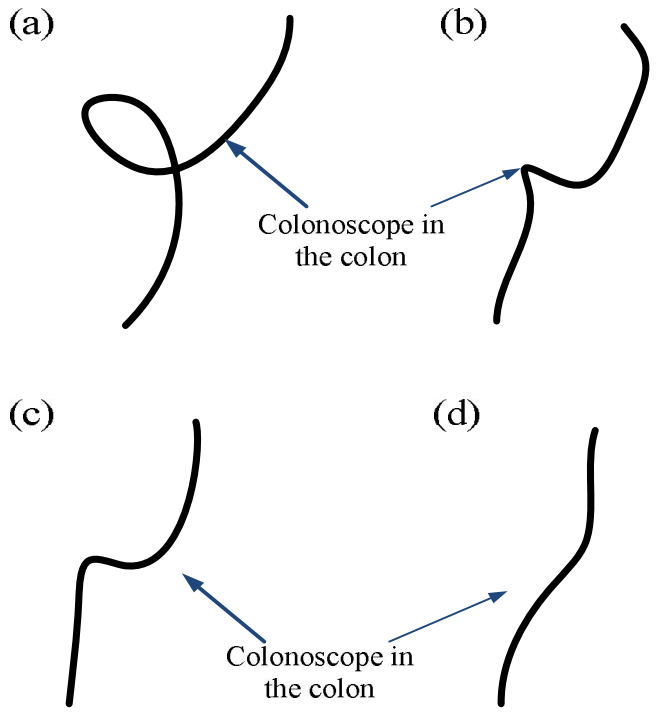

Figure 1.5 (a) tip of colonoscope reached the splenic flexure; (b) scope withdrawal with clockwise twisting reduces an alpha loop; (c) continued clockwise torque straightens the remaining loop; (d) straighted scope

In clinic, there are several maneuvers available to the physician confronted with a loop. One is to apply increased manual pressure to the left lower quadrant such that the sigmoid colon is made more "compact." Other useful maneuvers include "hooking the fold," which involves hooking the scope onto a corner of the colon while withdrawing the scope such that the tip does not lose ground. In some cases, changes in positioning of patient can also be useful in certain circumstances [16-21]. The use of such ancillary maneuvers may be helpful in up to 52% of attempts, indicating that in a significant number of cases the loop cannot be prevented when using the existing methods [22].

Loop formation in colonoscopy can lead to bowel perforation, bleeding from mesenteric tear, and premature termination of the procedure.

1.2 Research Objectives

There are currently several existing designs for overcoming loop formation in colonoscopy, some of which have been introduced to clinical work, including a variable stiffness colonoscope, an over-tube colonoscope, capsule endoscopy, a self-propelled endoscope, virtual colonoscopy, the Aer-O-Scope and the NeoGuide Endoscopy System (NES), and image-guided colonoscopy. However, empirical in-clinic assessment shows that none of these work very well in terms of overcoming loop formation [23]. This is the motivation for the research presented in this thesis.

A preliminary analysis by the author has led him to believe that all the existing attempts at solutions may have missed an important factor involving an engineering concept called "self-locking" and its underlying principle that governs the locking of the relative motion (or "stick") between two objects (colon and scope, in this case) [24]. This observation, coupled with the author's belief that medical procedures and operations must be performed in interactive human/machine fashion (or, simply speaking, that a complete automation for this procedure is both undesirable and less, if at all, viable), led the author to propose a new paradigm of thinking for colonoscopy called "doctor-assisted colonoscopy". This paradigm means that on the top of essential operations by the doctor with devices, assistive information and knolwege is provided through an engineering system. Under this new paradigm, the physician's role would be enhanced by new information involving the interaction between the scope and the colon such as

their contact force, scope positions, and orientation of the scope's distal end within the colon [25]. An accurate kinetic model is extremely important to providing this new information, and this thesis is devoted to the development of such a kinetic model.

From the aforementioned research questions to be answered by this thesis research, two objectives were proposed and they are stated as follows:

(1) To analyze the existing devices and solutions for overcoming loop formation in colonoscopy from an engineering design prospective, aiming to confirm the author's preliminary finding.

(2) To develop a kinetic model of the colonoscope that describes the motion of the colonoscope in the colon and also the contact force resulting from the external force/torque applied by the physician. Objective (2) can be further divided into three more specific objectives: (2a) to set up an experiment test-bed to identify and determine the parameters that should be included in the model; (2b) to set up a test-bed that can measure all the previously information mentioned in order to serve as a means to validate the model; and (2c) to establish the model from the first principle.

1.3 Organization of the Thesis

This thesis comprises of six chapters.

Chapter 1 gives an introduction to this research, necessary background pertinent to this thesis, and research objectives.

Chapter 2 presents an analysis of loop formation in colonoscopy. The analysis was conducted systematically with an engineering design theory and methodology called Axiomatic Design Theory (ADT). The ADT has two axioms; the first axiom regards the relationship between the functional and constraint requirement and device parameter, and only this first axiom was employed in the analysis. Also, clinical feedback for the existing devices was employed to examine its correlation with the engineering analysis.

Chapter 3 presents a literature review of the modeling of a cable-like object. This review outlines some emerging approaches to modeling a cable-like object, including dynamic splines, mass-spring models, the Kirchhoff's rod theory, the Cosserat theory, rigid bars with joints, and the finite beam element model (FBEM). Advantages and limitations of these approaches are discussed in this chapter. These methods all have certain advantages and disadvantages with respect to the modeling requirement. The goal of this review was to make a critical assessment of these methods and to justify the choice of the FBEM as the best and most suitable tool for modeling the colonoscope to be used for this research.

Chapter 4 presents the models of the colonoscope and the colon, and their interaction. For the colonoscope model, the Timoshenko beam element was employed, which accounts for the cross-sectional area, cross-section moment of inertia, and polar moment of inertia of the structure of the colonoscope. Each beam element had 6 degrees of freedom (DOFs) in translation and 6

DOFs in rotation in space and was connected to a neighboring beam element to represent the assembled colonoscope. The element had not only deformation but also position change, and its position was updated. In order to model the colon, the colon was defined as a set of hollow cylinder beam elements. The deformation of the colon was represented by a static equilibrium equation in which the stiffness matrix of the colon model was computed from a number of hollow cylinder beam elements. The parameters in the model of the colonoscope and the model of the colon were determined by the experiments in this research. Finally, the model of the scope-colon system which describes their interaction is presented.

Chapter 5 presents a validation of the mathematical model using an *ex-vivo* colonoscopy test-bed developed with this reaearch. A description of the built test-bed is given as well.

Chapter 6 gives the conclusion drawn from the results obtained, summarizes the contribution of the thesis, and outlines the future research work.

CHAPTER 2

ANALYSIS OF THE CAUSES OF COLONOSCOPE LOOPING AND EXISTING DEVICES AIMED AT OVERCOMING LOOP FORMATION

2.1 Introduction

This chapter provides an analysis of the causes of loop formation and evaluates the existing devices and solutions that attempt to overcome the looping problem in colonoscopy. Section 2.2 analyzes loop formation from a mechanical point of view. In Section 2.3, a framework of criteria for evaluating the existing devices and solutions that attempt to overcome the looping problem is established, which is based on Axiomatic Design Theory (ADT). Clinical feedback for the existing devices of colonoscopy technology is also consulted to examine its correlation with the engineering analysis. Section 2.4 presents a conclusion.

2.2 Mechanical Analysis of the Causes of Loop Formation in Colonoscopy

Loop formation generally begins when the colonoscope enters the sigmoid colon. At that point, an experienced physician often can straighten the scope, allowing it to then pass into the adjacent

descending colon. However, looping of the scope then again can occur once the tip of the scope reaches the sharp turn in the colon at the splenic flexure (note: the portion of the colon in the left upper quadrant close to the spleen; see Figure 1.1). Later, the tip of the scope reaches the other sharp turn, this one at the hepatic flexure, where the scope may form itself into a loop again. In the following sections, the causes of loop formation are explored from the point of view of the self-locking mechanism and Kirchhoff's rod stability theory.

2.2.1 Self-locking Mechanism

The interaction between the colon and the colonoscope is highly complex due to frictional contact between two deformable objects. Each contact point of the colonoscope with the colon has a friction state, either a static friction state or a dynamic friction state; therefore, when the colonoscope and the colon come into contact, there are generally two states in the tangential contact: stick state and slip state. The slip state occurs if the tangential force is greater than the limit of the static friction force, with the latter defined as the multiplication of the static frictional coefficient by the normal force. During the slip state, a relative slip between the colonoscope and the colon along the tangential direction occurs. Friction force is determined by multiplication of the dynamic frictional coefficient by the normal force applied on the contact [26]. For the stick state, the relative displacement of the contact points of two bodies is equal to zero (i.e., the ends of both contact points of the colonoscope and colon move together). Therefore, the stick state occurs at the distal end of the scope when loop formation occurs in the sigmoid colon.

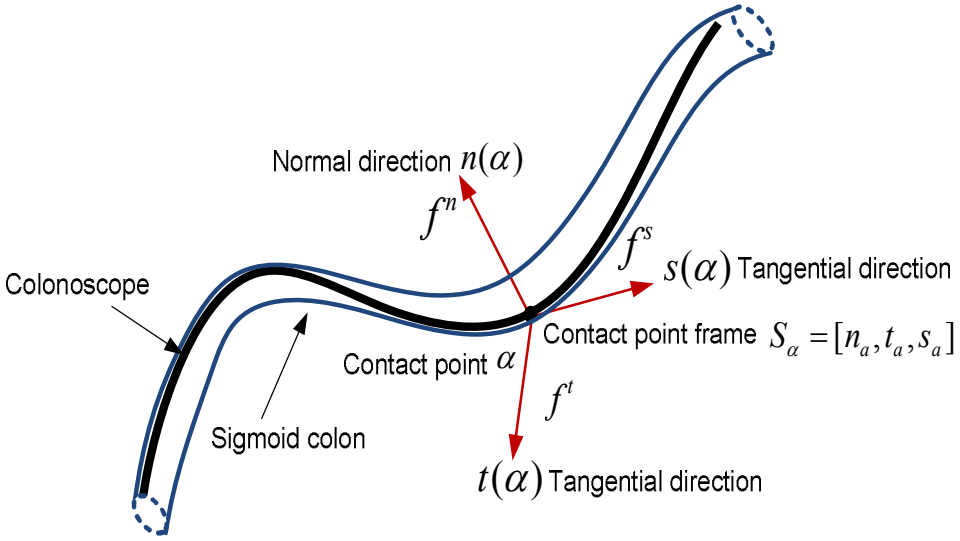

Figure 2.1 Analysis of the contact force by static frictional and dynamic frictional between the colonoscope and colon

Suppose that there is contact point frame $S_\alpha = [n_a, t_a, s_a]$ where n_a is a normal direction; f^n is a normal force; t_a and s_a are two component directions of the tangential direction of the colonoscope at the contact point and they are perpendicular to each other, and f^t, f^s respectively is forces along these component directions (see Figure 2.1).

The state of frictional force can be determined with Eq. (2.1) [26].

$$\begin{cases} \dfrac{\left\| \left[f^t \; f^s \right] \right\|}{\left\| f^n \right\|} < \mu_s & (a) \\ \dfrac{\left\| \left[f^t \; f^s \right] \right\|}{\left\| f^n \right\|} \geq \mu_s & (b) \end{cases} \tag{2.1}$$

where (a) indicates the occurrence of a sticking friction and (b) indicates the occurrence of a slip friction.

Defining $\frac{\left\| \left[f^t \; f^s \right] \right\|}{\left\| f^n \right\|} = \tan\alpha$, where α is called the driving force angle.

Based on the definition of friction angle β:

$$\beta = \arctan \mu_s \tag{2.2}$$

where μ_s is static frictional coefficient; β is friction angle.

$$\tan\beta = \mu_s \tag{2.3}$$

This leads to

$$\begin{cases} \tan\alpha < \tan\beta & (a) \\ \tan\alpha \geq \tan\beta & (b) \end{cases} \tag{2.4}$$

where (a) indicates a sticking state and (b) indicates a slip state.

Based on Eq. (2.4), the colonoscope remains stationary and does not move forward when $\alpha < \beta$. This phenomenon is called "self-locking." At this point, the loop becomes stretched if the physician continues to push the colonoscope. As for actual movements of the colonoscope, there are two variables: driving force F_p and driving force angle α (which is related to the curvature parameter θ with respect to the loop). During the state of self-locking, the colon tissue is distended by a significant contact force as a result of the increasing unwanted driving force. Finally, perforation of the colon may happen. Based on this analysis, if the driving force angle is greater than the friction force angle, loop formation could be avoided.

2.2.2 Kirchhoff's Rod Stability

The colon-scope system can be viewed as an elastic slender rod model. An elastic structure in which structural stability decreases with the increase of the load (load is the pushing force applied by the physician) ultimately becomes unstable. When the load applied exceeds its critical load on the rod, the colonoscope reaches an unstable state and naturally seeks another stable equilibrium state. The movement of the colonoscope to a new stable equilibrium state will involve an extremely large deformation when the scope relied on the colon and mesentery to increase its flexural rigidity. Ultimately, all axial forces applied to the external portion of the instrument contribute to loop formation. According to the foregoing analysis, structural instability accounts for the loop. Thus, the critical load is an important parameter for predicting structural stability. Critical load F_{cr} can be adapted from the rod model with the Kirchhoff's rod equilibrium equation, below [27].

$$F_{cr} = \frac{4\pi^2 EI \cos^3 \vartheta}{L^2(1+3\cos^2 \vartheta)} \tag{2.5}$$

where

L : length of the rod;

ϑ : spiral angle; and

EI : flexural rigidity of the rod.

The critical load can be increased by increasing the EI as shown in Eq. (2.5). The solution called "over-tube" (a tube through which the colonoscope is inserted and that serves to increase flexural rigidity of the colonoscope in the sigmoid colon) followed this thinking about loop formation. However, use of the over-tube has largely been abandoned because of the significant patient discomfort and huge risk of perforation reported [24]. Development of the variable stiffness colonoscope (VSC) followed the same thinking. The VSC has built-in variable stiffeners, however, the simple mechanism is not able to avoid the looping but brings an increased risk of perforation of the colon. A detailed engineering analysis of failure with these two devices will be given in the next section.

2.3 Evaluation of the Existing Devices and Solutions

2.3.1 Framework of Evaluation Criteria

This section will evaluate the existing devices and solutions for overcoming looping problem in colonoscopy. At first, a framework of criteria is established, which is based on engineering design theory.

In [28], Suh described design as an interplay between "*what* we want to achieve" and "*how* to achieve." The descriptor of "*what* we want to achieve" leads to form functional requirements (FRs) and constraint requriments (CRs). The CRs provide the conditions or contexts where the FRs are fulfilled. The descriptor of "how to achieve" is defined as the design parameters (DPs).

The design process is always to discover DPs to fulfill FRs under CRs. Details of the concepts of FR and CR can be found in the Ref. [28].

Evaluation of the existing devices and solutions to avoid the loop formation problem originates in the frameworks of the designs. The causes of the loop are considered to be FRs along with CRs, and the existing solutions are considered to be DPs. In light of the foregoing idea, axiomatic design theory (ADT) [29-33] was chosen for the evaluation owing to its "check point" role. The so-called check point role means that given DPs and FRs, the ADT evaluates the DPs. The ADT has two axioms: Axiom 1 and Axiom 2. They are stated as:

- Axiom 1: The Independence Axiom — Maintain the independence of the functional requirements (FRs)
- Axiom 2: The Information Axiom — Minimize the information content of the design

Axiom 1 governs the validity of a design, while Axiom 2 governs the "best" design or "optional" design. Let us first define the FRs and CRs representing the causes of loop formation. In Section 2.2, the analysis of loop formation showed that when the driving force angle is greater than the friction angle, loop formation can be avoided or prevented. The FR is defined as follows:

- FR: avoiding the stick-friction state of the distal end of the scope

It is noted that the definition of the FR (there is only one FR in this case) implies that the author believes that self-locking is the most basic cause for a loop to occur and that structural instability is dependent on the self-locking phenomenon. This is supported by calculation that the critical load for the structural instability is approximately equal to 1.82 N, nearly twice the critical load for the self-locking (see Appendix A and Appendix B). This further implies that on the occasion where structural instability may occur, there must be some geometric obstruction to the scope

from the colon — a sign of occurrence of self-locking. That is to say, the structural instability follows the self-locking phenomenon.

Constraints (CRs) are the bounds on acceptable solutions, i.e., operation time cost (CR_1), biopsy function (CR_2), and safe examination environment (CR_3) in colonoscopy. CRs are defined as:

- CR_1: operation time cost
- CR_2: biopsy function
- CR_3: safe examination environment

In the ADT, the DPs are solutions in the physical domain that characterizes the design that satisfies the FRs. In the application of the ADT to the evaluation problem here, the DPs represent various exising solutions intended to overcome the looping and they should either pull the scope rather than push force (DP_1) or make the driving force angle greater than the friction force angle when the scope is pushing forward (DP_2). In this study, the existing solutions were evaluated based on the first axiom only, as the attention was focused on revealing the the full effectiveness of the existing solutions.

2.3.2 Evaluation

This evaluation considers the following existing devices and solutions: the variable stiffness colonscope and the over-tube scope, the self-propelled endoscope, virtual colonoscopy, the Aer-O-Scope, the NeoGuide systems, imaging-guided colonosocpy. Some comments have been made regarding these solutions but without inclusion of any rigorous engineering analysis. The

methodology in the following consists of two steps: defining DPs for each existing solution and examining the design of the DPs fulfilling the FRs under the CRs.

2.3.2.1 Variable Stiffness Colonoscope

2.3.2.1.1 Evaluation of Design

The variable stiffness colonoscope (VSC) was developed by the Olympus^{TM} Corporation. The VSC has a built-in variable stiffener that can stiffen the insertion tube. The entire insertion tube with the exception of the bending section can be made floppier or stiffer by using the variable stiffness adjustment knob located at the hand control unit [34].

The principle behind the VSC is to vary the flexural stiffness of the scope in order to improve structural stability according to Eq. (2.5). DP is defined as:

- DP: stiffness change of the scope

Based on Eq. (2.6) (details of the derivation of this equation are found in Appendix C), a scope with a high flexural rigidity induce a high frictional force to the colon tissue, so then the scope fails to bend around the corner of the colon tissue and subsequently damages the colon tissue (so-called perforation of the colon).

$$F_f = \frac{\mu EI}{r^2}\left(\frac{12+\theta^2}{2\theta}\right) \tag{2.6}$$

where

μ : dynamic frictional coefficient;

EI : flexural rigidity of the scope;

r : radius of the scope curvature; and

θ : function of the arc-length l of the scope.

The overall function requirement (FR) mentioned previously is further deconstructed into two functional requirements: FR_1 is avoiding loop formation; FR_2 is avoiding perforation of the colon. DP is the change of the stiffness of the colonoscope and [A] is the design matrix. The design matrix of the variable stiffness of the scope is described as follows:

$$\begin{bmatrix} FR_1 \\ FR_2 \end{bmatrix} = \begin{bmatrix} A_{12} & \\ A_{21} & A_{22} \end{bmatrix} \begin{bmatrix} DP_1 \\ DP_2 \end{bmatrix} \tag{2.7}$$

where $[A_{21}]$ represents the effect of stiffness change on the perforation of the colon.

This design matrix indicates a decoupled design. Based on the ADT, an ideal design is an uncoupled design matrix, and each FR is controlled by only one DP and vice versa. Therefore, the design for the VSC has not met Axiom 1 of the ADT. For this reason, the DPs of the VSC do not met the criteria for devices to overcome loop formation.

2.3.2.1.2 Clinical Feedback

In clinic, the VSC has not been shown to be more useful or better than the conventional colonoscope, according to reports from the clinical experince [36-49]. Also, there are some

conflicting reports regarding its ability to facilitate cecal intubation and its increased risk of perforation of the colon [36, 37].

Shah et al. [48] performed a randomized controlled trial (RCT) to evaluate the effect of the VSC, and found that the operation time was shortened. This result indicated that the use of the VSC in clinical practice is more useful than use of the standard adult colonoscopy (SAC). However, there was one case of perforation of the sigmoid colon reported from the use of a pediatric VSC [49].

Xie et al. [38] conducted the systematic review of the use of the VSC compared with the SAC. Based on their studies, in practice, the VSC seems to offer only a small advantage over the SAC.

2.3.2.2 Over-tube Colonoscope

The use of an over-tube was thought to be effective in decreasing or eliminating the looping, in the very early years of colonoscopy, however, this device has not lived up to its expectations becasue significant pain and an increased risk of perforation, so this approach has been abandoned [50].

Recently, USGI^{TM} Medical Inc. introduced the Shape-Locking Guide (SG-1) (Figure 2.2) in an effort to revisit and improve the over-tube concept. The latter over-tube can be converted from a flexible to a rigid configuration on demand. Once the SG-1 reaches a desired position in the colon, and then the squeeze handle is activated, leading to stiffening of the over-tube in the

desired position. As a result, this device prevents the lateral transmission of force and discourages looping in the sigmoid colon in colonoscopy [51].

2.3.2.2.1 Evaluation of Design

In principle, the over-tube scope is similar to the VSC. The increased local flexural stiffness EI of the scope in the sigmoid colon can improve structural stability of the scope in the sigmoid colon.

In the use of over-tube colonoscopy, the over-tube slides over the colonoscope and the colonoscope slides through the over-tube, thus, the frictional force between the over-tube and the colonoscope is not negligible; this friction is much more than that between the over-tube and the colon tissue because the colon has slippery mucous layer. Technically, more force could be implemented by the physician to overcome additional friction force while the over-tube device is used in colonoscopy; however, this brings a risk of perforation of the colon. Using the same evaluation as that applied to the VSC, the design for the over-tube colonoscope does not meet Axiom 1 of the ADT. For this reason, the DPs of the over-tube colonoscope do not meet the criteria for devices that effectively overcome loop formation.

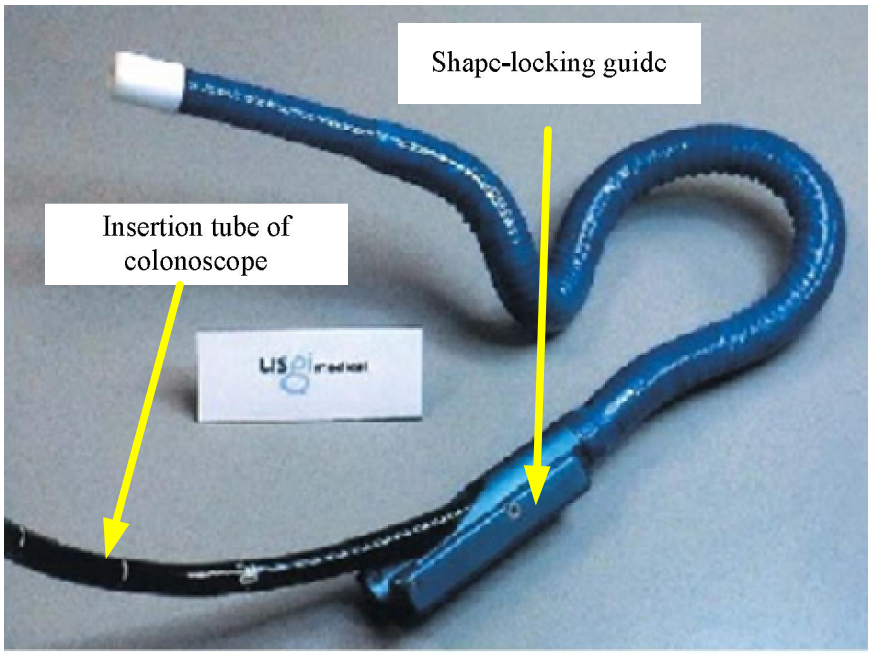

Figure 2.2 Shape-locking guide [51]*

(* Permission to use this figure is given in Appendix J)

2.3.2.2.2 Clinical Feedback

In clinic, loop formation in the transverse colon and in the first intubation in the sigmoid colon are not found to be avoidable by using this device. Additionally, the increased diameter (outer diameter is 21 mm) of the SG-1 may result in more discomfort for patients during colonoscopy [24].

2.3.2.3 Self-propelled Endoscope

2.3.2.3.1 Brief Review of Self-propelled Endoscope

With the development of microelectromechanical and microelectronic technologies, there have been significant advances in the field of medical devices including endoscopy. For example, capsule endoscopy, the patient swallows the capsule and it is self-driven through gastrointestinal natural peristalsis, enables a non-invasive diagnosis of the gastrointestinal tract [53, 54].

The capsule has a tinny camera, a light source, a transmitter, and a battery. During the examination, the camera takes photographs twice per second as the capsule passes through the digestive tract. The photographs are sent wirelessly to a small computer that is worn on the patient's belt, and photographs are then downloaded to a computer workstation for the physican's review [55, 56].

Given Imaging™ Ltd. released the Model-M2A capsular endoscope with a length of 26 mm and diameter of 11 mm in 2001 [57, 58]. The Endo Capsule that was released by an Olympus™ Corp. in 2005 is the the same size as the Model-M2A [59], as shown in Figure 2.3. Although the capsular endoscope has become popular among physicians, it presents three drawbacks. The first problem is its limited battery power, only providing 25 mW for 6–8 h [60]. The second problem is the impossibility of performing non-invasive biopsies. The third problem is that it does not allow a physician to take close images of particular interest [61]. Based on the latter bottleneck,

recently, researchers have presented capsular endoscopes that are based on several different locomotive principles. Following, a brief review of current state-of-the-art technology and systems for autonomous endoscopes is presented.

Figure 2.3 Endo Capsule

(http://www.olympusamerica.com/presspass/press_pass_cut/opp_enteroPro.asp)

(i) SMA Actuator

Ikuta et al. [62] used shape memory alloy (SMA) actuators to develop an automated endoscope. The experimental studies revealed that the SMA-actuated endoscope produced a snake-like motion, and therefore was able to move in the slippery colon.

Kim et al. developed a SMA-actuated locomotion mechanism for capsular endoscope [63]. This prototype, when was tested *in vitro*, was able to move in the gastrointestinal tract with a speed of 9.19 mm/min. However, this device required great power consumption.

Hosokawa et al. [64] devised a SMA-actuated capsular endoscope equipped with a propulsion system that simulates the locomotive mechanism of snails. The robot, which consisted of two SMA springs, was able to contract and elongate in response to an electric current, and stick to surfaces via a suction mechanism [65-66].

However, the response of the SMA actuator is very slow; thus, the SMA-actuated capsular endoscope cannot produce strokes quickly enough to produce movement.

(ii) Pneumatic Actuator

Dario et al. [67], Goh and Krishnan [68], and Phee et al. [69] developed several generations of inchworm-like capsular endoscopes based on the pneumatic actuators. The robots consisted of two types of pneumatic actuators: clamper and extensor. These devices were clamped onto terrain by using the clamper, and moved by the extensor. The experimentation with these devices *in vitro* has proven their ability to move in the colon without loop formation [70].

Kim et al. [71] presented a robotic colonoscope based on the pneumatic actuator. The robot was able to expand and retract to simulate inchworm-like locomotion. This device consisted of a camera, a light source, a water injection channel, and biopsy tools. Chen et al. [72] also presented a pneumatic-driven flexible robotic manipulator called ColobBot for use in colonoscopy.

However, these pneumatic-actuated robots exhibit bulky volume and have air pipes. These two factors can be obstacles for smooth movement in the colon.

(iii) Motor Mechanism

Goh et al. [73] developed several generations of robotic endoscopes based on the motor mechanism, such as the Mark VI, Mark VII, and Mark VIII model. These models were driven by two micromotors, and were able to move slowly across the slippery colonic specimens.

Kim et al. [74] devised two self-propelled robots by using micromotors, namely stretchable-body robot and spiral-body robot. These micromotor-actuated robots can generate sufficient propulsion and strokes as required.

Sukho et al. [75, 76] developed a paddling locomotive mechanism for the robot. The locomotive mechanism simulates the mechanical action of paddling a canoe to produce movement.

Stefanini et al. [77] presented a legged microrobot in 2006. Quirini et al. [78] also developed a novel legged locomotion mechanism for a miniaturized robot, in which the legged locomotion mechanism was used (a volume about 4-5 cm^3) (see Figure 2.4). A DC brushless motor was used to actuate the legs of the robot. The robot was equipped with four super-elastic legs to produce a speed ranging between 10 and 40 mm/min.

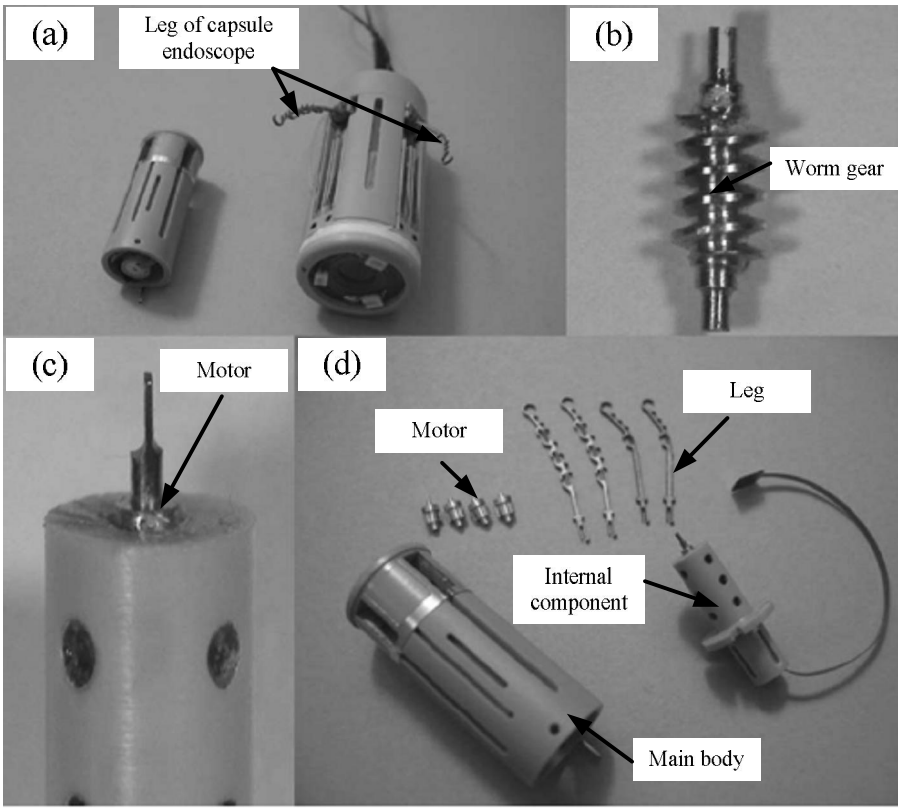

Figure 2.4 Capsule endoscope prototype (a) with closed legs and with open legs; (b) worm gear; (c) internal capsule body with motor shaft; (d) all components of the capsule [77]*

(* Permission to use this figure is given in Appendix J)

Valadstri et al. [79] devised a robotic-legged locomotion with 12 legs. This design represents a milestone in a pill-sized robot. A series of *in vivo* experiments demonstrated its ability to travel the entire colon in a short period of time.

Wang et al. [80] developed a wireless robotic endoscope using a micro-DC motor. This device consisted mainly of a locomotion system, a wireless power supply subsystem, and a communication subsystem. Although the endoscope performed with excellent dexterity, it cannot be applied for *in vivo* colonoscopy due to its short-range wireless power transmission.

(iv) Magnetic Field Control

At Tohoku University, Yamazaki et al. developed a capsular device with an inside permanent magnet and spiral structure [81]. An external rotational magnetic field was used to propel the capsule. *In vivo* and *in vitro* experiments demonstrated that the magnetic guidance system for the capsular endoscope was feasible. However, there is a safety concern assosciated with the use of the magnetic field radiation [82, 83].

Mosse et al. [84] developed an electrical simulation approach to propel a capsular endoscope. Five prototypes were tested in the small intestine, and moved reliably at a maximum speed of 4.5 mm/s.

Carpi et al. [85] exploited a magnetic shell to be applied the traditional capsular endoscope. The magnetic shell can interact with an external magnetic field, thus, this approach is able to control the movement of capsular endoscope and its orientation in the human body.

Ciuti et al. [86] proposed an active magnetic locomotive system to a capsular endoscope based on a human-machine interface and a 6 DOFs robotic arm for very previse guidance of the endoscope in the gastrointestinal tract.

(v) Hybrid System

Lee et al. [87] proposed a novel hybrid system for capsular endoscopes. The capsule's rotation and motion were controlled by magnetic forces. The capsular body had a screw propeller with five different flexible threads (see Figure 2.5). This design enhanced the capsule's advance in the curved gastrointestinal tract. Simi et al. [88] also proposed a hybrid locomotion system for an active endoscope in the gastrointestinal tract (see Figure 2.6).

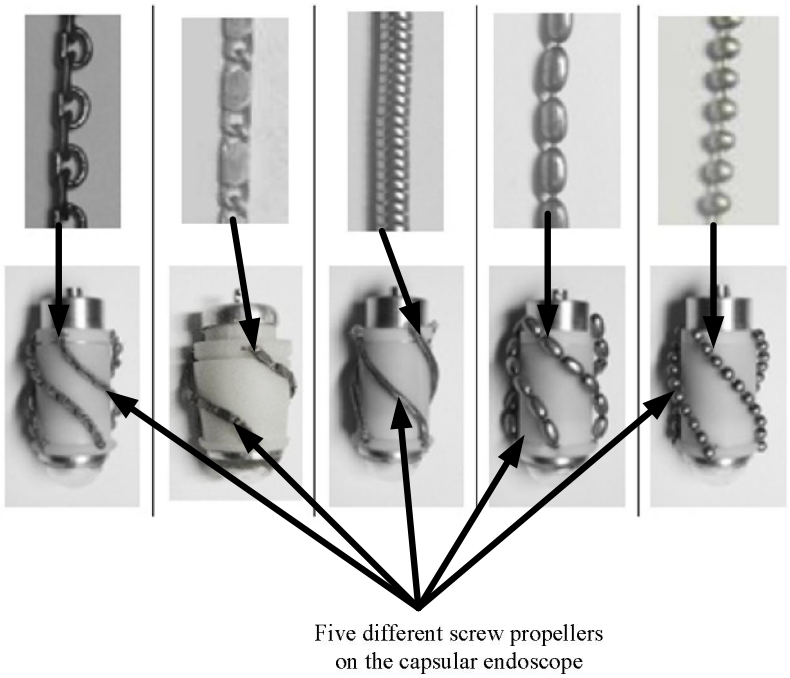

Figure 2.5 Five prototypes with different shapes of threads and screw [87]*

(* Permission to use this figure is given in Appendix J)

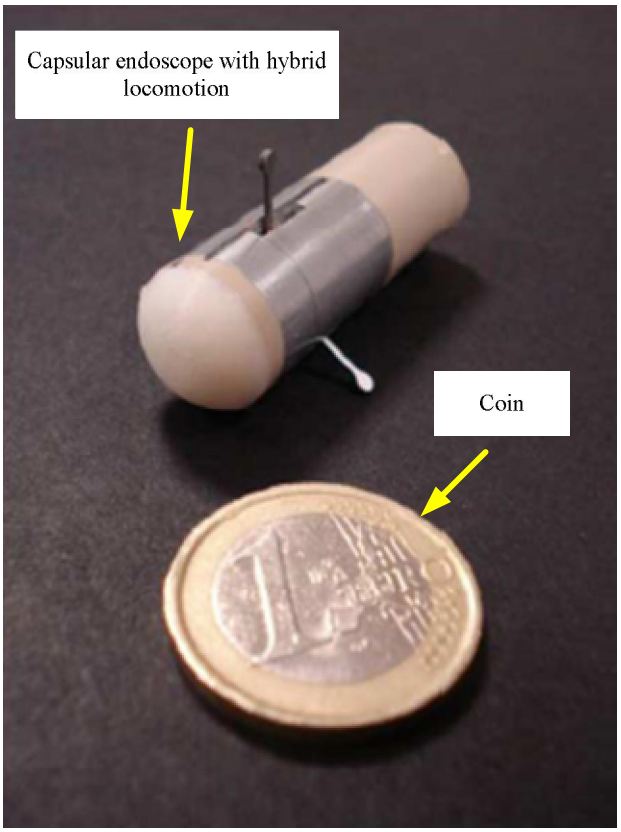

Figure 2.6 First hybrid locomotion capsule prototype [88]*

(* Permission to use this figure is given in Appendix J)

2.3.2.3.2 Evaluation of Locomotion Efficiency

A self-propelled endoscope could avoid the loop problem by employing pulling force instead of pushing force. A variety of microrobotic endoscopes based on different actuating mechanisms have been reviewed such as the SMA actuator, the pneumatic actuator, and the micromotor actuator, and so on. Table 2.1 shows the current state-of-the-art locomotive endoscopes. There are significant differences with regard to locomotion speed, driving force, and power consumption among the different locomotive principles.

For the self-propelled endoscope, there is a critical issue needing to be resolved, i.e., locomotion efficiency. The self-propelled endoscope needs to generate frictional force in order to clamp onto the colon tissue, then driving itself to advance. However, the colon is stretched when the endoscopye has a forward movement. When Δd is the theoretical stroke of the device during a time step and Δl is the elongation of the colon tissue, the effective stroke = Δd - Δl.

For the most efficient robotic endoscope (see Table 2.1), locomotion efficiency of the robotic endoscopy was estimated with Eq. (2.8) (details of the derivation of this equation are found in Appendix D):

$$\left\{ b_{xc}\left(\frac{\Delta l}{L}\right)^2 + d_{xc}\left(\frac{\Delta l}{L}\right)\cdot t_c \cdot \pi \cdot d_c + b_{xm}\left(\frac{\Delta l}{L}\right)^2 + d_{xm}\left(\frac{\Delta l}{L}\right)\cdot t_m \cdot h \right\} = F_f \tag{2.8}$$

The efficiency ratio was approximately 53%. For the most effective self-propelled endoscope, its speed is still much slower than that of manual insertion.

2.3.2.3.3 Evaluation of Design

The self-propelled endoscope's locomotion does not rely on external pushing and has no "self-locking" phenomenon that occurs during the examination. DP is defined as:

- DP: self-propelled mechanism

This design has met the functional requirements of the ADT. However, a further evaluatation of the self-propelled endoscopes against the CRs of the colonoscopy system shows that the DPs of the the self-propelled endoscopes fail to meet two of the CRs of the colonoscopy system, namely:

- CR_1: operation time cost
- CR_2: biopsy function

Table 2.1 Locomotive principles for self-propelled endoscopes [89]

Approaches	Locomotion speed (mm/s)	Driving force (N)	Locomotion principle	Control approach
Electrical simulation	4.5-6	0.3-0.6	Electrophysiology	Cable
SMA	0.1-0.3	1.4	Shape memory alloy effect	Cable
Magnetic control	5-10	1.5-3.0	Rotating magnetic field	Wireless
Legged locomotion	0.2-0.5	1.0-2.0	Biomimetics	Cable
Magnetic shell navigation	1-10	0.1-5	Static magnetic field propulsion	Wireless
Hybrid system	2-15	2-6	External magnetic and internal actuation	Wireless/Cable

2.3.2.4 Evaluation of Virtual Colonoscopy

Currently, computer tomography (CT) can be used for the colon screening. However, this technique has some drawbacks with regard to the diagnosing of colorectal diseases. First, CT is not able to detect polyps smaller than 10 mm. Second, any colour variations of mucosa may not be detected, so many abnormalities are missed. Third, this method is impossible to take any biopsies or remove polyps [90].

Further evaluation of virtual colonoscopy against the CRs of the colonoscopy system shows that the DPs of the virtual colonoscopy fail to meet two of the CRs of the colonoscopy system, namely:

- CR_2: biopsy function.
- CR_3: safe examination environment.

2.3.2.5 Evaluation of the Aer-O-Scope

GI View Ltd. [91-93] developed the Aer-O-Scope commercially available that was based on a self-propelled principle only for diagnosis of the colon. The Aeo-O-Scope consists of mainly a workstation and a disposable unit comprising of a rectal introducer, a supply cable, and a scope (see Figure 2.7). The propulsion mechanism has two balloons. One balloon is kept fixed in the rectum; the other balloon is mobile. The CO_2 gas pressure between the two inflated balloons drives the scope.

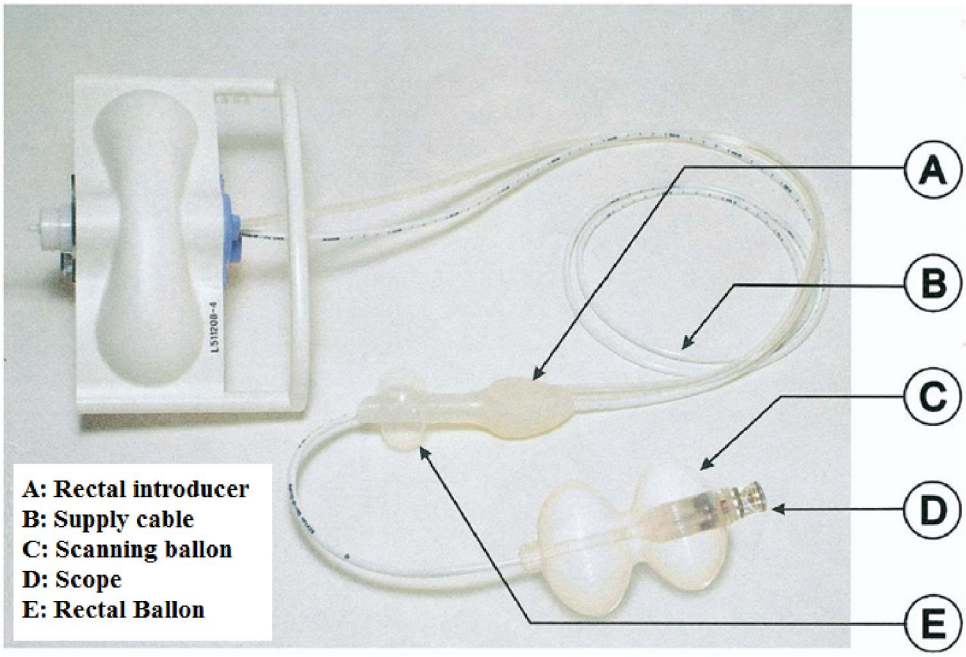

Figure 2.7 Aer-O-Scope disposable component [92]*

(* Permission to use this figure is given in Appendix J)

A pulling mechanism rather than pushing force propels the Aer-O-Scope. For the Aer-O-Scope, the DP is defined as:

- DPs: pulling mechanism

This design has met the functional requirements of the ADT. However, further evaluation of Aer-O-Scope against the CRs of the colonoscopy system reveals that the DPs of the Aer-O-Scope fail to meet one of the CRs of the colonoscopy system, namely:

- CR_2: biopsy function

In clinic, the Aer-O-Scope can be used only for visual diagnostic purposes.

2.3.2.6 Evaluation of the NeoGuide Endoscopy System

The NeoGuide Endoscopy System (NES) was developed by NeoGuide Systems Inc. [94]. This system has many common features with conventional scope. The entire insertion tube of the NES consisted of 25 segments that are controlled by the computer based on a "follow-the-leader" principle (see Figure 2.8 and Figure 2.9) [95, 96].

Figure 2.8 Console of the NES [95]*

(* Permission to use this figure is given in Appendix J)

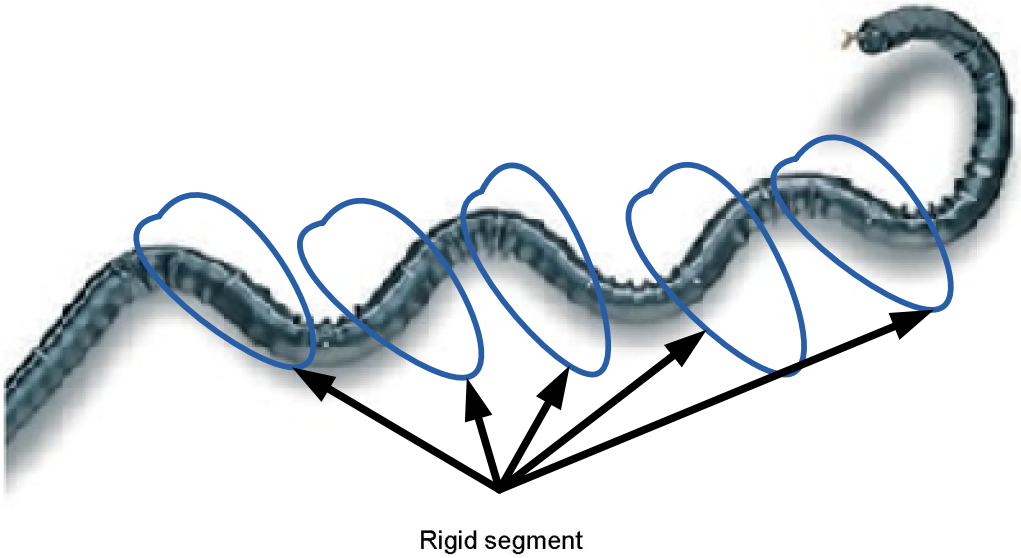

Figure 2.9 Insertion tube of the NES with multiple segments [95]*

(* Permission to use this figure is given in Appendix J)

The computer controls position of each segment. In this case, the shape of the scope in the colon cannot be changed randomly, i.e., the scope cannot be bent randomly due to external pushing force. Thus, the scope has no significant contact force acting on the colon tissue, so perforation of the colon may not occur.

For the NES, the DP is defined as:

- DP: the insertion tube following the trajectory of the tip of the scope

This design does not meet the functional requirements of the ADT. Further evaluation of the NES against the CRs of the colonoscopy system reveals that the DPs of the NES have met all three CRs of the colonoscopy system.

In clinic, Eickhoff et al. [96] performed the first human clinical trial with NES. The results of this study seem to be promising. However, some cases reported that the NES caused severe pain because of extra pushing force applied compared to the conventional colonoscope. Also, several cases reported occurrence of extensive non-typical loops [24].

2.3.2.7 Evaluation of Imaging-guided Colonoscopy

Imaging-guided colonoscopy provides real-time 3D views of the insertion tube configuration during the procedure. These techniques were achieved by using fluoroscopic guidance and magnetic endoscopic imaging (MEI) in Refs. [97-99]. Recently, Olympus Corp. designed a ScopeGuide that uses magnetic fields to provide a real-time 3D configuration of the colonoscope in colonoscopy. However, the radiation exposure is required during imaging-guided colonoscopy.

This design does not meet the functional requirements of the ADT; that is to say, this technique cannot prevent loop formation in colonoscopy.

Further evaluation of image-guided scope against the CRs of the colonoscopy system shows that the DPs of the image-guided scope fail to meet one of the CRs of the colonoscopy system, namely:

- CR_3: safe examination environment

2.4 Conclusions

In this chapter, a mechanical analysis of loop formation in colonoscopy was presented. Loop formation is a result of the self-locking phenomenon when driving force angle is less than frictional force angle. During the state of self-locking, a significant contact force distends the colon tissue, and finally perforation of the colon may occur during loop formation. Based on this analysis, a framework of criteria was established by instrumentally employing a design theory called the ADT.

The existing systems, including the VSC, the over-tube colonoscope, virtual colonoscopy, the self-propelled endoscope, virtual Colonoscopy, the Aer-O-Scope, the NES, and imaging-guided colonoscopy were evaluated. The results of the evaluation are summarized as shown in Table 2.2.

Table 2.2 Summary of evaluation results of the existing device and solutions

Existing Devices and Solutions	Functional Requirements (FRs)	Constraints Requirements (CRs)		
		CR_1	CR_2	CR_3
VSC	×	√	√	√
Over-tube colonoscope	×	√	√	√
Self-propelled endoscope	√	×	×	√
Virtual colonoscopy	√	√	×	×
Aer-O-Scope	√	√	×	√
NES	×	√	√	√
Imaging-guided colonoscopy	×	√	√	×

Clinical feedback for the existing devices was also reviewed to see whether the engineering analysis and clinical feedback agreed. The clinical feedback is summarized as follows:

(1) With the VSC, there are some conflicting reports about its ability to facilitate cecal intubation. This method is seen as a dangerous intrusion of the human colon because risk of perforation is high. The over-tube colonoscope prevents looping in the sigmoid colon but loop formation in the transverse colon may occur.

(2) The limitation of the Aer-O-Scope is such that they can be used only for visual diagnostic purposes because it does not have the function of removing premalignancies and polyps.

(3) For the self-propelled endoscope, it does not allow for therapeutic procedures to be carried out due to its special locomotion system. Furthermore, for the most effective self-propelled endoscope, its movement is 10 times slower than other manual insertion in the colon.

(4) The virtual colonoscopy can detect only large polyps and altogether misses diseases with colour variation symptoms.

(5) The NES is effective in preventing loop formation by comparison to the conventional colonoscope, but it may cause pain to patients and extensive non-typical loops during the colonoscopy.

(6) Imaging-guided colonoscopy offers a 3D configuration of looping in real-time. This approach provides physicians with visible information of the loop in the human body; however, this procedure requires an unsafe magnetic field.

In conclusion, both the engineering analysis and clinical feedback agree that the Aer-O-Scope is the best device for purposes of overcoming the looping problem. However, overall effectiveness of the Aer-O-Scope is restricted by its incapability to do biopsy. The root cause for inadequacy of all the currently existing devices in terms of overcoming the looping problem in colonoscopy is that they have failed to recognize the self-locking mechanism that is responsible for looping.

CHAPTER 3

APPROACHES TO MODELING DEFORMABLE OBJECTS:

LITERATURE REVIEW

3.1 Introduction

This chapter presents a literature review on modeling of deformable objects, in particular for cable-like objects. Section 3.2 introduces some approaches to modeling long and slender objects, including dynamic splines, mass-spring models (MSM), the Kirchhoff's rod theory, the Cosserat rod theory, rigid bars with joints, and finite beam element model (FBEM), and discusses their advantages and disadvantages with respect to the requirements for modeling. Section 3.3 gives a summary of these methods and discusses the choice of the FBEM as the most suitable tool for the modeling problem proposed as Objective 2 of the thesis (Chapter 1, Section 1.2).

3.2 Approaches to Modeling Deformable Objects

Over the past two decades, to facilitate minimally invasive interventional techniques, there has been rapid development and manufacture of intruments. An example of one such is the

endoscopic devices, catheter and guide wires and many others [108]. Such long and slender deformable instrument called "1D" elastic rod that is able to bend and twist in 3D space. It is one of a group of so-called "1D" objects, all of which share some common features including high tensile strength and low resistance to bending [109].

Based on elasticity theory, the dynamics of 1D objects can be described by mathematical formulations. Shabana [110] introduced three classic formulations for modeling of deformable systems, i.e., floating frame of reference, incremental finite element, and large rotation vector. A comprehensive review of the three methods can be found in Refs. [110-115].

Over the past several decades, dynamic splines [116-125], the Cosserat theory [148-156], the mass-spring model (MSM) [126-137], the Kirchhoff's rod theory [135-147], the rigid bars with joints [161-169], and the FBEM [170-191] have been applied to dynamic modeling of such 1D deformable objects. This review will visit all of the aforementioned methods and point out the limitations of each method with regard to the purpose of this study.

3.2.1 Dynamic Splines

The idea behind the dynamic splines method is that a 1D object can be modeled as a series of spline sections segmented by a set of control points. These control points are called the degrees of freedom of the system. The assumption of the dynamic splines method is that the object's shape always corresponds to that of the chosen spline model.

Three geometric splines are commonly utilized in the literature, namely Catmull-Rom (De Casteljau) (C^1), Cubic uniform B-Spline (C^2), and NUBS (generic) [120]. The splines can be represented by (n+1) control points q_i , and by (n+1) basis function b_i, expressed as

$$P(s,t) = \sum_{i=0}^{n} b_i(s) q_i(t) \tag{3.1}$$

where

P : position function;

t : time; and

s : horizontal ordinate.

Lagrangian formalism is used to represent the motion of the dynamic spline, and allows the external force and boundary conditions to be applied to the spline (see Ref. [125]). The equation of motion of dynamic spline is described by

$$\begin{cases} \dfrac{d}{dt}\dfrac{\partial T}{\partial \dot{q}_i} - \dfrac{\partial T}{\partial \dot{q}_i} - \left\{\dfrac{\partial \psi}{\partial \dot{q}_i}\right\}^t \{\lambda\} = Q_i \quad i = 1...4m \\ \{\psi\} = \{0\} \end{cases} \tag{3.2}$$

where

q_i : the ith generalized coordinate;

$\dot{q}_i$: dq_i/dt (t is the time);

T : kinetic energy of this system;

$\{\psi\}$: vector representing constraints of this system;

$\{\lambda\}$: vector including the Lagrange multipliers for each constraint; and

Q_i : sum of all forces acting on the q_i .

All forces acting on q_i consist of two contributions, and they are elastic forces that are generated by the deformation of objects and external forces and torques acting on the system.

In Ref. [116], Terzopoulos et al. presented a deformable model for computer graphics that included physics-based curves based on the Lagrangian Newton's equation. In Ref. [117], Qin and Terzopoulos proposed [117] dynamic non-uniform rational B-splines (DNURBS). They also combined the splines with physics laws after Terzopoulos's work.

Nocent and R´emion [118, 119] presented the dynamic material splines (DMSs). They considered splines control points as DOFs of the underlying continuous object. The continuous stretching energy was incorporated into the DMS and the Lagrange multipliers are used to constrain the point position and tangent orientation of the DMS.

Based on the Nocent and R´emion's work, Lenoir et al. [120-122] proposed a curvature energy formulation for the DMS. Alhtough the simulation was not geometrically exact, it did provide a real-time animation for the objects.

Walsum et al. [123] proposed a snake-based approach to model the catheter model. The model considered the internal energy, deformation of the catheter, and external energy. The catheter was defined by a fourth-order B-spline. In order to minimize the energy representation mentioned above, the control points along the B-spline were "moved" during the process of optimization.

Theetten et al. [124] presented a complete model for a deformable 1D object. The stretching, bending, and twisting energies were formulated as the continuous expression of an object that is mechanically rigorous and geometrically exact. The proposed model was validated by several classical test configurations, and good accuracy of this model was found. Thus, the suitability of their proposed model was proven.

The limitations of dynamic spline methods can be summarized as follows:

(1) Although this method can be employed to model complex contact configurations, it does not model the torsion of the objects.

(2) The dynamic spline method is a geometrically-based model, so it is difficult to account for the effects of inertia, damping, etc.

3.2.2 Mass-spring Model

The mass-spring model (MSM) is the simplest and most intuitive one from among all the deformable models. The object is discretized into a point-mass that has volume in three dimensions (or surfaces, i.e., 2D) in space as shown in Figure 3.1. These point-masses are connected to each other with springs that simulate the dynamics [126]. The motion of the point-mass is governed by Newton's second law, $f_i = m_i \ddot{x}_i$; thus, each point-mass of an object can be expressed by

$$M\ddot{X} = f(X, V) \tag{3.3}$$

where

X : position of point-mass;

V : velocity of point-mass;

$\ddot{X}$: acceleration of point-mass;

M : mass matrix of point-mass; and

F : internal and external forces acting on point-mass.

Thus, the motion equation of the MSM is governed by ordinary differential equations. Both internal and external force can be applied to the point-mass, then the motion equation can be solved simply [132, 133].

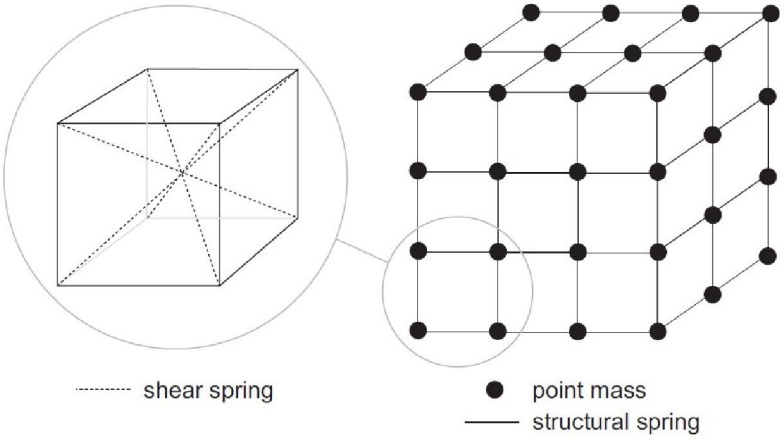

Figure 3.1 A mass-spring system [134]*

(* Permission to use this figure is given in Appendix J)

However, a deformable body also may dissipate energy in the process of deformation. In order to consider this engery, "viscoelastic springs" were used to damp out relative motion [134]; thus, a viscous force may be applied to each spring between point-masses. It can be expressed by

$$f_i = k_d (v_j - v_i) \tag{3.4}$$

where

k_d : spring's damping constant;

v_i v_j : velocity for point mass i and point mass j; and

f_i : viscous force between point mass i and point mass j.

Thus, the MSM method enables the deformable object to model the damping factor.

Application of the MSM for computer graphics can be found in [126-134]. Further, The MSM is the simplest approximation of elasticity theory, so as a result the MSM is relatively inaccurate. This reduced accuracy may be acceptable in its application to film and games, but overall the MSM is not recommended for accurate modeling.

3.2.3 Kirchhoff's Rod Theory

Kirchhoff proposed a model for three-dimensional elasticity in the early 1900s, then developed a mathematical formulation that was similar to a then-existing equation that described motion of a rigid body. Later, Clebsh modified Kirchhoff's rod theory by adding the factor of initial curvature. Love completed Kirchhoff's rod theory by adding the ordinary approximation theory. Kirchhoff's rod theory is built upon elasticity theory; thus it provides accurate representation for deformable objects. There are several assumptions in Kirchhoff's rod theory as follows [135]:

(1) The cross-section of the rod is identical throughout, and the flexural rigidities (EIs) along the principal axes of the rod should be kept constant.

(2) The material of the rod is homogenous and isotropic.

(3) The length of the rod must be large compared to the size of the cross-section.

(4) Axial and shear deformations both are negligible.

(5) Distributed force and moments along the rod both are negligible.

(6) The applied external forces should be conservative.

There can be many practical problems in the application of Kirchhoff's rod theory to modeling; for example, in ocean engineering work on marine cables. Kirchhoff's rod theory is used to analyze both loop formation and the stability of the rod, taking into consideration a variety of loads and boundary conditions. Recently, in biology biomechanics research (involving, for example, cilia, flagella, DNA, and so on) Kirchhoff's rod theory was used to investigate the stability mechanism [136-146].

However, in this study, Kirchhoff's rod theory is not suitable for modeling the colonoscope since the contact force from the colon tissue cannot be discarded.

3.2.4 Cosserat Rod Theory

In 1907, Cosserat brothers Eugèn and Franço proposed a new formulation for describing the continuum mechanics (now called Cosserat theory) as applied to deformable rods and shells. In their formulation, the stresses and the rotational DOFs of the deformable object were considered as independent variables, and this work was published in Refs. [148-161]. To the present day, Cosserat rod theory remains a well-known approach for investigation of nonlinear elasticity for deformable object. A comprehensive discussion of this subject was given in Antman's book [162].

In Cosserat rod theory, the elastic rod is regarded as a long and thin deformable body, its length larger than the of cross-section area. The rod is defined as the continuous point-mass (also called the element). When the Lagrange equation of motion is applied to the rod, its large bending and twisting deformations can be captured.

Recently, several projects have reported use of Cosserat theory for computer animation [148-156], and indicated high-fidelity simulation.

However, Cosserat rod theory shares the assumption with Kirchhoff's rod theory that distributed force and moments along the rod are discarded. Thus, this method too is not suitable to model the colonoscope in this study.

3.2.5 Rigid Bars and Joints

The 1D object can be modeled by a number of bars that are connected by joints. This structure is called a bar-and-joint system. This system often can be seen in the area of robotic manipulation [162].

The Newton-Euler formulation as shown in Eq. (3.5) is applied to find the dynamics of the system [166]:

$$M(q)\ddot{q} + V(q,\dot{q}) = G(q) \tag{3.5}$$

where

$M(q)$: inertia tensor;

$V(q,\dot{q})$: generalized force vector representing coriolis and gravitational forces;

$G(q)$: generalized forces;

$\ddot{q}$: acceleration of the link; and

$\dot{q}$: velocity of the link.

When external forces are applied to the system, the position of each link can be found by integrating Eq. (3.5) [161].

Körner et al. [163, 164] developed a computer-based training simulator for colonoscopy based on the bar-and-joint model. They used 20 elements of articulated link for their scope model. However, the fidelity provided by this simulator was poor.

Konings et al. [165] proposed a model for guide-wire navigation in interventional radiology simulation based on a model of rigid bars and joints. The model was validated using a 2D planar phantom. The experimental results indicated good accuracy of the model.

Ikuta et al. [166-169] proposed a virtual endoscopy simulator with force sensation based on a model of rigid bars and joints. The forward dynamics based on a simplified Newton-Euler equation were used in their study. The Newton-Euler equation was simplified by discarded inertia and centrifugal and coriolis forces. However, the endoscope model has shown unrealistic simulation.

3.2.6 Finite Beam Element Model

Structural analysis is typically used to investigate the behaviours of structures. There are two methods for structural analysis: analytical methods and numerical methods. The drawback of analytical methods is that only simple structural configurations can be analyzed. Thus, for complex structures, only the numerical methods can be used. The finite element method (FEM) is an effective numerical technique [170].

The structure is discretized by an appropriate element such as a beam element for a 1D member of a structure, a plate for a 2D member of a structure, and so on. An equilibrium equation based on the principle of virtual work with the assumption of a linear relation of the displacement and applied load is used for linear analysis. Linear analysis includes geometrical linearity (i.e., infinitesimal displacement) and linear elastic material (i.e., material linearity) [171]. However, nonlinear analysis should be used if involving material nonlinearity such as nonlinear stress-strain relation of materials and large displacement for a structure.

The dynamic equilibrium equation of the FEM is expressed by [172]:

$$M\ddot{U} + C\dot{U} + KU = F \tag{3.6}$$

where

M : mass matrix of element;

C : damping matrix of element;

K : stiffness matrix of element;

U : nodal displacement of element; and

F : loading on element.

Mass matrix M, stiffness matrix K, and damping matrix C of Eq. (3.6) are independent of time. For a linear system, these matrices are kept fixed in the procedure of integration. However, for a nonlinear system, these matrices are updated at each time-step.

There are two schemes that are used for the integration of Eq. (3.6): explicit scheme and implicit scheme. They are expressed by Eq. (3.7) and (3.8), respectively [198]:

$$U_{n+1}\,|_{\exp} = f(U_n, \dot{U}_n, \ddot{U}_n, U_{n-1}, \ldots) \tag{3.7}$$

$$U_{n+1}|_{imp} = f(U_n, \dot{U}_{n+1}, \ddot{U}_{n+1}, \ldots) \tag{3.8}$$

where Δt is the time-step and U_n is nodal displacement at the time $n\Delta t$.

There are several different numerical methods that are used in the explicit scheme, e.g., the central difference method, two-cycle interaction with trapezoidal rule, and the fourth-order Rung-Kutta method. In the implicit scheme, the Houbolt method, the Wilson Theta method, the Newmark Beta method, and the Park Stiffly stable method are used. The advantage of the explicit methods is that less computation is required compared to that required by implicit methods. One application of the explicit methods is the commercial software ANSYS^{TM}, which offers an accurate and easy-to-use solver for the dynamic equilibrium equation of the FEM. However, explicit methods can be unstable numerically if the time-step is larger than the critical value. The advantage of implicit methods is that they offer more stability than do explicit methods [198].

For modeling of a 1D deformable object, a beam element is commonly used in the FEM. There are two categories of beam models: the Euler-Bernoulli beam model and the Timoshenko beam model. There exist two assumptions in the Euler-Bernoulli model: that the transverse shear deformation is discarded and that the remaining plane of the cross-section of beam element is normal to the neutral axis of the beam element after its deformation. In the Timoshenko beam theory, there is only one assumption that the plane sections remain a planar shape and are perpendicular to the neutral axis [191].

Anderson et al. [194, 195] developed a real-time interactive simulator called daVinci (Visual Navigation of Catheter Insertion) using the finite 3D beam elements for vascular catheterization procedures. Their physics-based catheter model consists of a set of connected beam elements that

can capture bending, twisting, and other deformations. Recently, Cotin et al. [196, 197] developed a catheter simulator using finite beam elements. The catheter model based on FBEM provided very high-fidelity simulation for interventional neuroradiology.

3.3 Conclusions

In this chapter, several techniques for modeling deformable bodies were reviewed; their limitations are summarized in Table 3.1. The dynamic splines method is suitable for modeling of complex configurations of objects, and it is able to model systems of 3 DOFs. The torsional behaviour is not captured by this method. The dynamic splines method is a geometrically-based (non-physically-based) model. This method is commonly applied to computer-based animation where comparatively less accuracy is required. The MSM is the simplest and most intuitive model. Discrete point-masses are connected to each other by a network of mass-less springs. This method has been used to model skin, cloth, and so on for computer animation. The MSM is the simplest approximation of elasticity theory; the main advantage of the MSM method is its very fast computational efficiency. The FBEM provides a solid foundation to model 1D deformable object accurately. This physics-based model can capture bending, twisting and other deformations of the structure, which was chosen to model the kinetics of the colonoscope in Chapter 4.

Table 3.1 Major characteristics of different approaches to modeling deformable object

Characteristics of the models	Dynamic splines	Mass-spring-model	Kirchhoff's rod theory	Cosserat Rod theory	Rigid bars with joints	FBEM
Governing equations of motion	Euler- Lagrange equation	Newton's second law	Newton-Euler / Euler-Lagrange equation	Euler-Lagrange equation	Newton-Euler equation	Matrix structural analysis
DOFs	3	3	6	6	6	6
Non-linear behaviour	no	no	yes	yes	no	yes
Solution techniques	numerical solution	numerical solution	numerical solution	numerical solution	numerical solution	numerical solution
Model fidelity	less accurate	less accurate	accurate	accurate	less accurate	accurate

CHAPTER 4

THE MODEL OF THE COLONOSCOPE AND THE COLON

4.1 Introduction

In colonoscopy, the colonoscope is manipulated for intubation into the colon. The colonoscope has a flexible body which does not have distinct joints and segments, and it can be bent at any point. During the colonoscopy procedure, the scope moves with respect to the colon subject to the friction between the scope and colon and external force. Just like any moving object, the scope has inertia, damping, and stiffness.

During colonoscopy, the colon deforms in a complex way since it is constrained loosely at a number of points by the attachment called mesenteries or peritoneal fixations. The colon itself is basically quite flexible and can be considered a soft elastic-viscous tube. The colon can be lengthened when it is stretched by the colonoscope. In a normal situation, the colon is constrained by the mesenteries to remain in position within the abdominal cavity. However, despite constraint by mesenteries, the colon will move when it interacts with the scope. The dynamic behaviour of the colon is not significant compared to that of the scope, so in this study the inertia and damping of the colon can be disregarded.

In this chapter, the mathematical models for the scope and the colon will be developed. The model development also includes the parameter determination by the experiments. In particular, in Section 4.2, the model for the scope is presented, and in Section 4.3, the model of the colon is presented. The model for the scope-colon system that describes their interaction is presented in Section 4.4.

4.2 The Model for the Colonoscope

4.2.1 Equilibrium Equation for the Colonoscope

In order to model the kinetics of the colonoscope, an accurate representation of the scope is required. As discussed previously in Chapter 3, several techniques are available for modeling a cable-like object. Finite element method (FEM) was chosen as a tool for the modeling owing to the complex shape of the scope in the colon. In particular, the Timoshenko beam element was chosen because the beam model can capture the deformations of the scope including bending, twisting, and tensional compression. The scope is modeled as a set of beam elements. Each beam element has 6 DOFs in translation and 6 DOFs in rotation in space. The force-motion of the scope can be represented by Eq. (4.1) below. During each time step, by using the updated position instead of the original position of each beam element, a nonlinear finite beam element model for the scope is implemented to obtain the new position of the scope.

$$[M(U)]\{\ddot{U}\}+[C(U)]\{\dot{U}\}+[K(U)]\{U\}=\{F\} \tag{4.1}$$

where

$[K]$: stiffness matrix of the scope;

$[M]$: mass matrix of the scope;

$[C]$: damping matrix of the scope;

$\{F\}$: external force F_e and contact force F_c. The external force, i.e., force from the physician who manipulates the colonoscope, is also represented in the form of nodal force;

$[U]$: a column matrix of displacements corresponding to force vector $\{F\}$, and the force vector $\{F\}$ is applied at the nodal ends of each beam element, and the displacement of each beam element is then computed.

(i) Stiffness Matrix of the Scope

Stiffness matrix of the scope $[K]$ is a form of band matrix due to the serial structure of beam elements of the scope (a node is shared by two elements except for the end node). The stiffness matrix $[K_e]$ of the beam element is on the order of 12×12; see Eq. (4.2). Details for the derivation of the stiffness matrix $[k_e]$ of the beam element are given in Appendix E.

The coordinate of the beam element described in its local coorindate must be transformed to the global coordinate system. The transformation matrix $[\Lambda]$ is expressed by Eq. (4.3) below. This leads to the relation between $[K_e]$ in the local coordinate system and $[K]$ in the global frame as shown in Eq. (4.4) (MATLAB codes of stiffness matrix $[K]$ are given in Appendix F).

$$
[K_e] = \frac{E}{l}
\left[\begin{array}{cccccc|cccccc}
A & & & & & & & & & & & \\
0 & \frac{12I_z}{l^2(1+\phi_y)} & & & & & & & & & & \\
0 & 0 & \frac{12I_y}{l^2(1+\phi_z)} & & & & & & \textit{symmetric} & & & \\
0 & 0 & 0 & \frac{GJ}{E} & & & & & & & & \\
0 & 0 & \frac{-6I_y}{l(1+\phi_z)} & 0 & \frac{(4+\phi_z)I_y}{1+\phi_z} & & & & & & & \\
0 & \frac{6I_z}{l(1+\phi_y)} & 0 & 0 & 0 & \frac{(4+\phi_z)I_y}{1+\phi_y} & & & & & & \\
\hline
-A & 0 & 0 & 0 & 0 & 0 & A & & & & & \\
0 & \frac{-12I_z}{l^2(1+\phi_y)} & 0 & 0 & 0 & \frac{-6I_z}{l(1+\phi_y)} & 0 & \frac{12I_z}{l^2(1+\phi_y)} & & & & \\
0 & 0 & \frac{-12I_y}{l^2(1+\phi_z)} & 0 & \frac{6I_y}{l(1+\phi_z)} & 0 & 0 & 0 & \frac{12I_y}{l^2(1+\phi_z)} & & & \\
0 & 0 & 0 & \frac{-GJ}{l} & 0 & 0 & 0 & 0 & 0 & \frac{GJ}{E} & & \\
0 & 0 & \frac{6I_y}{l(1+\phi_z)} & 0 & \frac{(2-\phi_z)I_y}{1+\phi_z} & 0 & 0 & 0 & \frac{6I_y}{l(1+\phi_z)} & 0 & \frac{(4+\phi_z)I_y}{1+\phi_z} & \\
0 & \frac{6I_z}{l(1+\phi_y)} & 0 & 0 & 0 & \frac{(2-\phi_y)I_z}{1+\phi_y} & 0 & \frac{-6I_z}{l(1+\phi_y)} & 0 & 0 & 0 & \frac{(4+\phi_z)I_y}{1+\phi_z}
\end{array}\right] \tag{4.2}
$$

where

E : Young's modulus;

ν : Possion's ratio;

A : cross-sectional area of the beam and l is the length of the beam;

I_y : cross-section moments of inertia along y axis;

I_z : cross-section moments of inertia along z axis;

ϕ_y : shear deformation parameters, defined as $\phi_y = \frac{12EI_z}{GA_{sy}l^2}$ with A_{sy} the shear area along y axis; and

ϕ_z : shear deformation parameters, defined as $\phi_z = \frac{12EI_y}{GA_{sz}l^2}$ with A_{sz} the shear area along z axis.

$$
\begin{cases}
[\Lambda]_{12\times12} = \begin{bmatrix} [\lambda] & [0] & [0] & [0] \\ [0] & [\lambda] & [0] & [0] \\ [0] & [0] & [\lambda] & [0] \\ [0] & [0] & [0] & [\lambda] \end{bmatrix} \\
[\lambda]_{3\times3} = \begin{bmatrix} l_{ox} & m_{ox} & n_{ox} \\ l_{oy} & m_{oy} & n_{oy} \\ l_{oz} & m_{oz} & n_{oz} \end{bmatrix} \\
[0]_{3\times3} = \begin{bmatrix} 0 & 0 & 0 \\ 0 & 0 & 0 \\ 0 & 0 & 0 \end{bmatrix} \\
l_{ox} = \dfrac{X_j - X_i}{l} \\
m_{ox} = \dfrac{Y_j - Y_i}{l} \\
n_{ox} = \dfrac{Z_j - Z_i}{l}
\end{cases}
\tag{4.3}
$$

where X_k, Y_k, Z_k indicate the coordinates of node k ($k = i, j$) in the global coordinate system [199].

$$
[K] = [\Lambda]^T [K_e][\Lambda] \tag{4.4}
$$

(ii) Mass Matrix of the Scope

The mass matrix $[M_e]$ of the beam element is on the order of 12×12, expressed by Eq. (4.5). Details for the derivation of the mass matrix $[M_e]$ of the beam element can be found in Appendix G.

$$[M_e] = \rho Al \left[\begin{array}{cccccc|cccccc}
\frac{1}{3} & & & & & & & & & & & \\
0 & \frac{13}{35}+\frac{6I_z}{5Al^2} & & & & & & & & & & \\
0 & 0 & \frac{13}{35}+\frac{6I_z}{5Al^2} & & & & & & \textit{symmetric} & & & \\
0 & 0 & 0 & \frac{J_x}{3A} & & & & & & & & \\
0 & 0 & -\frac{11l}{201}-\frac{I_y}{10Al} & 0 & \frac{l^2}{105}+\frac{2I_y}{15A} & & & & & & & \\
0 & \frac{11l}{201}+\frac{I_z}{10Al} & 0 & 0 & 0 & \frac{l^2}{105}+\frac{2I_y}{15A} & & & & & & \\
\hline
\frac{1}{6} & 0 & 0 & 0 & 0 & 0 & \frac{1}{3} & & & & & \\
0 & \frac{9}{70}-\frac{6I_z}{5Al^2} & 0 & 0 & 0 & \frac{13l}{420}-\frac{I_z}{10Al} & 0 & \frac{13}{35}+\frac{6I_z}{5Al^2} & & & & \\
0 & 0 & \frac{9}{70}-\frac{6I_y}{5Al^2} & 0 & -\frac{13l}{420}+\frac{I_y}{10Al} & 0 & 0 & 0 & \frac{13}{35}+\frac{6I_y}{5Al^2} & & & \\
0 & 0 & 0 & \frac{J_x}{3A} & 0 & 0 & 0 & 0 & 0 & \frac{J_x}{3A} & & \\
0 & 0 & \frac{13l}{420}-\frac{I_y}{10Al} & 0 & -\frac{l^2}{140}-\frac{I_y}{30A} & 0 & 0 & 0 & \frac{11l}{201}+\frac{I_y}{10Al} & 0 & \frac{l^2}{105}+\frac{2I_y}{15A} & \\
0 & -\frac{13l}{420}+\frac{I_z}{10Al} & 0 & 0 & 0 & -\frac{l^2}{140}-\frac{I_z}{30A} & 0 & -\frac{11l}{201}-\frac{I_z}{10Al} & 0 & 0 & 0 & \frac{l^2}{105}+\frac{2I_z}{15A}
\end{array}\right] \tag{4.5}$$

where

I_y : rotatory inertia also called the moments of inertia along y axis;

I_z : rotatory inertia also called the moments of inertia along z axis;

J_x : torsional inertia also called the polar moment of inertia along x axis;

A : cross-sectional area of the beam; and

l : length of the beam.

With the same transformation matrix [Λ] for the stiffness matrix of the scope, the mass or inertia matrix of the scope in the global coordinate system can be determined by Eq. (4.6) (MATLAB codes of the mass matrix [M] are given in Appendix H).

$$[M] = [\Lambda]^T [M_e][\Lambda] \tag{4.6}$$

(iii) Damping Matrix of the Scope

The most effective way to represent the damping matrix is through an equivalent Rayleigh Damping expressed by Eq. (4.7). Rayleigh Damping is a linear combination of the mass and stiffness matrices.

$$[C] = \alpha[M] + \beta[K] \tag{4.7}$$

where α, β are determined by the experiment.

In the following sections, parameters in the model for the scope are determined experimentally via the Olympus^{TM} colonoscope CF-Q160L colonoscope, including flexural rigidity and Rayleigh damping coefficient, respectively.

4.2.2 Experimental Determination of Flexural Rigidity of the Scope

Measurements of the flexural rigidity of the colonoscopes were reported in Refs. [200-208]. The conclusion was that the flexural rigidity of the colonoscope depends on the individual colonoscope (different models and their use situations). For example, Nemirovaski [200-202] did testing on several Olympus^{TM} colonoscopes. Wehrmeyer et al. [204] did experiments on newer Olympus^{TM} and Pentax^{TM} colonoscopes with and without a stiffener inserted in the biopsy channel, and they found that the flexural rigidities of these colonoscopes were in the range of 160-240 N·cm^2. Dogramadzi et al. [206] presented the effect of temperature on flexural rigidity. Their results showed an approximate 15% reduction in flexural rigidity at body temperature (about 37^o) over room temperature (about 25^o). Hellier et al. [208] also measured both flexural rigidity and torsional rigidity of colonoscopes at room temperture (about 25^o) and body temperature (about 37^o), respectively. They conducted a series of experiments to determine flexural rigidity and torsional rigidity of the Olympus^{TM} colonoscope CF-140S. They found that along the length of the colonoscope, flexural rigidity of the Olympus^{TM} colonoscope varied between 260 and 440 N·cm^2 and torsional rigidity varied between 68 and 88 N·cm^2/deg.

For the particular colonoscope used in this study, measurement of flexural rigidity is thus necessary. The following sections will describe that measurement as performed in this study.

4.2.2.1 Experimental Design

The apparatus for flexural rigidity measurement in this study was the Instron-3366 single column testing machine. A test-rig with a 120 mm span for a three-point bending test was made (see Figure 4.1), and it was mounted on the Instron-3366 testing machine as shown in Figure 4.2 (a). The Olympus^{TM} CF-Q160L colonoscope was put in place and supported by the rig as shown in Figure 4.2 (b). The colonoscope was supported by two rollers which had a span of 120 mm between them, and a load P was applied at the mid-point to produce a displacement δ. Flexural rigidity *EI* was calculated by [208]

$$EI = \frac{PL^3}{48\delta} \tag{4.8}$$

where L is the span of the rig.

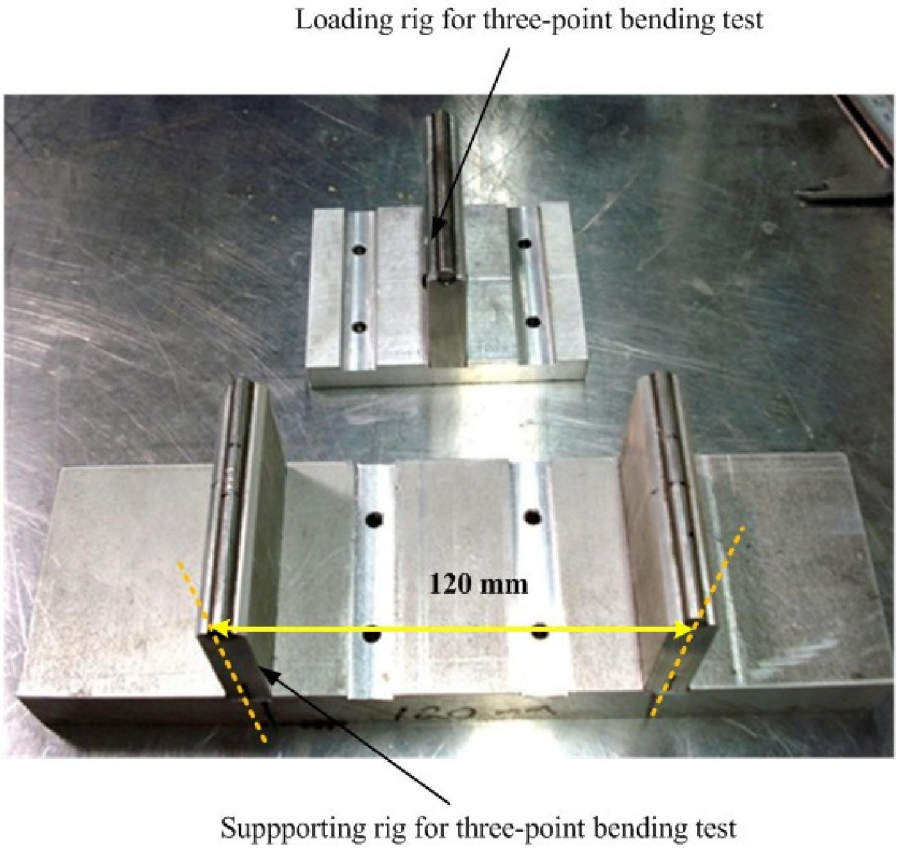

Figure 4.1 Test rig with 120 mm span

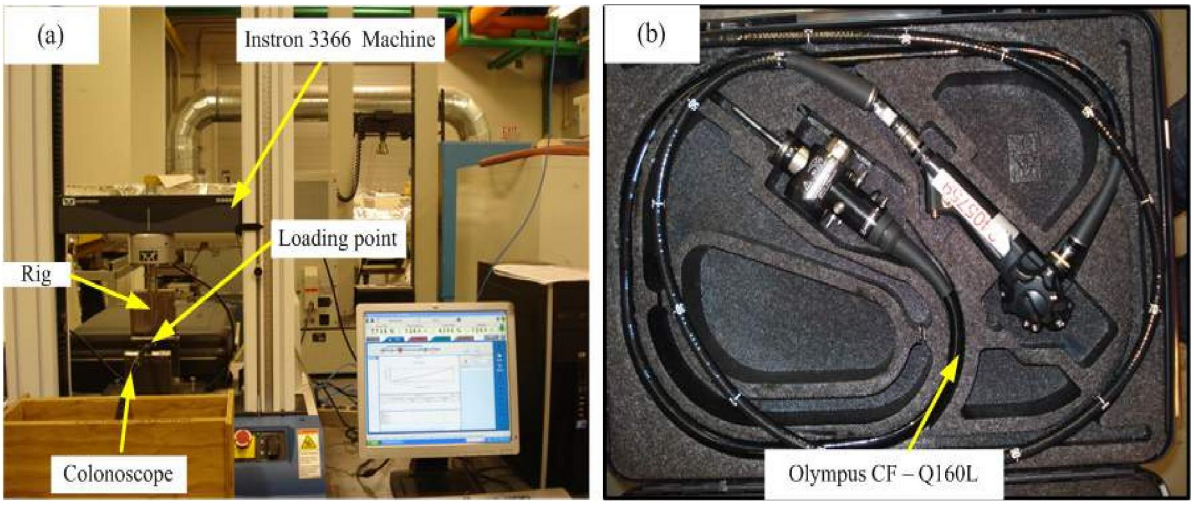

Figure 4.2 Three-point bending testing for the CF-Q160L colonoscope

4.2.2.2 Methods

Several factors should be noted with regard to the installation of the tester and colonoscope as follows:

(1) The Instron machine was horizontally laid down to ensure that the bending of the scope occurred in the horizontal plane only;

(2) The maximum displacement δ of the loading point at 12 mm (see Figure 4.3) was limited to prevent a large deflection of the scope.

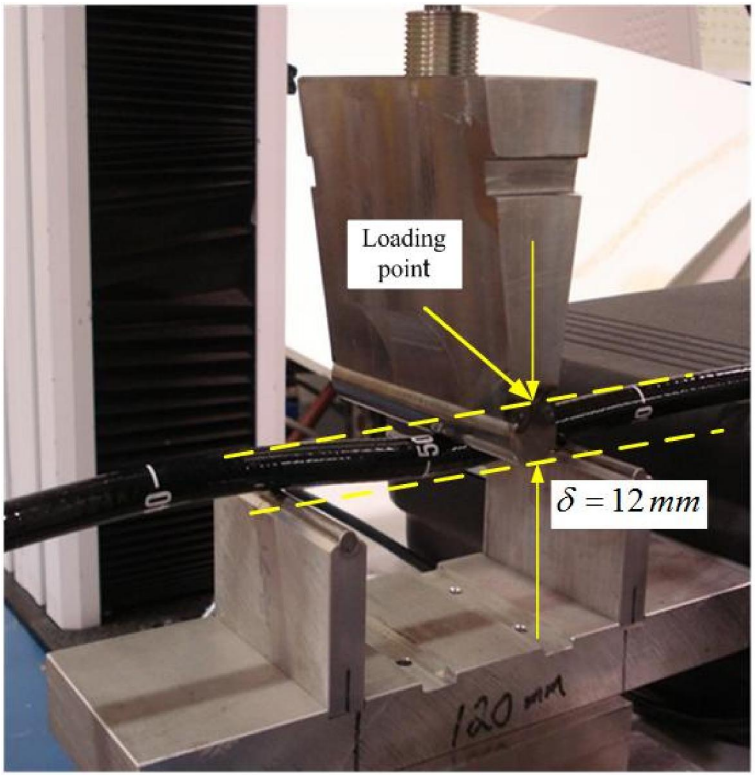

Figure 4.3 Loading point on the CF-Q160L colonoscope

In the measurement of flexural rigidity of the scope the environmental temperature was 25 ℃, and the following procedure was taken:

Step 1: The load was applied at certain positions along the insertion tube of the scope. The loading points were set along the colonoscope length beginning at the tip of the colonoscope with 21 cm, 31 cm, 41 cm, . . . 141 cm, and 151 cm (14 in total). Thus there were 14 spots where loading was imposed on the insertion tube of the scope. Note that the distal end of the scope (from 0 mm to 20 cm) was not included in the testing because it consists of more fragile components. Each test was repeated five times.

Step 2: The scope was formed into a loop (note: that the purpose of this testing was to detect if there is any significant difference of flexural rigidity of the scope when the colonoscope is in a loop) [208]. An example of the loop is shown in Figure 4.4; the loop is 50 mm in circumference.

Step 3: The effect of the tip angulation on flexural rigidity of the colonoscope was determined. This was done by placing the scope on the rig in a straight configuration and then manipulating the control unit to achieve full deflection of the tip [208].

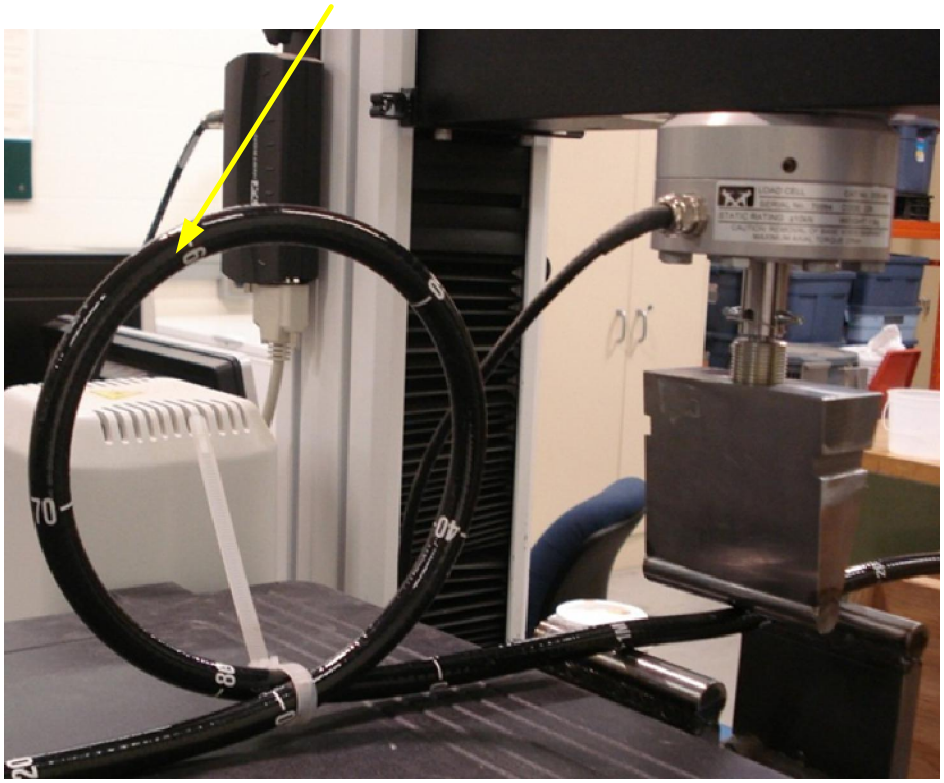

Figure 4.4 Flexural rigidity testing of colonoscope with a loop configuration

4.2.2.2 Results

Figure 4.5 shows the load-deflection relation with the loading point at 51 cm away from the tip of the scope. From this figure, a good linearity (with R^2= 99.3%) can be seen. From the information presented in Figure 4.5, flexural rigidity can be obtained. Figure 4.6 shows the measured rigidity of the scope corresponding to the loading points with a confidence level of 95%. From this figure it can be seen that the EI varies along the colonoscope length, which suggests that there is a locational effect on flexural rigidity. The distal section has a lower EI than do the proximal sections of the colonoscope. Overall, the flexural rigidity of the CF-Q160L

colonoscope is close to that of the one measured by Hellier et al. [208]. Torsional rigidity of the CF-Q160L colonoscope was not further measured and the results from Hellier et al. [208] were employed for this study.

Figure 4.7 shows a comparison of the average EI of the CF-Q160L colonoscope between the scope with a loop configuration and without a loop configuration. From this figure it can be seen that the average EI of the scope with a loop configuration is slightly higher than that of the scope without a loop. Their difference is about 10 $N \cdot cm^2$, which suggests that looping has an effect on flexural rigidity. The reason for this may be that the internal components (for instance, wires, optic fiber, and springs) of the colonoscope change to become more tense when the scope contains a loop.

Figure 4.8 shows a comparison of the average EI of the CF-Q160L colonoscope between the scope with tip deflection and one without tip deflection. From this figure, it can be seen that under tip deflection the EI at certain testing points along the colonoscope length is a little higher than that of the straightened scope (i.e., without tip deflection). The reason for this result may be that the angulation cables inside the insertion tube of the scope were tensed when the tip was deflected, while in the straightened scope the auguation wires were not under tension [208].

Overall, the flexural rigidities of the Olympus^{TM} CF-Q160L colonoscope are in the range of 260-660 $N \cdot cm^2$. The effects due to location, looping, and tip deflection of the EI of the Olympus^{TM} CF-Q160L colonoscope were found in this study.

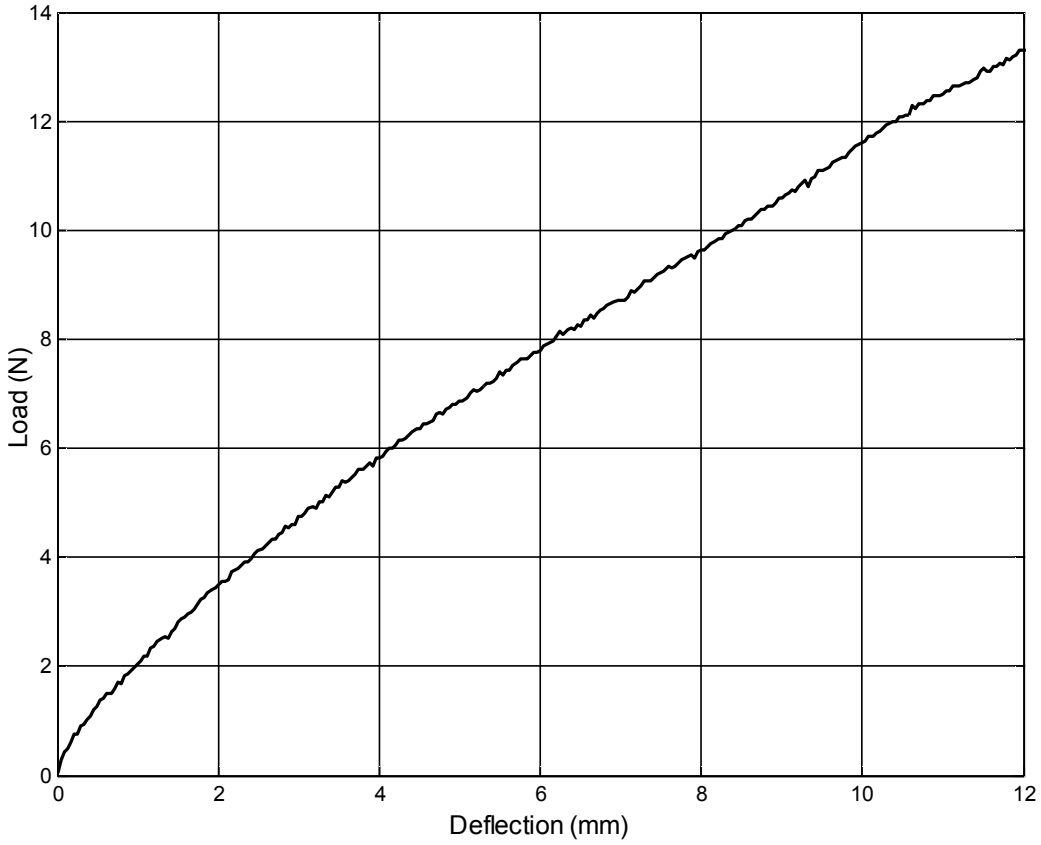

Figure 4.5 Load-deflection relation with the loading point at 51 cm away from tip of scope

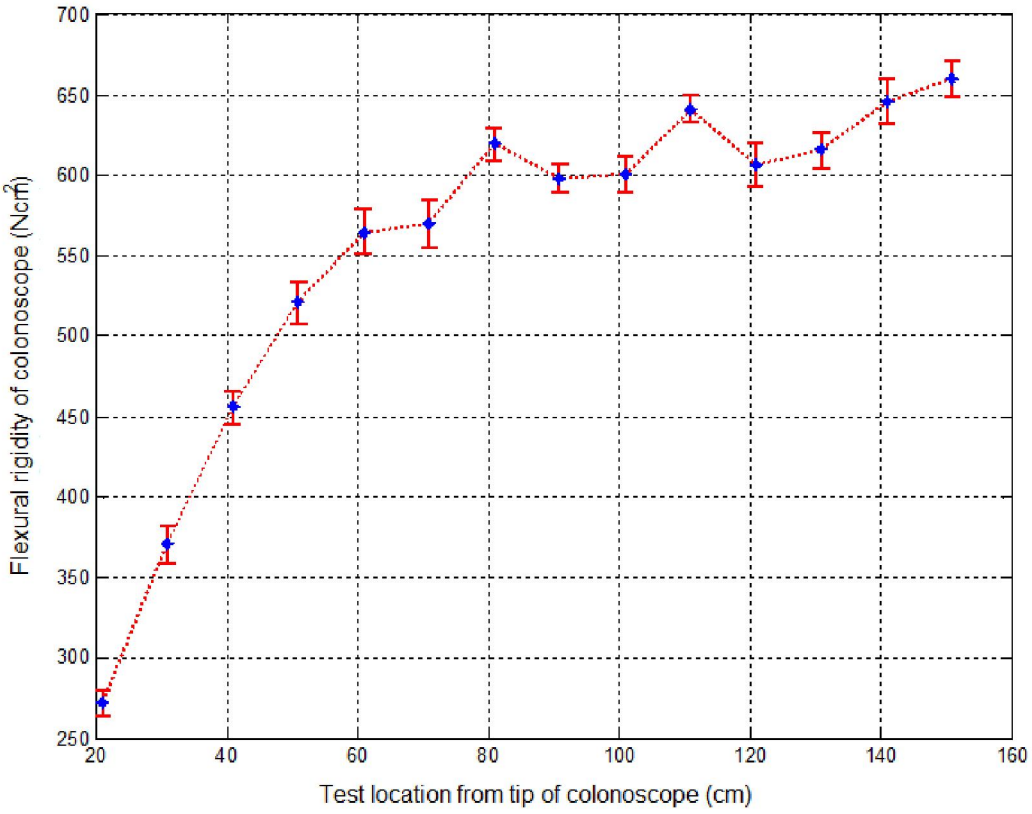

Figure 4.6 Flexural rigidities with 95% confidence interval bars of the CF-Q160L colonoscope

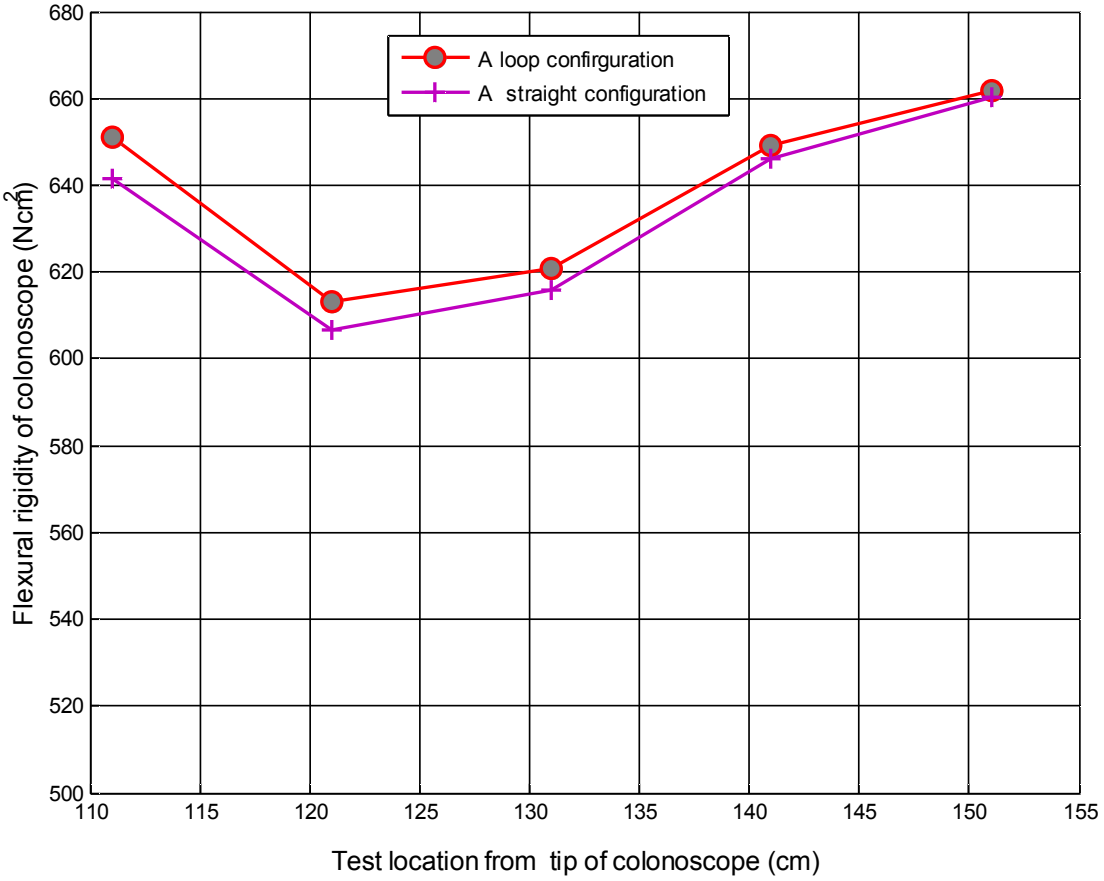

Figure 4.7 Comparison of the average EI of the CF-Q160L colonoscope between the scope with a loop configuration and without a loop configuration

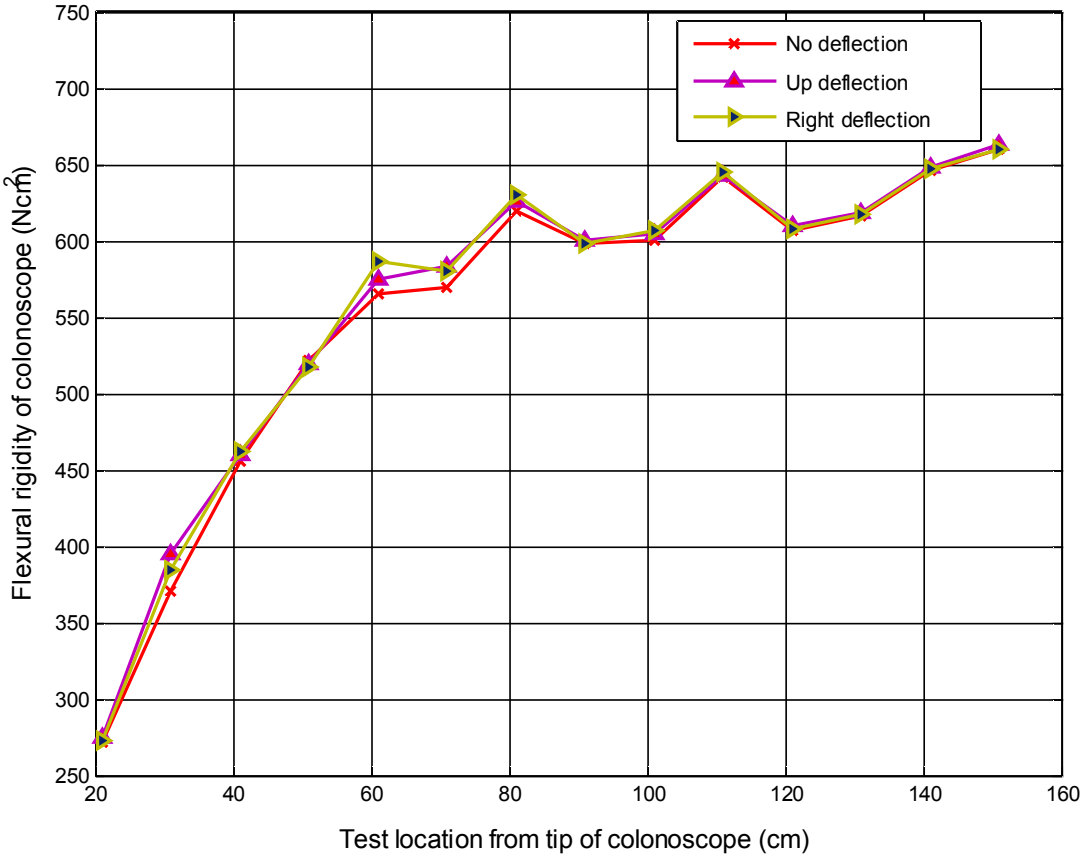

Figure 4.8 Comparison of average EI of the CF-Q160L colonoscope with tip deflection and without tip deflection

4.2.3 Experimental Determination of Damping Matrix of the Scope

Experimental determination of the damping matrix is difficult. The most common way to determine damping matrix is to view it as a linear combination of the mass and stiffness matrices as shown in Eq. (4.7). The damping model is also known as "Rayleigh damping" or "classical damping" or "proportional damping" [209]. This classical damping model is applied to all

viscous damping systems but to non-viscous damped systems; see Ref. [209] for details. In the literature, Rayleigh damping has been successfully applied to vibration analysis [210-218]. In short, it is reasonable for this study to make use of the Rayleigh damping. Eq. (4.9) denotes the relation between the Rayleigh damping coefficients and its natural frequency ω_i and damping ratio ς_i in the ith normal mode [199]:

$$2\varsigma_i\omega_i = \alpha + \beta\omega_i^2 \tag{4.9}$$

Eq. (4.9) leads to

$$\varsigma_i = \frac{\alpha}{2\omega_i} + \frac{\beta\omega_i}{2} \tag{4.10}$$

For Eq. (4.10), when ω_i is small, the first term $\frac{\alpha}{2\omega_i}$ dominates at the initial stage, then term $\frac{\beta\omega_i}{2}$ starts to dominate the equation and the value of $\frac{\alpha}{2\omega_i}$ diminishes while ω_i increases (see Figure 4.9).

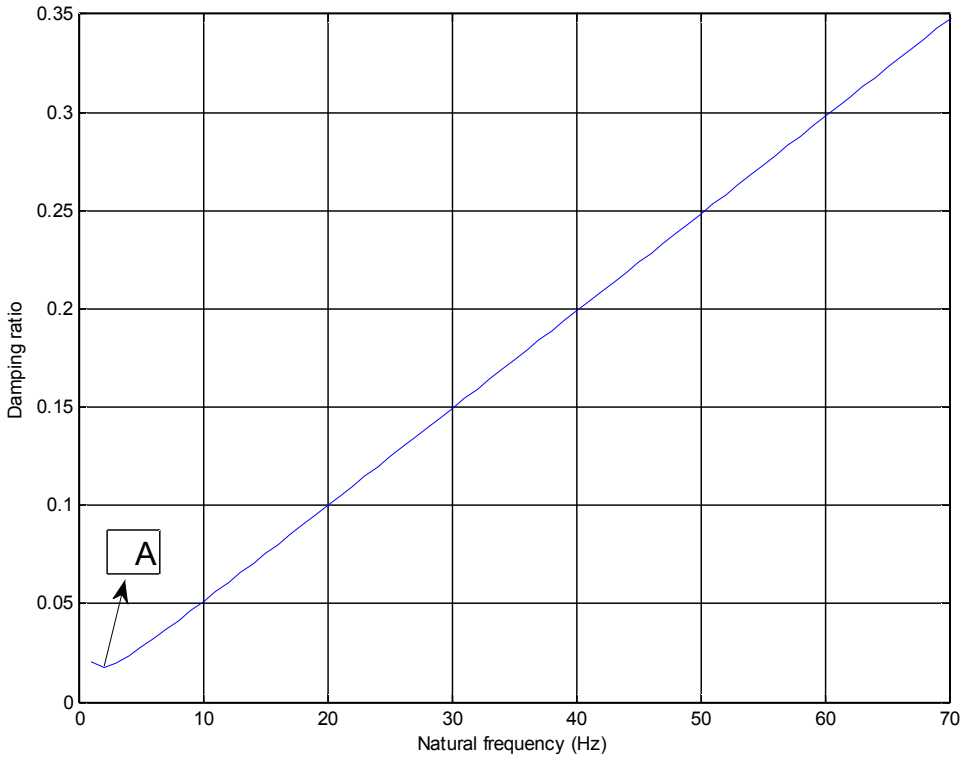

Figure 4.9 Variation of damping ratio with natural frequency of the system

Figure 4.9 shows a non-linear damping property with respect to the frequency from the beginning to point A, and the linear relationship between damping ratio and natural frequency. Furthermore, considering the fact that the non-linear range is very small, the damping ratio can be viewed as linearly proportional to the frequency of the system. Based on this analysis, only the first few modes were considered and the other modal parameters were proportional to the ones in the low modes. Thus, there was no need to measure ς_n (when the system is in high modes). In fact, modal parameter ς_n in high modes cannot be measured accurately by experiment [210]. In most cases, the first three modal parameters can be found by vibration experiments. Chowdhury et al. [210] presented a method for computation of the Rayleigh

damping coefficients. This method ensures a rational estimate of the Rayleigh damping coefficients α and β.

Thus, given a set of values $\omega_1, \omega_2, \ldots \omega_n$ and their corresponding $\zeta_1, \zeta_2, \ldots \zeta_n$ for a system, for the ith mode of the system (1<i<n), the damping ratio ς_i can be obtained by a linear extrapolation [210]:

$$\varsigma_i = \frac{\varsigma_m - \varsigma_1}{\omega_m - \omega_1}(\omega_i - \omega_m) + \varsigma_m \ (m < i < 2.5m) \tag{4.11}$$

where

ς_1 : damping ratio for the first mode;

ω_1 : natural frequency for the first mode;

ς_m : damping ratio for the mth mode;

ω_m : natural frequency for the mth mode;

ς_i : damping ratio for the ith mode; and

ω_i : natural frequency for the ith mode.

From Eq. (4.11), $\varsigma_m, \varsigma_{2.5m}, \omega_m, \omega_{2.5m}$ are obtained and the Rayleigh damping coefficients α and β can then be found by

$$\begin{cases} \beta = \dfrac{2\varsigma_m\omega_m - 2\varsigma_{2.5m}\omega_{2.5m}}{\omega_m^2 - \omega_{2.5m}^2} \\ \alpha = 2\varsigma_m\omega_m - \beta\omega_m^2 \end{cases} \tag{4.12}$$

Chowdhury's method was widely used in the literature for [211-218]. In practice, the first three mode parameters of Chowdhury's method were used to estimate the Raleigh damping coefficients.

In this research, Chowdhury's method was used to find the damping matrix for the scope. With regard to the scope, a few natural frequencies in high modes can be found using the FE model of the scope. MATLAB codes for this can be found in Appendix I. The results for the first ten natural frequencies of the scope are shown in Figure 4.10.

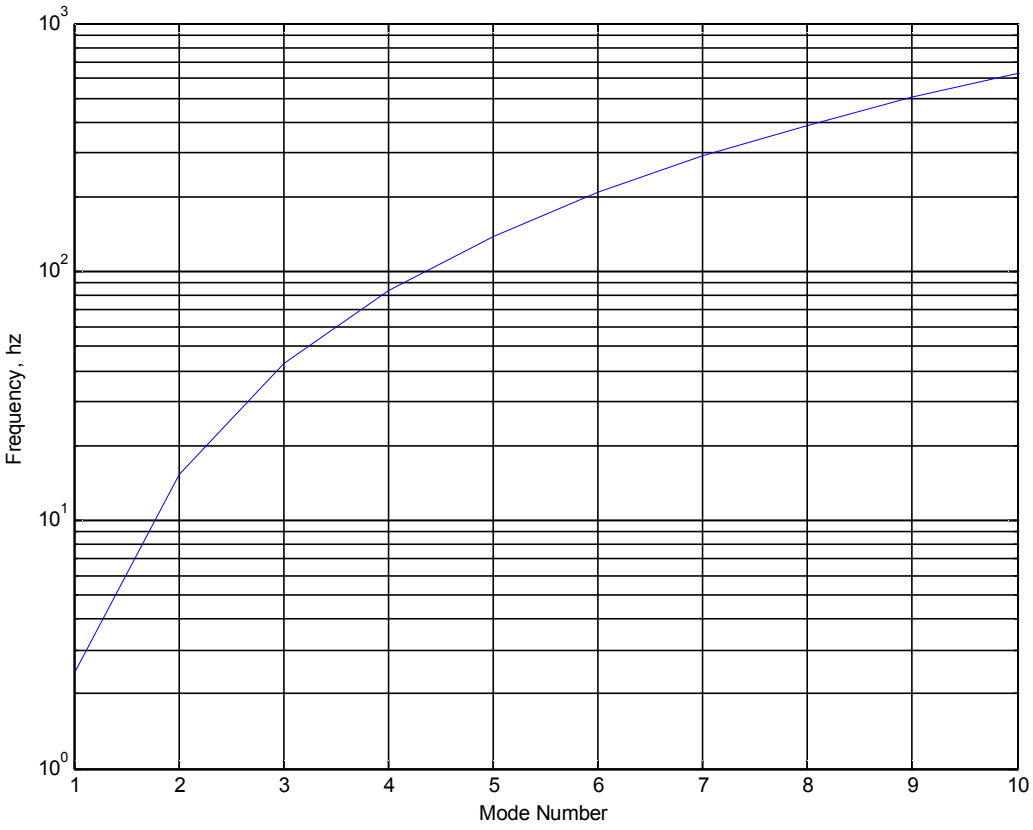

Figure 4.10 First several natural frequencies of the FBED of the scope

In the following section, the forced vibration experiment to determine the first few damping ratios is described.

4.2.3.1 Forced Vibration Experiment

In the testing, there were two assumptions for the modal parameters of the scope. (1) Each segment along the length of the scope had the same damping property. The reason for this assumption is that the distal end of the scope has inside components from those in other segments of the insertion tube of the scope; and (2) External forces, such as pushing force by the physician, and contact force with the colon, had no effect on the modal parameters of the scope.

4.2.3.1.1 Equipment and Method

There were three main components to the vibration experiment: excitation of the structure, sensing of the response, and data acquisition. These are explained below.

The colonoscope can be excited in two main ways: (a) using an exciter or shaker, and (b) using an impulse hammer. The advantage of (a) is the provision of a waveform as the driving signal given to a structure. This enables prescribing of a particular frequency-band. In addition, the steady-state sinusoidal driving is suitable for measurement of the frequency response at different frequencies directly. In this experiment, an exciter was chosen.

The response sensor in this case is an accelerometer. In this experiment, Brüel & Kjær^{TM} 4371 was used. Signals from the shaker and from the accelerometers were amplified using a charge

amplifier, namely the Amplidfer Brüel & Kjær™ 2635. The Brüel & Kjær™ dynamic signal analyzer PHOTON+ was used for data processing.

The colonoscope was clamped at 20 cm away from the distal end during the forced vibration testing. The experiment setup of the colonoscope's vibration testing is shown in Figure 4.11.

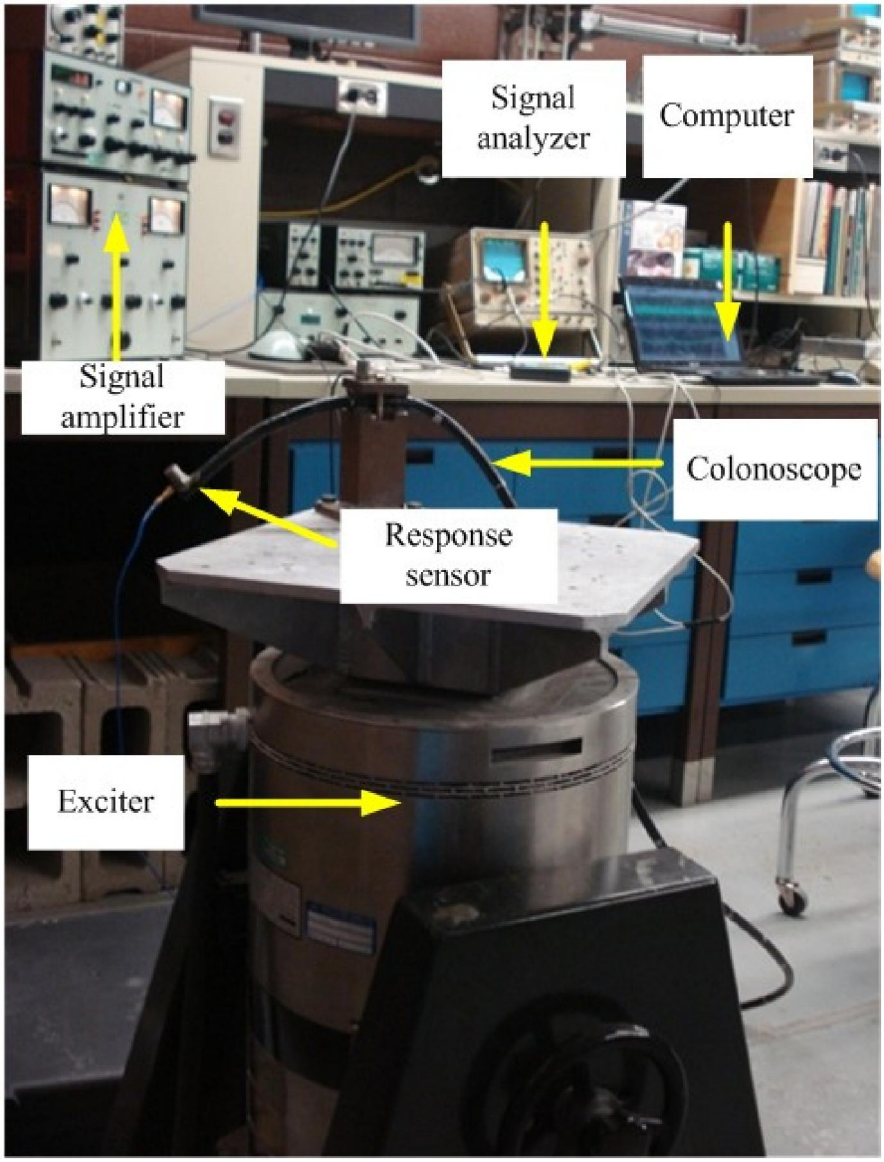

Figure 4.11 Forced vibration experiment of the CF-Q160L colonoscope

4.2.3.1.2 Results

In this section, the results obtained from the forced vibration testing of the colonoscope are described. Figure 4.12 shows the results of frequency versus vibration transmissibility of the CF-Q160L colonoscope obtained from the forced vibration testing. The vibration transmissibility is a non-dimension ratio of the response acceleration amplitude of scope in steady-state forced vibration to excitation acceleration amplitude. The vibration transmissibility T_r of a system can be described by [217]

$$T_r = \sqrt{\frac{1+(2\varsigma\lambda)^2}{(1-\lambda^2)^2+(2\varsigma\lambda)^2}} \tag{4.13}$$

where

λ : frequency ratio;

T_r : vibration transmissibility; and

ς : damping ratio.

When $\lambda = 1$ (i.e., the system is in a resonance state), the damping ratio ς can be found by

$$\varsigma = \frac{1}{2}\sqrt{\frac{1}{T_r^2-1}} \tag{4.14}$$

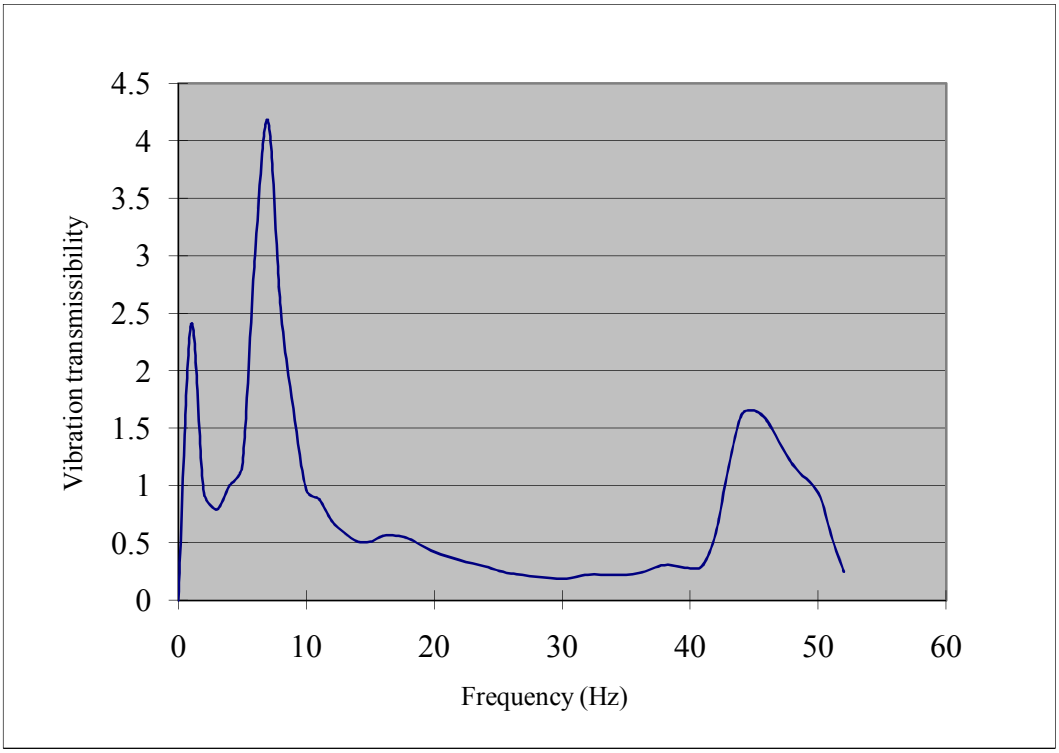

Figure 4.12 Relation between amplitude ratio and frequency for the CF-Q160L colonoscope

Table 4.1 Relation between natural frequency and damping ratio for the first few modes of the CF-Q160L colonoscope

Resonance frequency (Hz)	Damping ratio
1 (0.1*)	0.209 (0.019)
7 (1.8)	0.085 (0.040)
44 (2.6)	0.384 (0.048)

* The number in parenthesis indicates the standard deviations

4.2.3.2 Damping Matrix of the Scope

The damping ratios obtained from the above experiment were used to determine the Rayleigh damping ratios in the damping matrix that is decribed in the following.

Selecting $\varsigma_2 = 0.085$ and $\varsigma_3 = 0.364$ to extrapolate damping ratios for the high modes of 4, 5, 6 and 7 using Eq. (4.11) leads to

$$\begin{cases} \varsigma_4 = \dfrac{\varsigma_3 - \varsigma_2}{\omega_3 - \omega_2}(\omega_4 - \omega_3) + \varsigma_3 = 0.7072 \\ \varsigma_5 = \dfrac{\varsigma_3 - \varsigma_2}{\omega_3 - \omega_2}(\omega_5 - \omega_3) + \varsigma_3 = 1.1436 \\ \varsigma_6 = \dfrac{\varsigma_3 - \varsigma_2}{\omega_3 - \omega_2}(\omega_6 - \omega_3) + \varsigma_3 = 1.6931 \\ \varsigma_7 = \dfrac{\varsigma_3 - \varsigma_2}{\omega_3 - \omega_2}(\omega_7 - \omega_3) + \varsigma_3 = 2.3558 \end{cases}$$

Eq. (4.12) estimates for the Raleigh damping coefficients as:

$$\begin{cases} \beta = \dfrac{2\varsigma_2\omega_2 - 2\varsigma_7\omega_7}{\omega_2^2 - \omega_7^2} = 0.0164 \\ \alpha = 2\varsigma_2\omega_2 - \beta\omega_2^2 = 0.3864 \end{cases}$$

Now, the damping matrice $[C]$ of the scope is expressed by

$$[C] = 0.3864 \cdot [M] + 0.0164 \cdot [K] \tag{4.15}$$

where $[M]$ = the mass matrix of the colonoscope; $[K]$ = the stiffness matrix of the colonoscope.

4.2.4 Colonoscope Cantilever Experiment

The CF-Q160L colonoscope was clamped at 80 cm from the distal end to deform under its self-weight as shown in Figure 4.13 [162]. The points on the scope were measured by graph paper (see on Figure 4.13, the interval between two neighbouring points is 50 mm along the scope). The results for displacement of these points on the scope due to self-weight are shown in Table 4.2.

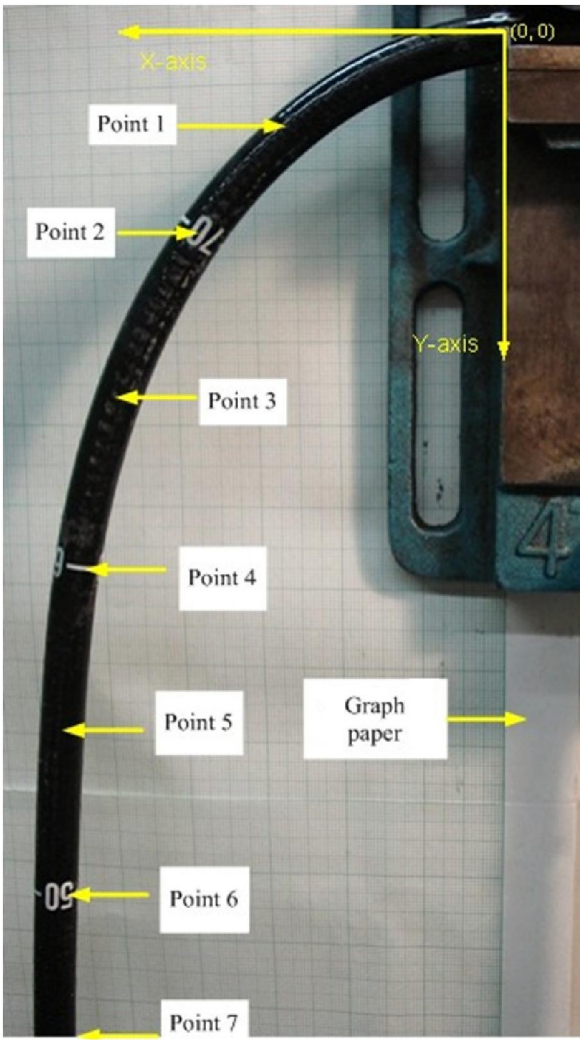

Figure 4.13 CF-Q160L colonoscope cantilever experiment

Table 4.2 Results for displacement of points on the scope under its self-weight

Point (i)	Displacement along X-axis (mm)	Displacement along Y-axis (mm)
1	0	0
2	-3	-26
3	-29	-62
4	-60	-113
5	-100	-163
6	-146	-219
7	-196	-265
8	-247	-310
9	-300	-362
10	-352	-414

The FBEM of the scope had 16 elements with each being 50 mm length and having the EI value of 350 $N \cdot cm^2$. The deformed colonoscope under its self-weight is shown in Figure 4.14. The results for nodal displacement of the simulated cantilever colonoscope are shown in Table 4.3.

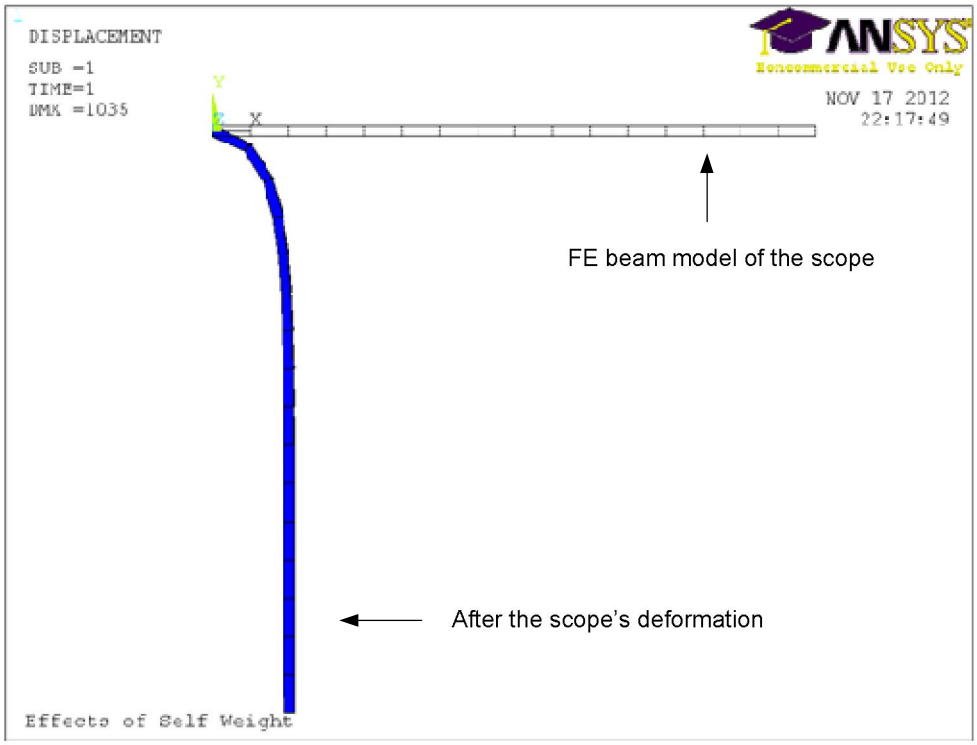

Figure 4.14 Deformed configuration of FE beam model of colonoscope

Table 4.3 Nodal displacement for simulated cantilever scope using EI of 350 N·cm^2

Node (i)	Displacement along X-axis (mm)	Displacement along Y-axis (mm)
1	0	0
2	-4.6247	-21.256
3	-28.144	-63.833
4	-64.581	-112.1
5	-107.68	-161.76
6	-154.08	-211.75
7	-202.14	-261.82
8	-251.07	-311.91
9	-300.44	-361.99
10	-350.07	-412.07

In Section 4.2.2, it was shown that the range of flexural rigidities of the scope was between 250 $N \cdot cm^2$ and 680 $N \cdot cm^2$ due to the locational effect, looping effect, and effect of tip deflection on the EI of the scope. Thus, the FE model of the scope needs to be tested using different EIs.

Table 4.4 and Table 4.5 show nodal displacement for the simulated cantilever scope using EIs of 480 $N \cdot cm^2$ and 600 $N \cdot cm^2$, respectively. A comparison between the measured deflection and simulated deflection of the colonoscope using these EIs is shown in Figure 4.15. Figure 4.15 shows no significant difference between experimental and simulation results. Thus, the FE model of the scope is reliable in terms of accuracy.

Table 4.4 Nodal displacement for simulated cantilever scope using EI of 480 $N \cdot cm^2$

Node (i)	Displacements along X-axis (mm)	Displacements along Y-axis (mm)
1	0	0
2	-4.517	-21.014
3	-27.665	-63.353
4	-63.746	-111.52
5	-106.58	-161.13
6	-152.81	-211.1
7	-200.76	-261.17
8	-249.61	-311.25
9	-298.94	-361.33
10	-348.53	-411.41

Table 4.5 Nodal displacement for simulated cantilever scope using EI of 600 N·cm^2

Node (i)	Displacement along X-axis (mm)	Displacement along Y-axis (mm)
1	0	0
2	-4.237	-20.369
3	-26.394	-62.049
4	-61.497	-109.91
5	-103.6	-159.4
6	-149.34	-209.33
7	-196.96	-259.37
8	-245.59	-309.44
9	-294.78	-359.51
10	-344.27	-409.58

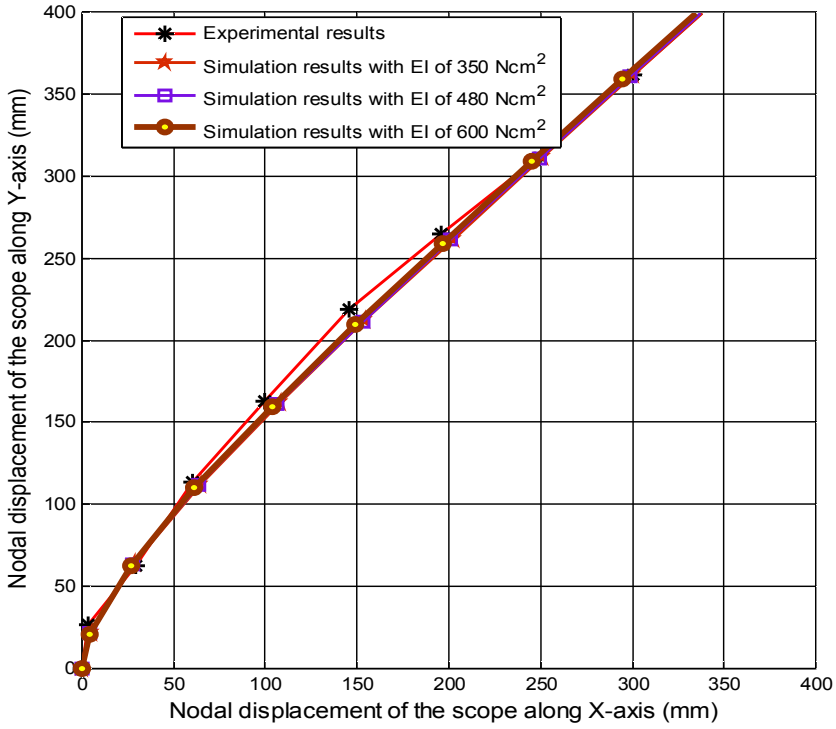

Figure 4.15 Comparison of measured and simulated deflections of the colonoscope using the different EIs

4.3 The Model for the Colon

4.3.1 Equilibrium Equation for the Colon

For the colon, the following assumptions were made:

(1) The colon tube consists of a number of hollow-cylinder Timoshenko beam elements;

(2) The colon has a constant inner diameter and wall thickness along its length;

(3) The colon folds are disregarded;

(4) The mass or inertia and damping of the colon can be neglected due to their insignificant dynamic behaviours in colonoscopy.

Based on these assumptions, the colon was modeled as a set of hollow cylinder Timoshenko beam elements. Each element had 6 DOFs in translation and 6 DOFs in rotation. The force-motion of the colon was represented by a static equilibrium equation, which is expressed by

$$[K_c]\{U_c\} = \{F_c\} \tag{4.16}$$

where

$[K_c]$: stiffness matrix of the colon;

$[U_c]$: column matrix of displacement corresponding to contact force vector $\{F_c\}$; and

$\{F_c\}$: contact force between scope and colon, applied at nodal ends of each beam element.

The stiffness matrix of the colon $[K_c]$ is a form of band matrix due to the serial beam element of the colon. The stiffness matrix $[K_e]$ of the hollow cylinder beam element is on the order of 12×12, expressed by Eq. (4.2). The global stiffness matrix $[K_c]$ was computed by

$$[K_c] = [\Lambda]^T [K_e][\Lambda] \tag{4.17}$$

where $[\Lambda]$ was found with Eq. (4.3).

In order to determine the stiffness matrix $[K_c]$ for the colon in Eq. (4.17), the geometrical model and mechanical model of the colon must be known in advance. In the following sections, the geometrical model and mechanical model of the colon will be discussed.

4.3.2 Geometrical Model of the Colon

The deformation of the colon is divided into two directions: radial direction (transverse direction) and longitudinal direction (centerline along the colon tube). The deformation along the radial direction is negligible. Therefore, only the deformation along the longitudinal direction was considered. The centerline of the entire colon was represented by $r_i = [x_i, y_i, z_i]^T$, which indicates the coordinates of points on the centerlines in the global system (see Figure 4.16). During the colonoscopy procedure, the colon attempts to adapt to the scope. Therefore, the geometrical model of the colon also was determined by the scope's shape.

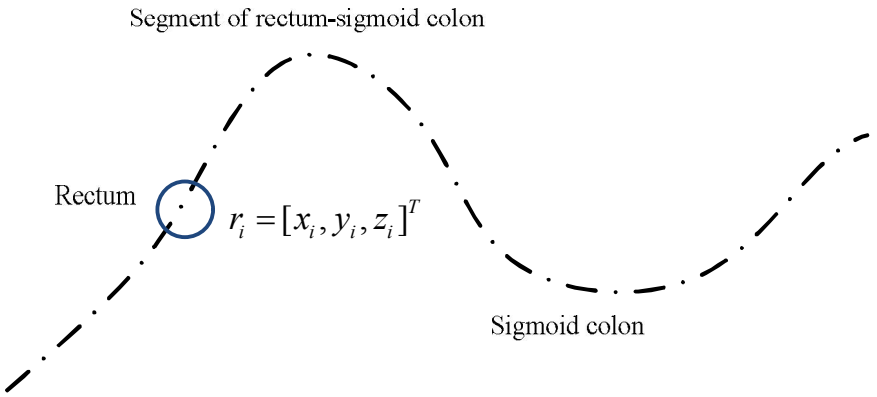

Figure 4.16 Centerline model of the colon

4.3.3 Mechanical Model of the Colon

Yamada performed a variety of experiments to find out the mechanical properties and characteristics of the human colon [219]. He found that the stress-strain relation for colon tissue was non-linear and mechanical properties were similar to those of porcine colon, which were studied in Refs. [220, 221]. The pig is a superior experimental animal model because of its comparatively close resemblance to the human in terms of internal anatomy and physiology [222-224]. The porcine colon was used in this study.

4.3.3.1 Tensile Experiment of the Colon

The Instron-3366 single column testing machine was used for the tensile experiment. Specimens from different parts of the porcine colon tissue were prepared and tested including rectum, sigmoid colon, descending colon, transverse colon, and descending colon. The dimensions of

each sample were approximately 10 cm in length and 2 to 3 cm in width. Tensile testing was performed on each sample (see Figure 4.17).

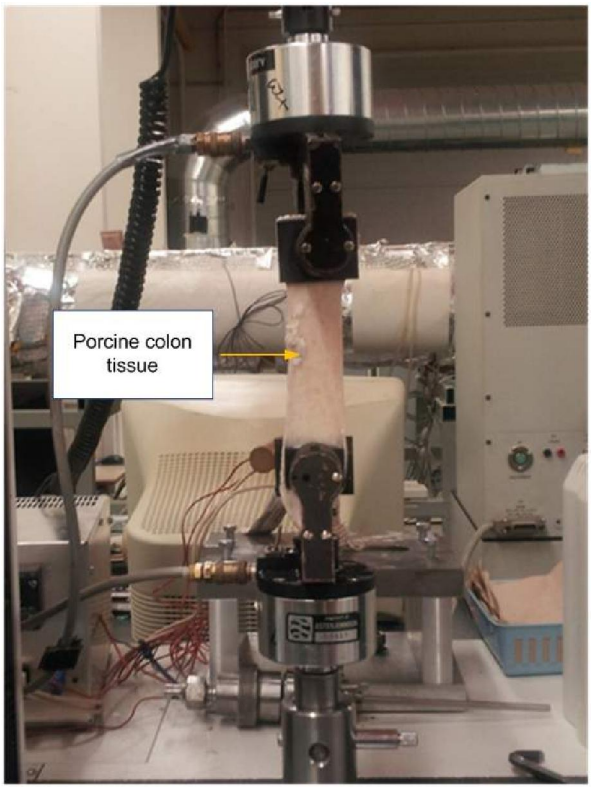

Figure 4.17 Tension testing for porcine colon tissue

4.3.3.2 Results

(1) Figure 4.18 shows the relation between loading and extension of the rectum along the longitudinal direction. The relation between loading and extension of the transverse colon along the transversal direction is shown in Figure 4.19.

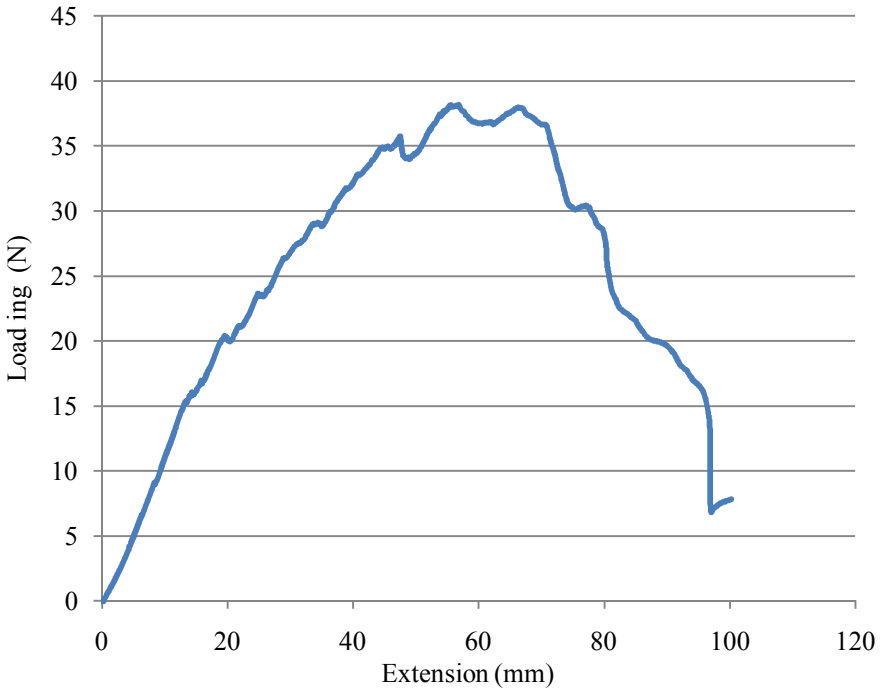

Figure 4.18 Relation between loading and extension of the rectum along the longitudinal direction

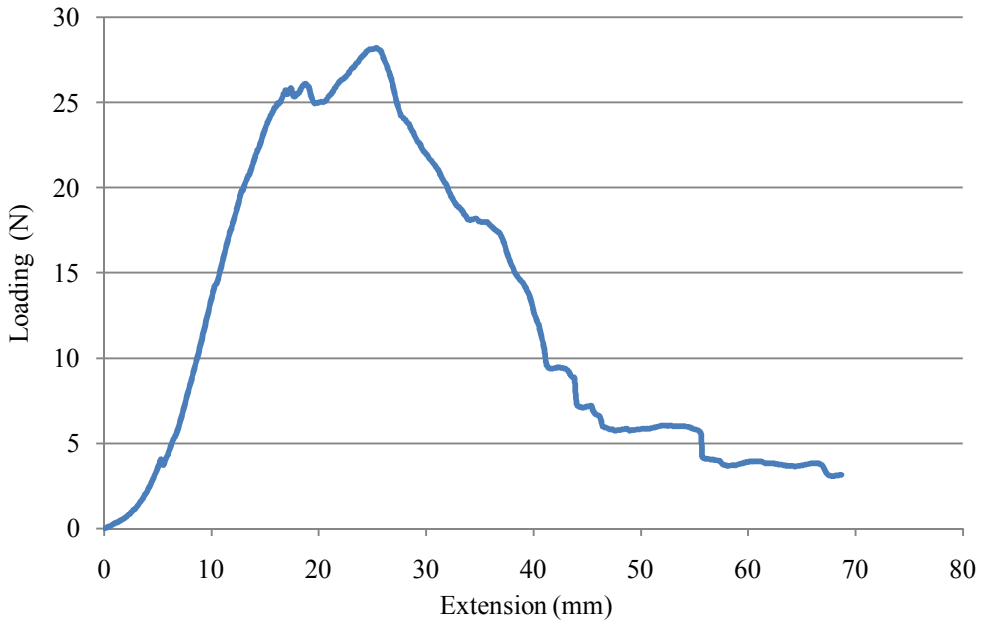

Figure 4.19 Relation between loading and extension of the transverse colon along the transversal direction

(2) According to the corresponding length, width, and thickness of each specimen, the relation between the stress and strain for different parts of the porcine colon are shown in Figure 4.20.

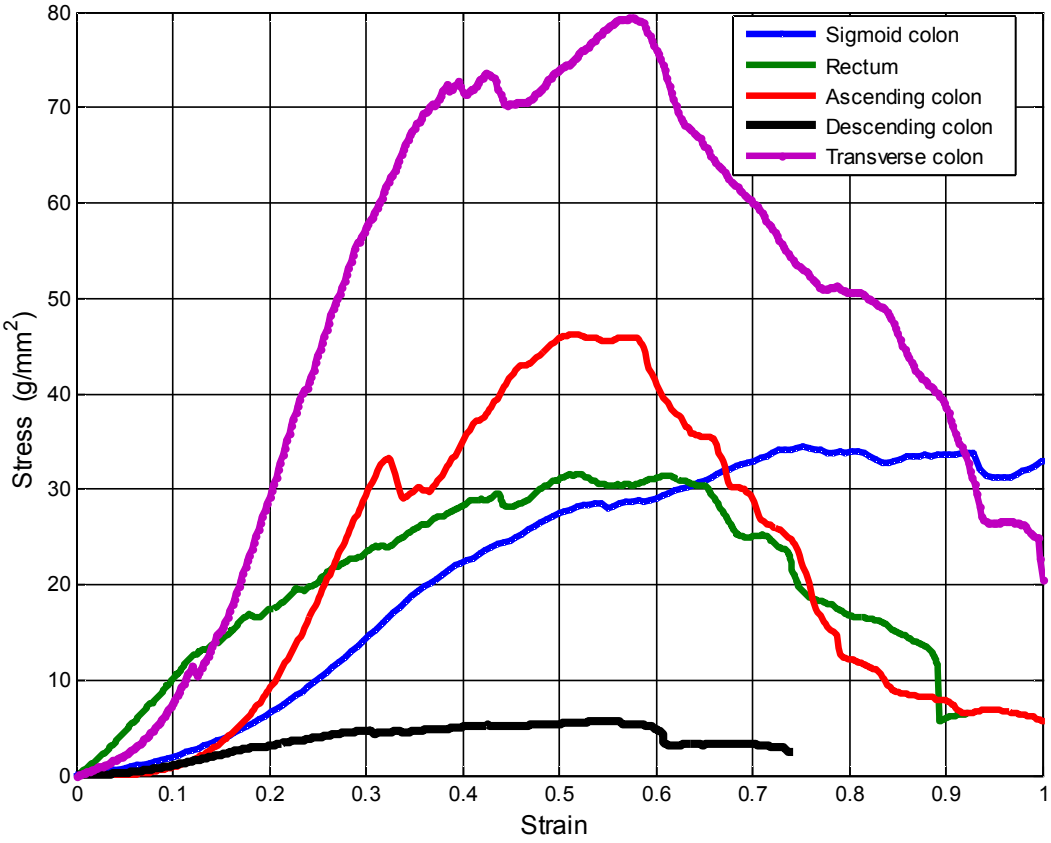

Figure 4.20 Relation between stress and strain for different parts of porcine colon

(3) Figure 4.20 shows the relation between the engineering stress and strain for the porcine colon. However, if the elongation of the colon is up to 120% of the original length, the reduced cross-section areas of the colon tissue should be considered. Therefore, the engineering stress-strain curve was transformed to the true stress-strain curve in this case. The true stress and strain were computed using Eq. (4.18). The true stress-strain curves of porcine colon tissue are shown in Figure 4.21. From Figure 4.21, for small strains, engineering and true stress-strain curves almost overlapped but there were significant differences for the stress when the strain became large due to a reduction of cross-section areas of colon tissue.

$$\begin{cases} \sigma_t = \sigma_e(1+\varepsilon_e) \\ \varepsilon_t = In(1+\varepsilon_e) \end{cases} \tag{4.18}$$

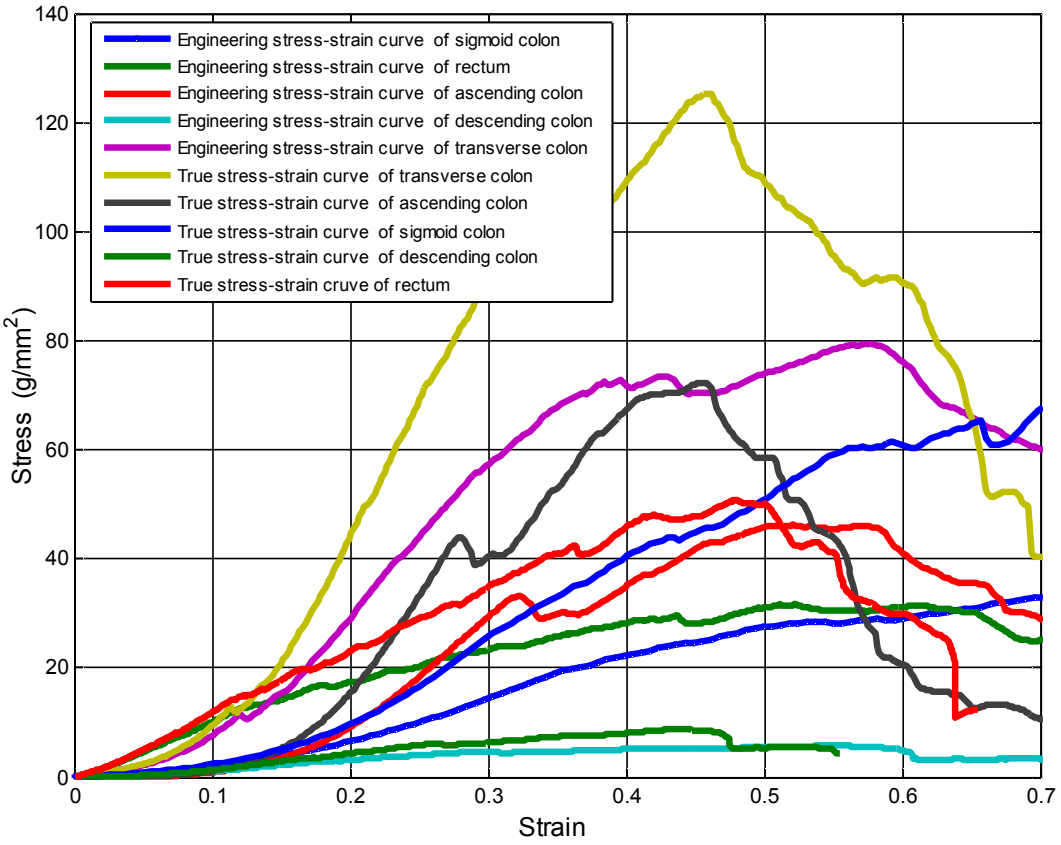

Figure 4.21 True stress-strain curves for each part of porcine colon tissue

(4) The sigmoid colon tissue can be considered as a linear elastic relationship between the stress and the strain (with $R^2 = 0.970$) when their strain is approximately between 0 and 0.20. Table 4.6 gives the mean value of Young's modulus for each part of the porcine colon tissue based on the aforementioned strain.

Table 4.6 Mean value of Young's modulus for each part of porcine colon tissue

	Mean value of Young's modulus (KPa)				
	Rectum	Sigmoid colon	Descending colon	Transverse colon	Ascending colon
Longitudinal direction	398	360	318	892	781
Transverse direction	375	320	296	810	753

4.4 Contact Model

In this section, the contact model between the colonoscope and the colon is illustrated. Contact forces computed from the contact model will be applied to the kinetics model of the colonoscope in order to solve the force-motion equation of the scope as shown in Eq. (4.1).

The contact model is an important aspect in the area of simulation for medical devices; thus a large number of contact models have been developed in the literature. Comprehensive literature reviews on this subject can be found in Refs. [225, 226]. In general, three categories of contact models are available: (1) classical rigid body contact formulation, (2) complementarity formulation, and (3) compliant contact formulation. There are two types of contact constraints: (a) interpenetration contact such as surgical needle, surgical suture, and so on, and (b) non-interpenetration contact such as the catheter, laparoscopic devices for surgery, and so on. The

contact system of the scope-colon can be categorized as a kind of non-interpenetration contact. For this case, the complementarity formulation is typically used, i.e., contact force computation is formulated into a Linear Complementarity Problem (LCP) by linearizing the Signorini's problem, details of which can be found in Refs. [227-240]. For the LCP, the contact force is computed by the mechanical compliance from the finite element models of two deformable objects and the contact space. The contact force f_n is computed with Eq. (4.19) [227].

$$\begin{cases} f_n \geq 0 \\ \delta_n = [W] f_n + \delta_n^f \geq 0 \\ f_n \perp \delta_n \end{cases} \tag{4.19}$$

where

δ_n : contact space;

f_n : contact force; and

$[W]$: mechanical compliance (also called Delassus operator), which is found by [227].

$$[W] = \left(\frac{[M_1]}{h^2} + \frac{[C_1]}{h} + [K_1] + \frac{[M_2]}{h^2} + \frac{[C_2]}{h} + [K_2] \right)^{-1} \tag{4.20}$$

where

$[M_1]$ and $[M_2]$: mass matrix of FE model for two contact bodies;

$[C_1]$ and $[C_2]$: damping matrix of FE model for two contact bodies;

$[K_1]$ and $[K_2]$: stiffness matrix of FE model for two contact bodies;

h : time step; and

δ_n^f : free motion in contact space.

When the scope and colon come into contact, each contact point of the scope with the colon has a friction state, either stick (static friction state) or slip (dynamic friction state). The relative motion of the contact point between the scope and the colon is equal to zero in the case of the stick state. During the slip state, relative motion between the scope and the colon along the tangential direction occurs (non-interpenetration contact), so the friction force for the contact point is determined by the multiplication of the frictional coefficient by the normal contact force. However, Signorini's law does not consider the frictional force in the contact space. In the case of the contact model with consideration of the frictional force, Coulomb's law should be added into the LCP (so-called LCP with friction), which leads to the two equations below [227]:

$$f_{\vec{T}} = -\mu \left\| f_{\vec{n}} \right\| \frac{\delta_{\vec{T}}}{\left\| \delta_{\vec{T}} \right\|} \tag{4.21}$$

$$\begin{bmatrix} \delta_{\vec{n}} \\ \delta_{\vec{t}} \\ \delta_{\vec{s}} \end{bmatrix} = [W] \begin{bmatrix} f_{\vec{n}} \\ f_{\vec{t}} \\ f_{\vec{s}} \end{bmatrix} + \begin{bmatrix} \delta_{\vec{n}}^{f} \\ \delta_{\vec{t}}^{f} \\ \delta_{\vec{s}}^{f} \end{bmatrix} \tag{4.22}$$

where

$\vec{T}$: vector in the plane ($\vec{t}$, $\vec{s}$) of contact space, $\vec{n}$ is in normal direction in contact space and is perpendicular to $\vec{T}$;

$f_{\vec{T}}$: contact force in the plane ($\vec{t}$, $\vec{s}$) of contact space, which is resultant force of $f_{\vec{s}}$ and $f_{\vec{t}}$;

$f_{\vec{n}}$: contact force along normal direction of contact space;

μ : friction coefficient; and

$\delta_{\vec{n}}^{f}$, $\delta_{\vec{t}}^{f}$, $\delta_{\vec{s}}^{f}$: free motion in contact space.

For an LCP with friction, single nodal contact can be simply solved by the Newton-Raphson method [240]. However, for the contact system of the scope-colon there are multiple-node contacts with the frictional force at the same time. For the multiple-node contact problem, considering a contact point α among m instantaneous contact points, the contact force for contact point α can be computed by Eq. (4.23) [235].

$$\delta_\alpha - [W_{aa}] f_\alpha = \sum_{\beta}^{\alpha-1} [W_{\alpha\beta}] f_\beta + \sum_{\beta=\alpha+1}^{m} [W_{\alpha\beta}] f_\beta + \delta_\alpha^f \tag{4.23}$$

where $[W_{\alpha\beta}]$ is defined as the mechanical coupling between contact points α and β ($\beta = 1 \ldots a-1, a+1, \ldots m$).

Therefore, for the contact system of the scope-colon, considering a contact α on the node i of the scope, there are three vectors in the contact space for this node: one along the contact normal direction (denoted by n) and two along the tangential direction (denoted by t and s). The mechanical coupling of contact point α is contact point β. Eq. (4.20) and Eq. (4.23) lead to the contact model below:

$$\begin{cases} \delta_\alpha - [W_{aa}] f_\alpha = \sum_{\beta}^{\alpha-1} [W_{\alpha\beta}] f_\beta + \sum_{\beta=\alpha+1}^{m} [W_{\alpha\beta}] f_\beta + \delta_\alpha^f \\ [W_{a\beta}] = \left(\dfrac{[M]}{h^2} + \dfrac{[C]}{h} + [K_s] + [K_c] \right)^{-1} \end{cases} \tag{4.24}$$

where

$[M]$: mass matrix for FE model of the scope;

$[C]$: damping matrix for FE model of the scope;

$[K_s]$: stiffness matrix for FE model of the scope;

$[K_c]$: stiffness matrix for FE model of the colon;

δ_α^f : free motion of the scope;

h : time step; and

f_α : contact force for contact point α of the scope.

Free motion of the scope means the deformation of the beam elements under its self-weight and external manipulation (the physician's external operation), and it can be solved with Eq. (4.1) (see Section 4.2.1).

Eq. (4.24) can be solved by a Gauss-Seidel (GS)-like algorithm. Duriez [232] proposed a GS-like algorithm to solve the LCP with friction for a guaranteed coverage. Details of a GS-like algorithm can be found in Ref. [235] (Chapter 20, Section 20.5.3). SOFA (simulation open-framework architecture) is open-source research-based software compiled in a Visual C++ environment, and it provides an efficient solver using a GS-like algorithm to solve the LCP with friction. It is available in SOFA (see LCPCalc.h and LCPCalc.cpp).

4.5 Conclusions

In this chapter, the model of the scope and the model of the colon were presented. For the colonoscope model, the Timoshenko beam finite element method was employed, which was able to account for the cross-sectional area, cross-section moment of inertia, and polar moment of inertia of the structure of the colonoscope. Each beam element had 6 DOFs in translation and 6 DOFs in rotation in space. Each beam element was connected to a neighbouring element to

represent the assembled colonoscope. The element had not only deformation but also motion, and its position was updated. In order to model the colon, the colon was defined as a set of hollow cylinder Timoshenko beam elements. The force-motion of the colon was represented by a static equilibrium equation, in which the stiffness matrix $[K_c]$ of the colon model was computed in terms of a number of hollow cylinder beams. The parameters in the model of the colonoscope as well as the model of the colon were determined by the experiments. Finally, the model of the scope-colon system which describes their interaction was presented.

CHAPTER 5

MODEL VALIDATION ON AN *EX-VIVO* COLONOSCOPY TEST-BED

5.1 Introduction

This chapter provides a description of the validation of the mathematical model described in Chapter 4. The validation was performed on a built colonoscopy test-bed. The pig model was used owing to its close resemblance to the human in terms of internal anatomy and physiology. The test-bed consisted of mainly a human-based colon tray and porcine colon tissue. Various position sensors and force sensors were put in place to measure the movement behaviour of the scope (in the colon) as controlled by the physician, including both position and force of the scope.

In this study, an *ex-vivo* colonoscopy test-bed using porcine colon tissue and a human-based "colon tray" was built. Input of the mathematical model is external force and torque applied by the physician; output of the mathematical model is motion of the colonoscope. The test-bed had the ability to capture precise colonoscope movement as it moved into the colon, i.e., for collection of kinematic and kinetic data in colonoscopy.

This chapter is organized as follows. Section 5.2 presents the built *ex-vivo* colonoscopy test-bed including sensors, instruments, and data collection. In Section 5.3, the comparison of the model predicted or simulation results and experimental results is described. Section 5.4 discusses sources of errors between the experimental and simulation results, which gives a basis for further improvement of the model as well as of the test-bed. Section 5.5 presents the conclusions.

5.2 Experiments

5.2.1 Experimental Setup

Ascension Trakstar-2 System (Ascension Technologies Corp., Burlington, VT), which typically is used in medicine for guiding small biopsy needles to lesions and guide-wires within the patient's body, was a good option for capturing the motion of the scope in the colon. The sensor has 0.9 mm outer diameters and enables track 6 DOFs: X-axis, Y-axis, Z-axis, yaw angle, pitch angle, and roll angle. In this study, Ascension Trakstar-2 with model-90 sensors was used to track the motion of the colonoscope in the colon.

Louis et al. [241] developed the Colonoscopy Force Monitor (CFM) (Artann Laboratories, Trenton, NJ) to improve training of physicians and establish best practices for performing colonoscopy by the quantitative characterization of an expert skill. With the application of the CFM, it was expected that the frequency and levels of significantly painful colonoscopy and risks of perforation of the colon would be reduced. The CFM is a hand-held force-measuring attachment that was mounted on the colonoscope shaft and provides the physician with real-time

feedback on the force and torque applied during colonoscopy. In this study, the CFM was used to collect the input information for colonoscopy.

In general, we developed a test-bed that consisted of a human-based "colon tray" (Medical Innovations International Inc., Rochester, NY), porcine colon tissue (supplied by Medical Innovations International Inc., Rochester, NY), the CFM (Artann Laboratories, Trenton, NJ), a flexible force sensor (Tekscan Inc., Boston, MA), Ascension Trakstar-2 System (Ascension Technologies Corp., Burlington, VT), and an Olympus^{TM} CF-Q160L colonoscope (Olympus Corp., Tokyo). Details of each component are described as follows:

(1) The porcine colon tissue was laid in human configuration on a board referred to as the "colon tray." Specific regions of the colon were fixed with a mesh material to represent the immobile intra-abdominal attachment areas of the colon (see Figure 5.1).

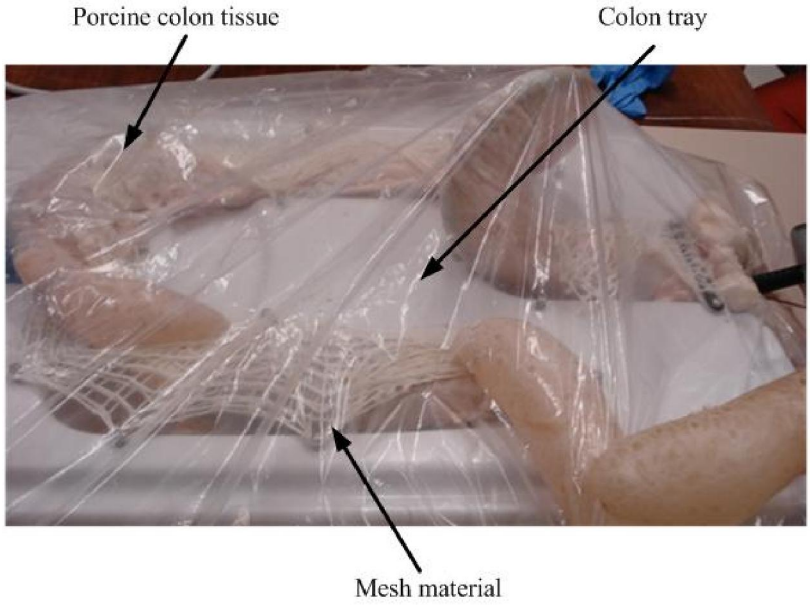

Figure 5.1 Human-based colon tray with the porcine colon tissue

(2) The CFM continually measured, displayed, and stored the push/pull, clockwise, and counter-clockwise torque applied to the insertion tube of the colonoscope (Figure 5.2). The CFM system consisted of 2 components: (1) hand-held wireless colonoscope attachment and (2) computer. The CFM was connected to a computer. Force and torque readings were logged at a sampling rate of 30 Hz.

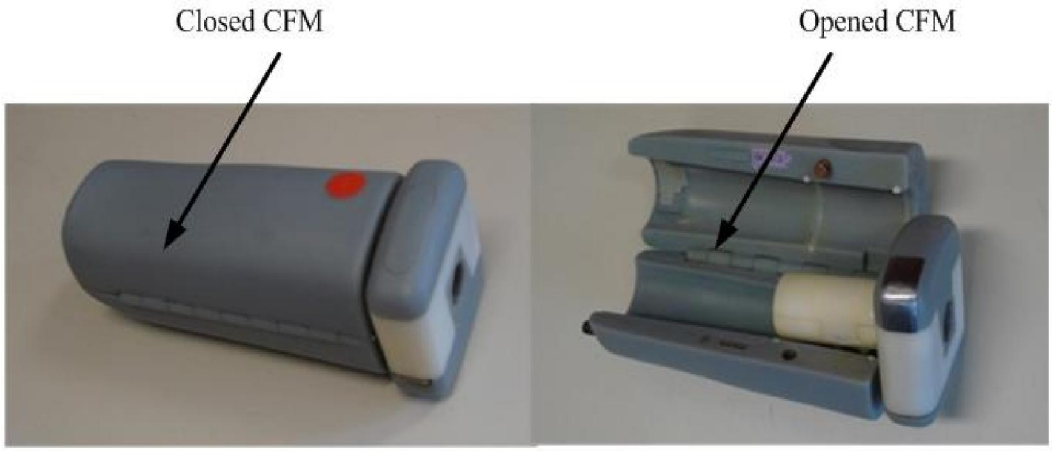

Figure 5.2 CFM for force and torque measurement

(3) The flexible force sensor is a paper-thin (0.008") Flexiforce B201 sensor (Tekscan Inc., Boston, MA). The system has a handle connected to the force sensor. The plastic ELF (Economical Load and Force) handle contains data acquisition electronics with USB connection and interface to B201 sensors (see Figure 5.3). The flexible force sensor was applied to the colonoscope insertion tube to collect the data for the normal contact force between the scope and colon tissue. The flexible force sensor was calibrated to preload 4 N, 6 N, 8 N, 15 N force and adjusted to the proper sensitivity using an Instron-3366 machine. The plastic ELF handle was connected to a computer. The normal force readings were logged at a sampling rate of 30 Hz.

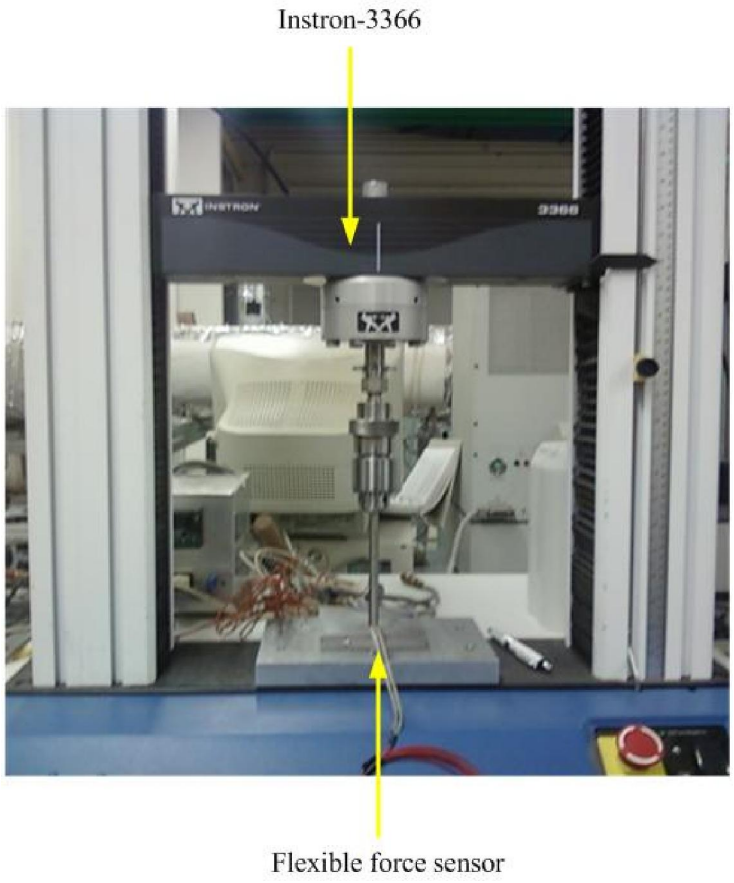

Figure 5.3 Calibrating flexiforce sensor

(4) Ascension Trakstar-2 System consisted of electronic main unit, flat-plate electromagnetic transmitter, and four Model-90 position sensors (see Figure 5.4). The first two position sensors were used to track the motion of the colonoscope in the colon; the third one was used to position the CFM; the fourth one was used to detect the deformation of scope in sigmoid colon. Thus, the CF-Q160L colonoscope was equipped with Sensor 1 and Senor 2 These two sensors were placed at 0 cm, 20 cm from the distal end of the scope. Sensor 3 that attached on the CFM was to position the point of input exerted by the CFM (see Figure 5.5). Sensor 4 was sutured onto the part of the sigmoid colon that alternatively detected the deformation of scope in sigmoid colon where the loop forms in real-time (see Figure 5.6). The flat-plate transmitter was placed at 40 cm below the colon tray model. The origin of

global coordinate of position sensors was directly underneath the joint between sigmoid colon and rectum on the colon tray. The Ascension Trakstar-2 System was connected to an Intel 3.0 GHz computer with 4GB RAM. The position readings were logged at a sampling rate of 30 Hz.

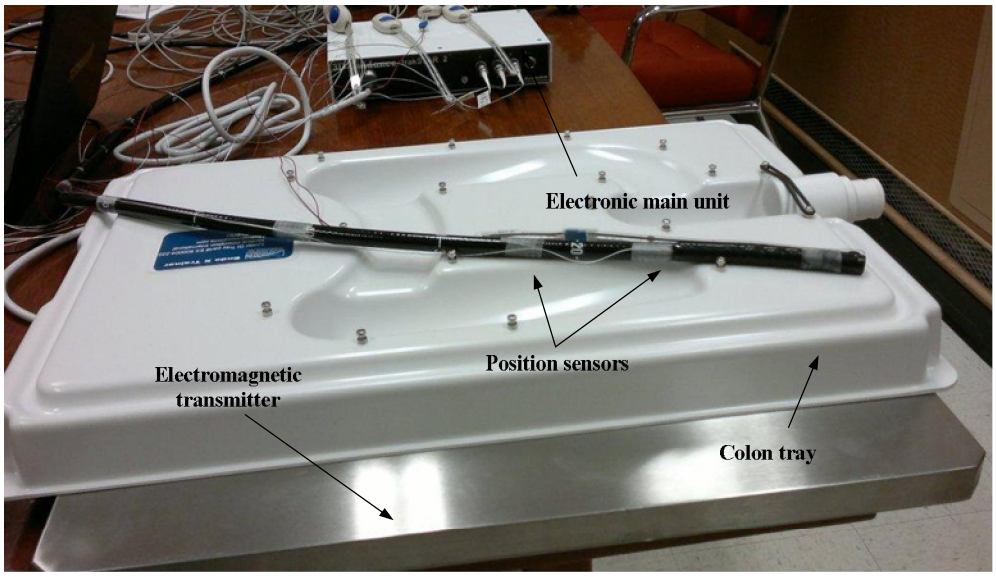

Figure 5.4 Ascension Trakstar-2 System

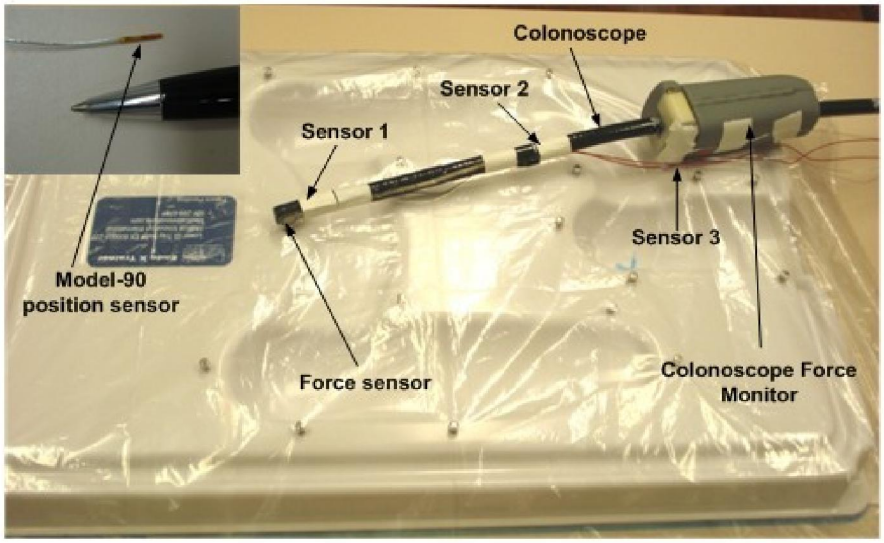

Figure 5.5 Colonoscope equipped with sensors

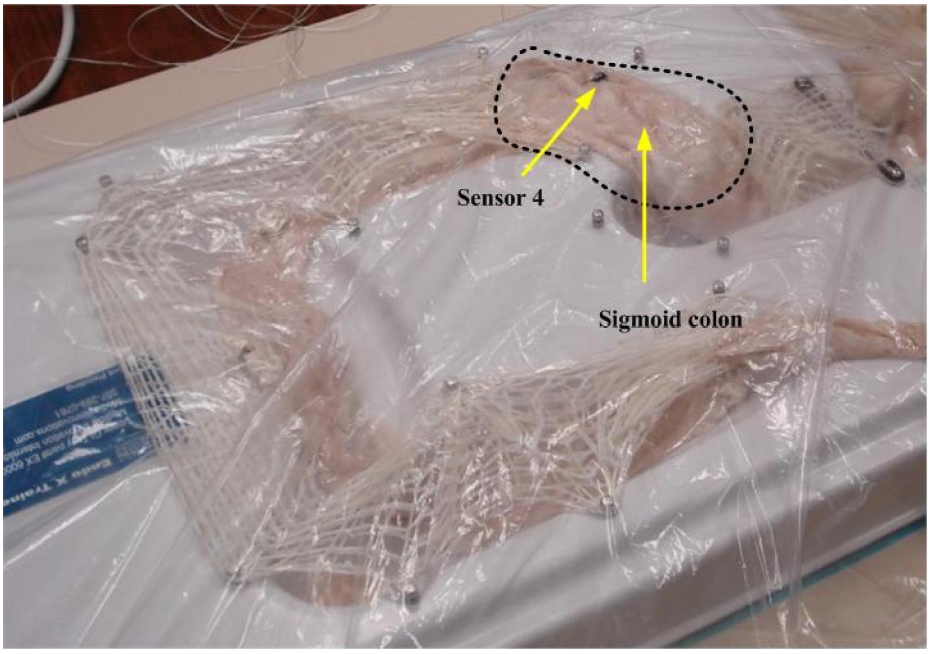

Figure 5.6 Sensor 4 sutured on sigmoid colon

5.2.2 Methods

The following procedure was followed:

Step 1: Getting the geometric shape of the colon. The position sensor recorded the nodal coordinates of the centerline of the colon tray (i.e., the centerline model of the colon) as shown in Figure 4.16.

Step 2: Performing standard techniques for colonoscopy, including lubricating the insertion tube and insufflating air into the colon.

Step 3: Setting the logged data from three sensors at 30 Hz. Three-stream data were collected by the same computer based on time-stamped synchronization.

Step 4: Implementing the external manipulation (force F and torque T) by the physician. During the colonoscopy, external forces and torques were recorded by the CFM. An example of the external force during the complete colonoscopy as collected by the CFM is shown in Figure 5.7; the external torque applied by the operator is shown in Figure 5.8. The motion of the colonoscope was recorded by position sensors. The motion of the tip of the colonoscope was recorded by Sensor 1, which recorded the tip's position with respect to X-axis, Y-axis, and Z-axis (unit: millimeter) as well as azimuth angle along X-axis, roll angle along Y-axis, and elevation angle along Z-axis (unit: Degree). One example of two synchronized data of external force applied by the physician and the tip's motion of the scope is shown in Figure 5.9. Sensor 1 recorded the tip's rotation of the scope as shown in Figure 5.10. The trajectories of the three position sensors located along the X-axis, along the Y-axis and along the Z-axis is shown in Figure 5.11. The contact force between the tip of the scope and the colon was recorded by a flexible force sensor. An example of two synchronized data of external force applied by the physician and contact force between the tip of the scope and the colon is shown in Figure 5.12. From Figure 5.12, it can be seen that contact force of the tip of the scope against the colon wall increased when the scope was in the sigmoid colon, which indicates that the tip of the scope had more frictional force compared to that generated in other regions of the colon.

Step 5: Repeating the procedure on each porcine colon tissue (there were in total three sets of the colon tissue).

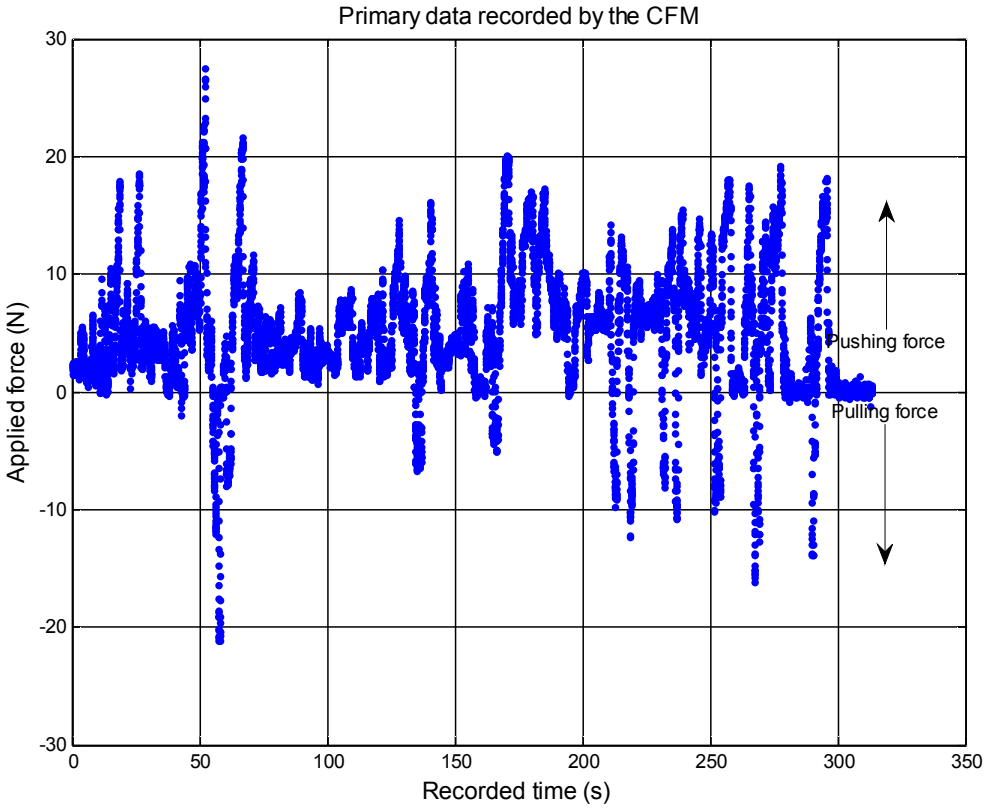

Figure 5.7 Primary pushing and pulling forces during a complete colonoscopy

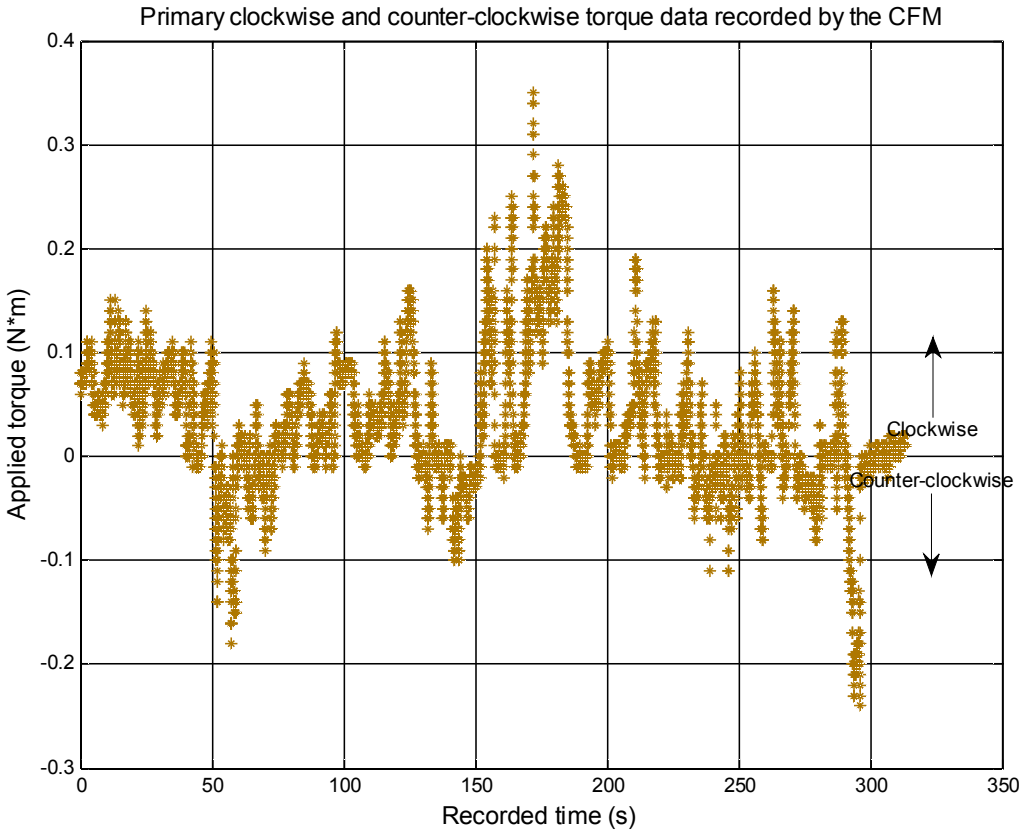

Figure 5.8 Primary clockwise and counter-clockwise torque during a complete colonoscopy

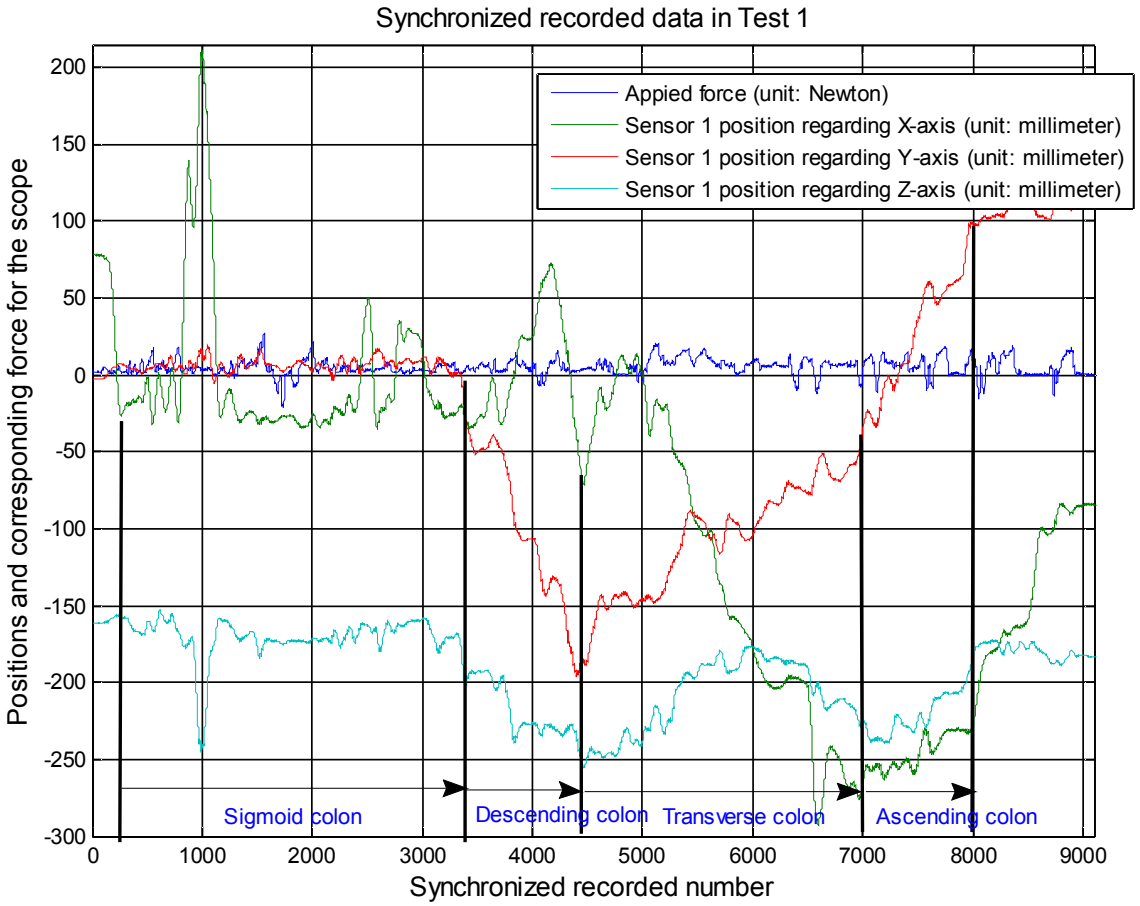

Figure 5.9 Primary synchronized data regarding input force and output motion

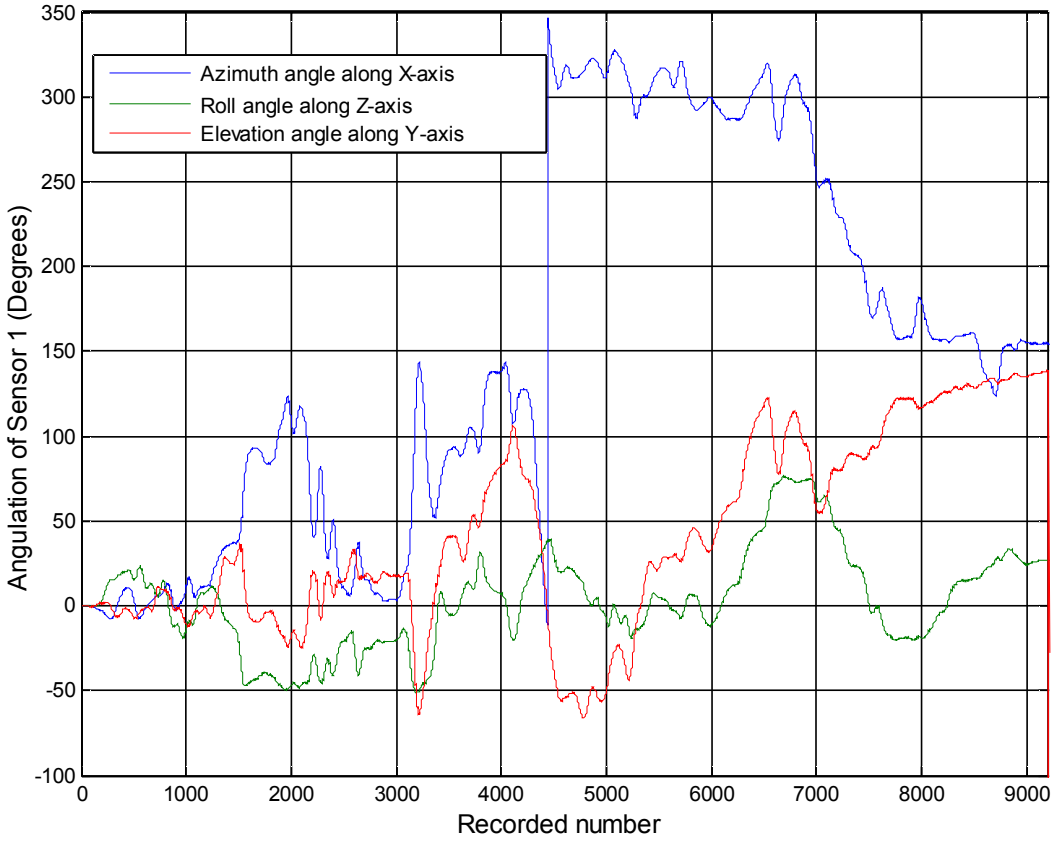

Figure 5.10 Tip's angulations along X-axis, Y-axis, and Z-axis of scope

(a)


Trajectories of the three sensors along X-axis
Sensor 2 attached 20 cm from the tip of the scope
Sensor 3 attached onto the CFM
Sensor 1 attached at the tip of the scope
Position (mm)
Recorded number
400
300
200
100
0
-100
-200
-300
0
1000
2000
3000
4000
5000
6000
7000
8000
9000

(b)

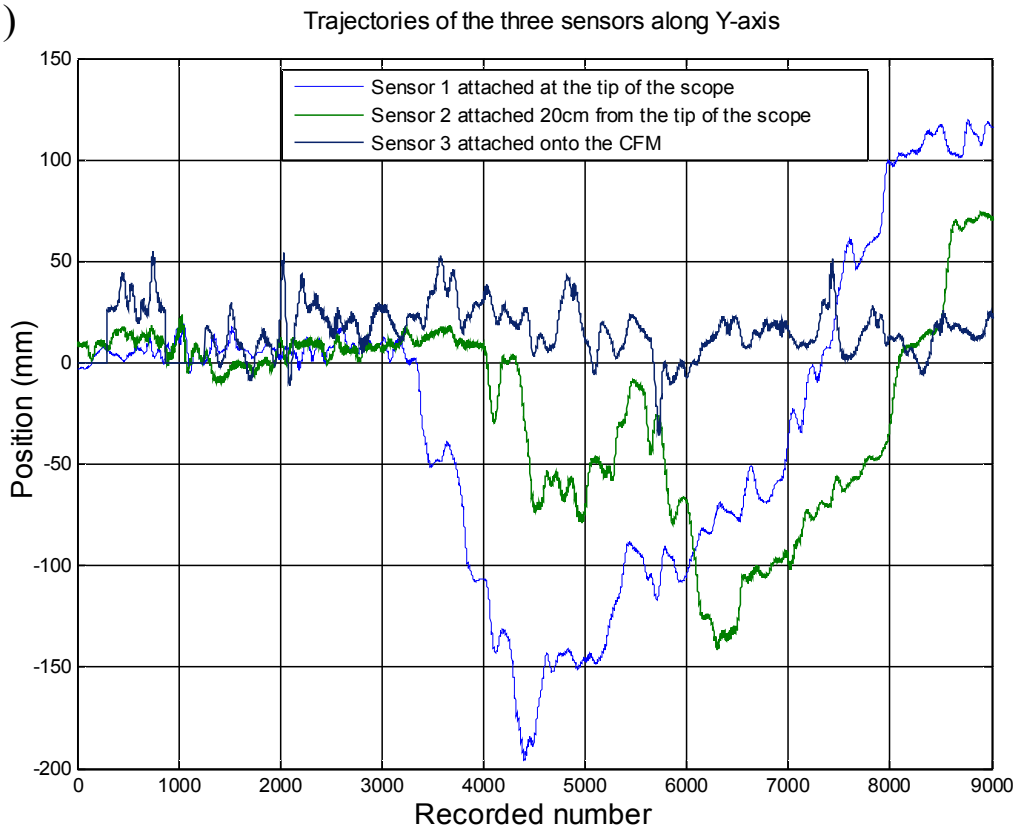
Trajectories of the three sensors along Y-axis
Sensor 1 attached at the tip of the scope
Sensor 2 attached 20cm from the tip of the scope
Sensor 3 attached onto the CFM
Position (mm)
Recorded number
150
100
50
0
-50
-100
-150
-200
0
1000
2000
3000
4000
5000
6000
7000
8000
9000

(c)

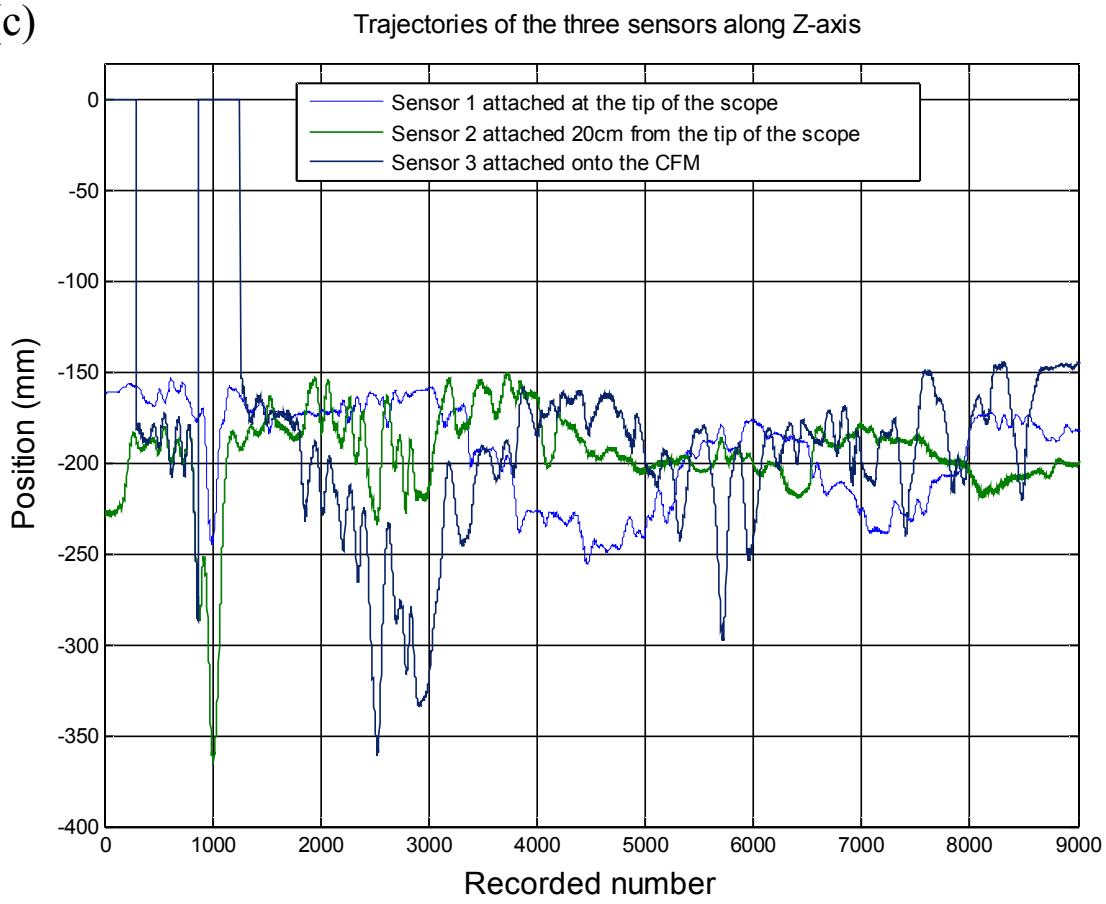

Figure 5.11 (a) trajectories of the three position sensors along X-axis; (b) trajectories of the three position sensors along Y-axis; (c) trajectories of the three sensors along Z-axis

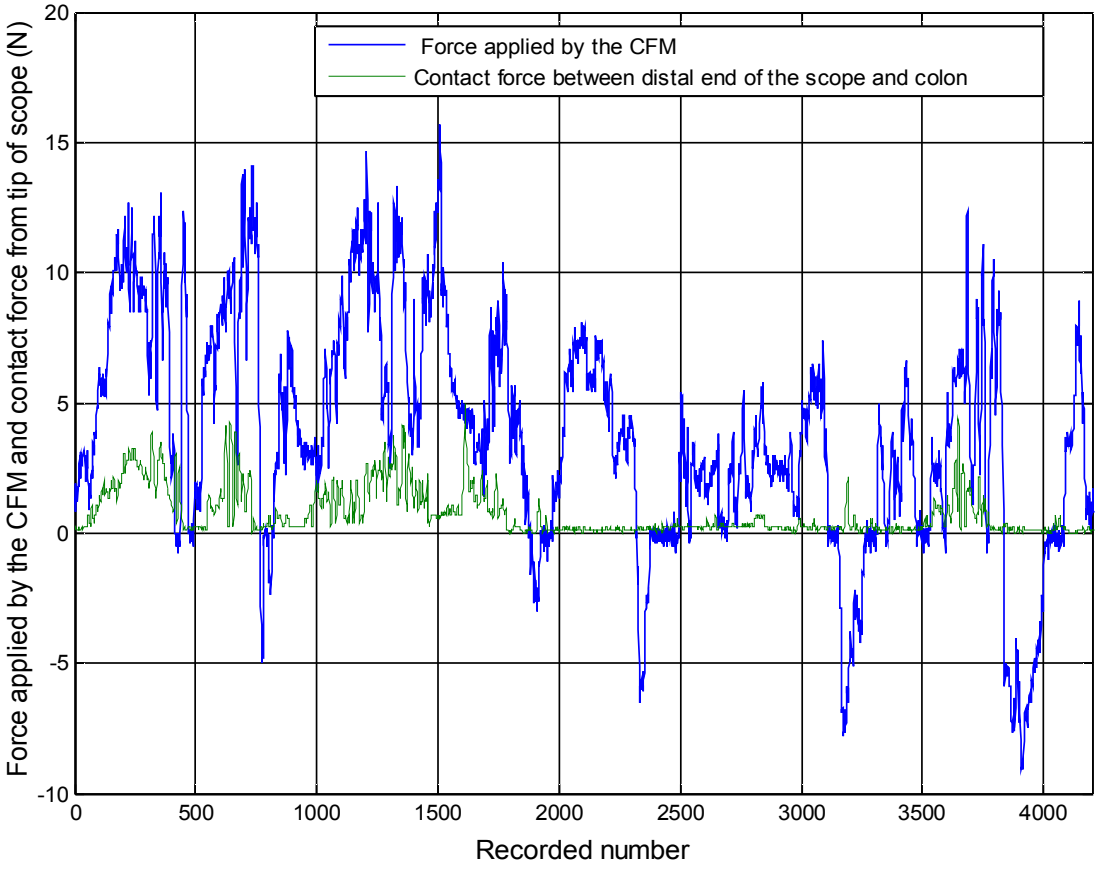

Figure 5.12 Comparsion between external force applied by the CFM and contact force between tip of the scope and colon

5.3 Comparison of Experimental and Simulation Results

The FBEM of the colonoscope was simulated by the following five steps.

Step 1: Assembly of the Beam Elements into the Colonoscope

The initial coordinates (x, y, z) of the nodes of the beam elements of the scope were known, which are related to the colon tray. There were sensors on these places.

Locations of the four position sensors were described in Section 5.2.1. These sensors not only recorded the displacements of the scope but also read the nodal coordinates of the beam elements of the scope in three dimension (x, y, z), which determined the position of the scope in the colon. Sensor 1 recorded the coordinate of the tip of the scope. Sensor 2 recorded one nodal coordinate, which was on the junction of the distal end and insertion tube of the scope (i.e., 20 cm away from the tip of the scope). Sensor 3 was attached to the CFM to record the coordinate of the input force exerted by the CFM, and there was no relative motion between the CFM and the scope during the operation because the CFM firmly griped the scope. Sensor 4 was sutured onto the sigmoid colon, and tracked the scope's shape in the sigmoid colon. The origin of the global frame of the position sensors was underneath the joint between the sigmoid colon and rectum on the colon tray, which was kept fixed during the experiment (see Figure 5.13).

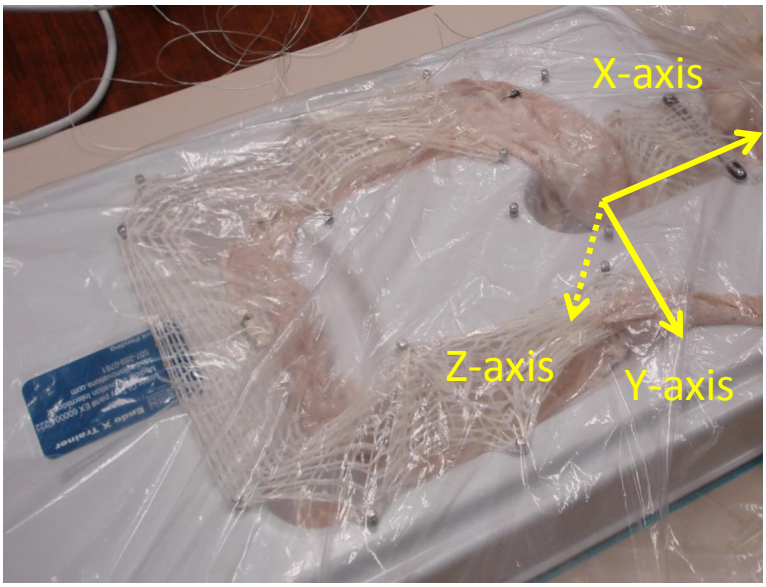

Figure 5.13 Origin of coordinate frame of position sensors

Step 2: Defining Material Properties of the Beam Elements of the Scope

The flexural rigidity of the CF-Q160L colonoscope is in the range of 260 to 660 N·cm^2 because its flexural rigidity is subject to the constraints of the location, looping, and tip deflection effects. The average EI (350 N·cm^2) of the CF-Q160L colonoscope was used for the FE model of the scope. As a matter of fact, the flexural rigidity of the CF-Q160L colonoscope is close to that of the one measured by Hellier et al. [222]. For this reason, torsional rigidity of CF-Q160L colonoscope was not further tested in this study, and the results from Hellier et al. [222] were employed. Specifically, torsional rigidity of the scope was 7000 N·mm^2, and this measurment was used in the FE model of the scope. Inherent physical properties of the CF-Q160L colonoscope such as its radius and weight were measured to determine its density, and the area moment of inertia and the polar moment of inertia. These parameters were used to determine the stiffness matrix of the scope [K_s] as well as the mass matrix of the FE model of the scope. The

damping matrix [C] of the CF-Q160L colonoscope was determined by the experiment described in Chapter 4. Eq. (4.19) was used to determine the damping matrix of the FE model of the scope.

Step 3: Computation of the Free Motion of the Scope

In this step, there was no contact force between the colon and scope. The motion of the scope was called "free" motion δ as shown in Eq. (4.24) [26]. The free motion of the colonoscope was found by solving Eq. (4.1) for all forces except contact force. The free motion corresponds to the deformation of the scope under its self-weight and external forces (external forces applied by the physician were recorded with the CFM).

Step 4: Computation of the Contact Force between the Scope and the Colon

The contact force was determined with Eq. (4.24) of Chapter 4. In Eq. (4.24), the construction of mechanical compliance [W] includes the mass matrix [M] for the scope, the damping matrix [C] for the scope, the stiffness matrices for both the scope and the colon. The mass matrix [M], the damping matrix [C] and the stiffness matrix [K_s] of the scope were determined at Step 1. In order to determine the stiffness matrix [K_c] for the colon, the sigmoid colon's Young Modulus (E) was used in this study (E = 360 KPa). The frictional coefficient μ = 0.25 between the scope and the colon was used [102].

Step 5: Computation of the Motion of the Scope with Contact Force

After the contact force were found at Step 4, the force-motion equation of the scope was computed by the input force/torque and contact forces from the colon. This step is so-called contact correction [26]. The time step 0.033 was chosen. The final motion of the scope was found at this step.

For one complete colonoscopy, extensive data were collected. These data were distinct according to where the colonoscope moved within the colon, i.e., sigmoid colon, descending colon, transervse colon, and ascending colon, and they will be referred to as the four regions of the colon. The data in the four aforementioned regions were selected.

When the scope was in each region of the colon the motion of the scope was computed with the mathematical model, given the input force and position of the scope in the colon. Two examples of the input force when the scope was in different regions are shown in Figure 5.14 and Figure 5.15.

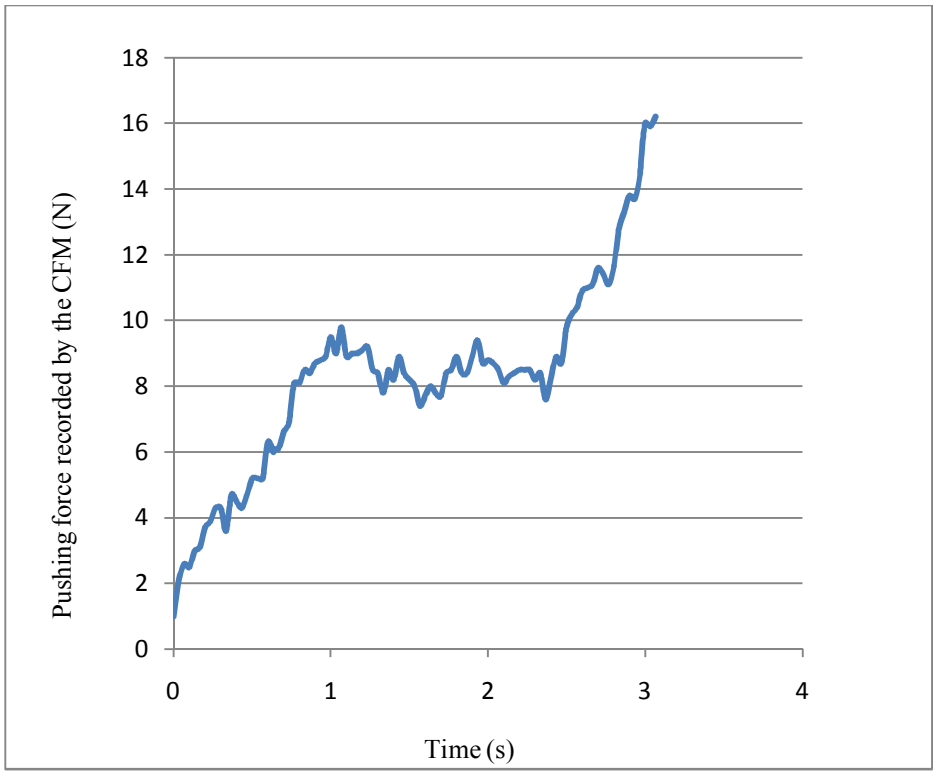

Figure 5.14 Force recorded by the CFM in the descending colon (Example 1)

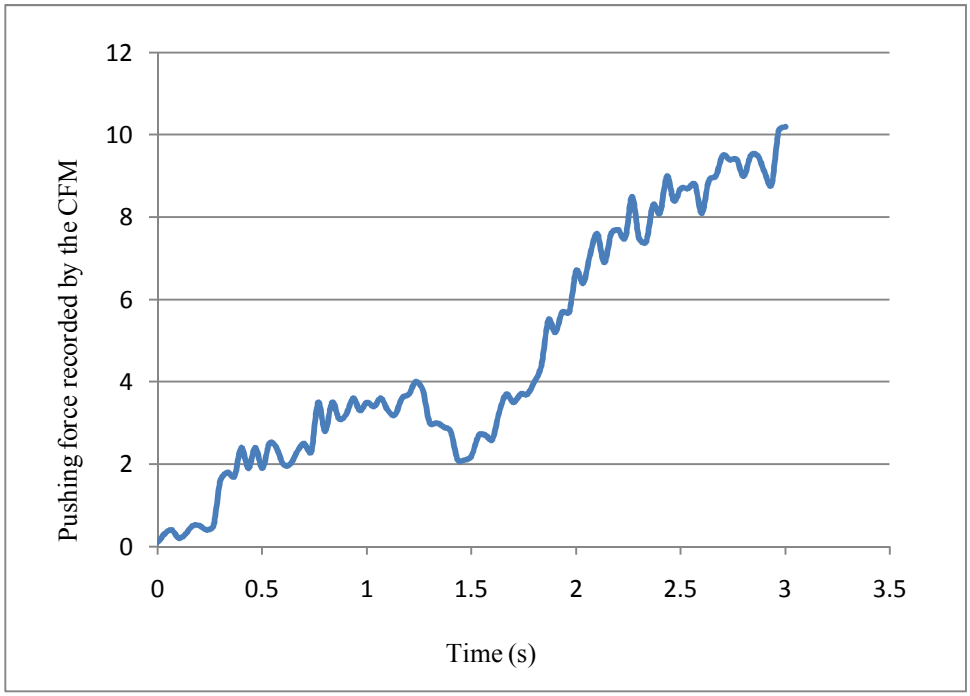

Figure 5.15 Force recorded by the CFM in the sigmoid colon (Example 2)

Comparison of the displacement of the distal end of the scope between the model predicted or simulation results and experimental results will be presented in the following section. The errors between the simulation and experimental results will be discussed.

When the scope was in the descending colon, the distal end of the scope had two active DOF displacements along the X-axis and the Z-axis (displacements along the Y-axis were constrained because of the immobile intra-abdominal attachment areas of the descending colon), respectively. Figure 5.16 shows a comparison of the displacement of the distal end of the scope along the X-axis between simulation and experimental results. Figure 5.17 shows a comparison between simulation and experimental results of elevation angle of the scope about the Y-axis. Root mean square error (RMSE) of the displacement of the distal end of the scope along the X-axis in the descending colon was found to be about 1.597 mm. RMSE of the elevation angle of the scope about the Y-axis in the descending colon was found to be about 0.156 degrees.

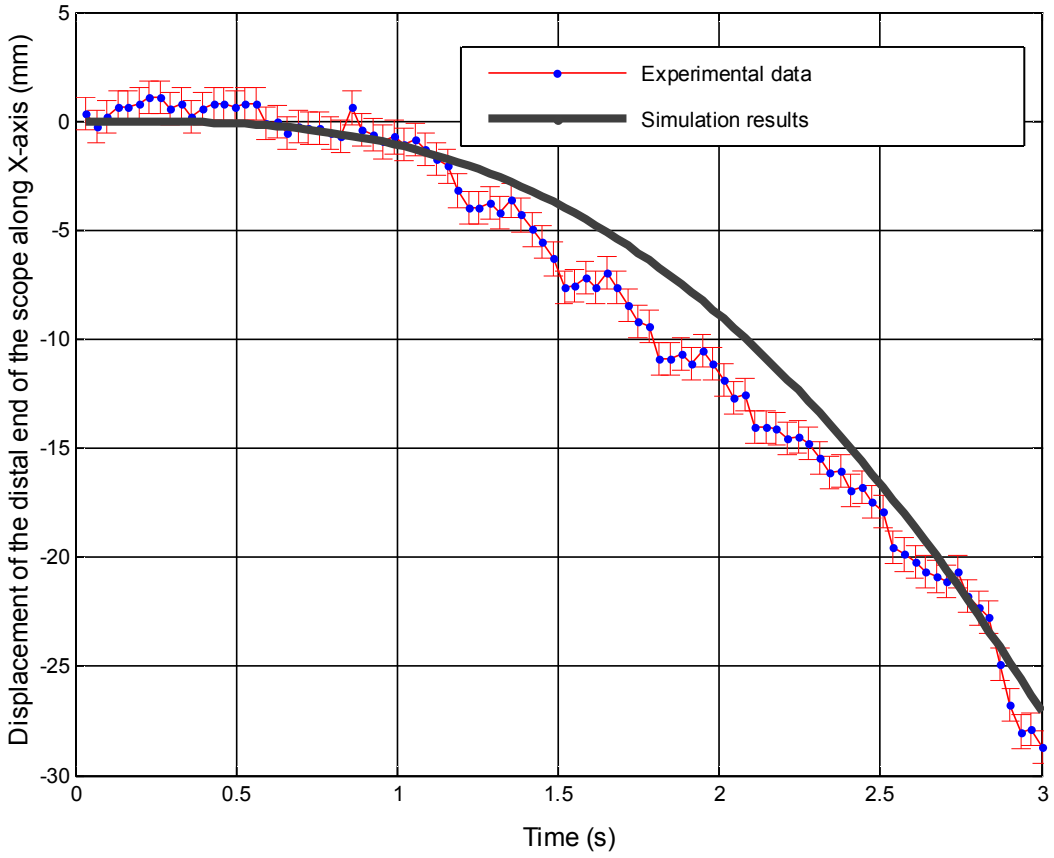

Figure 5.16 Comparison between simulation and experimental results of the displacement of the distal end of the scope along the X-axis with scope in descending colon

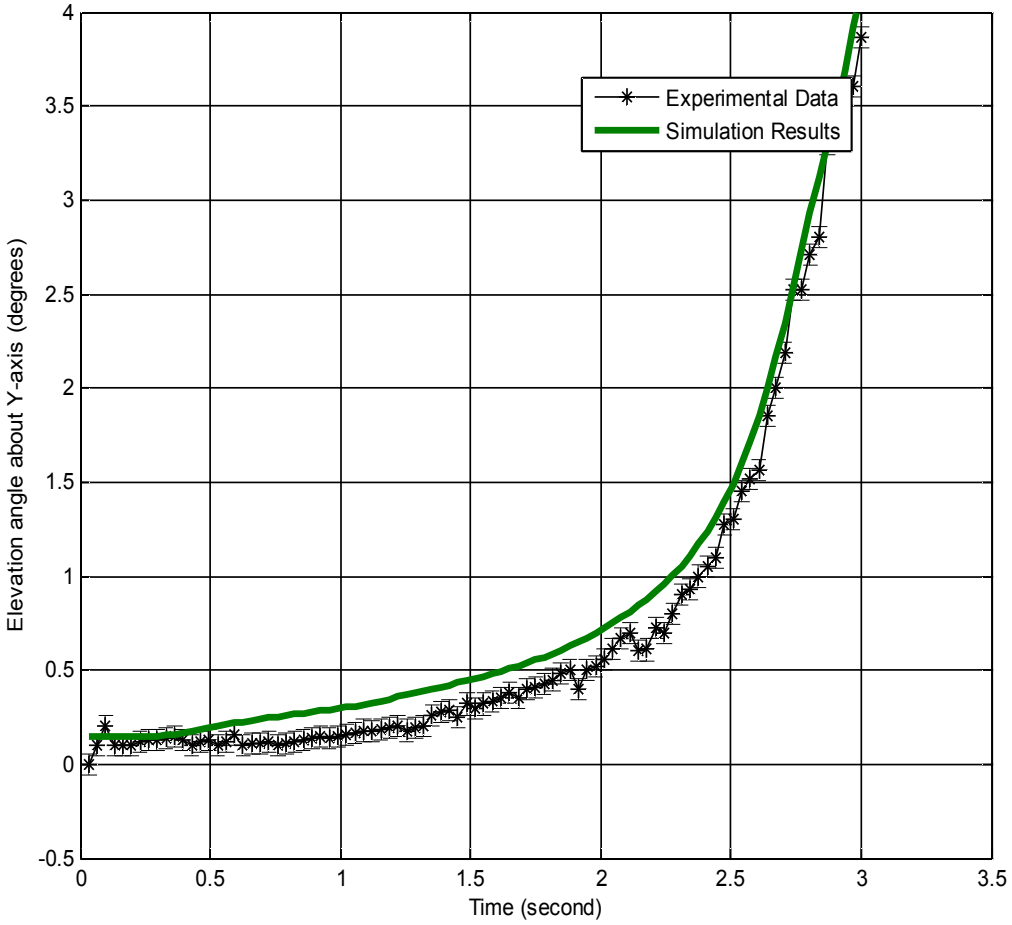

Figure 5.17 Comparison between simulation and experimental results of the elevation angle of the distal end of the scope about the Y-axis with scope in descending colon

Figure 5.18 shows a comparison between simulation and experimental results of the displacement of the distal end of the scope along the Y-axis when the scope was in the transverse colon. RMSE of the displacement of the scope along the Y-axis in the transverse colon was found to be about 2.105 mm.

Figure 5.19 shows a comparison between simulation and experimental results of the displacement of the distal end of the scope along the X-axis when the scope was in the ascending colon. RMSE of the displacement of the distal end of the scope along the X-axis in the ascending colon was found to be about 0.9606 mm.

The simulation results showed more displacement than did the experimental results when the scope was in the ascending colon. The plausible explanation of more displacement from the simulation results is that the retraction force from the stretched colon was not incorporated into the mathematical model. When the scope was moving in the ascending colon, the scope looped with the sigmoid colon. As a result, the sigmoid colon was stretched by the scope. The retraction force from the stretched sigmoid colon gripped the scope, which was acting as a kind of resisting force. In the simulation, this resisting force was not considered, which implied that the scope had less resisting force than it actually did. Thus, more displacement of the distal end of the scope was generated when the scope was in the ascending colon.

Figure 5.20 shows a comparison between simulation and experimental results of the displacement of the distal end of the scope along the Y-axis. RMSE of the displacement of the scope along the Y-axis in the sigmoid colon was found to be about 4.9820 mm. By comparison to the error generated for other regions of the colon, the error when the scope was in the sigmoid colon was large. The potential reason for this error was due to the mobility of the sigmoid colon. The mobility of the sigmoid colon caused significant disturbance to the distal end of the scope. This disturbance can be seen in the experimental results as shown in Figure 5.20.

A summary of the RMSE of displacement of the distal end of the scope in different regions of the colon is given; see Table 5.1.

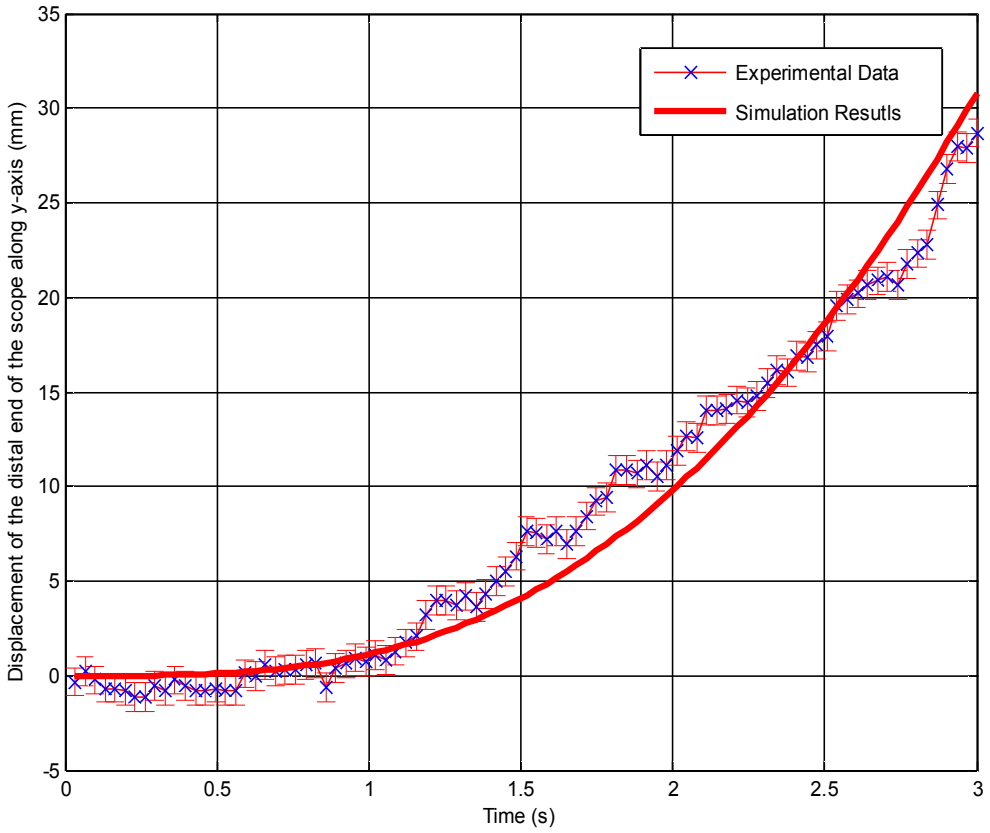

Figure 5.18 Comparison between simulation and experimental results of the displacement of the distal end of the scope along the Y-axis with scope in transverse colon

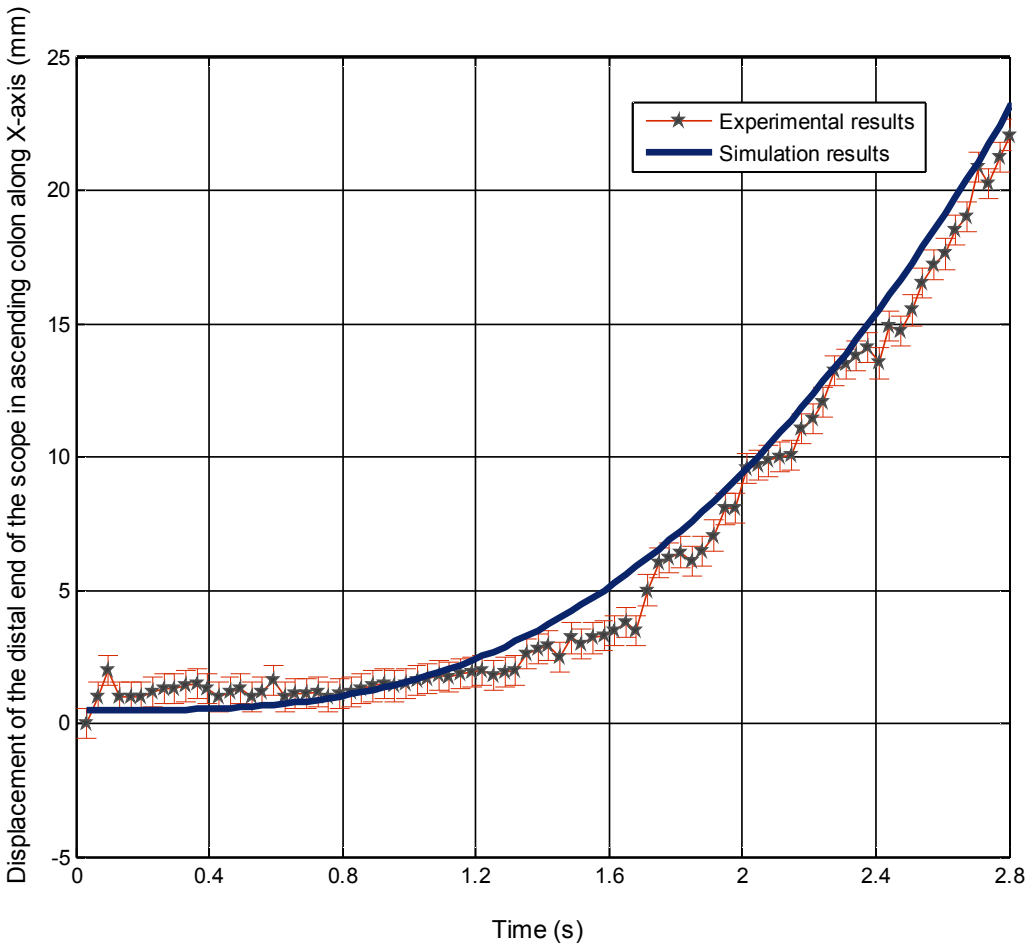

Figure 5.19 Comparison between simulation and experimental results of the displacement of the distal end of the scope along the X-axis with scope in ascending colon

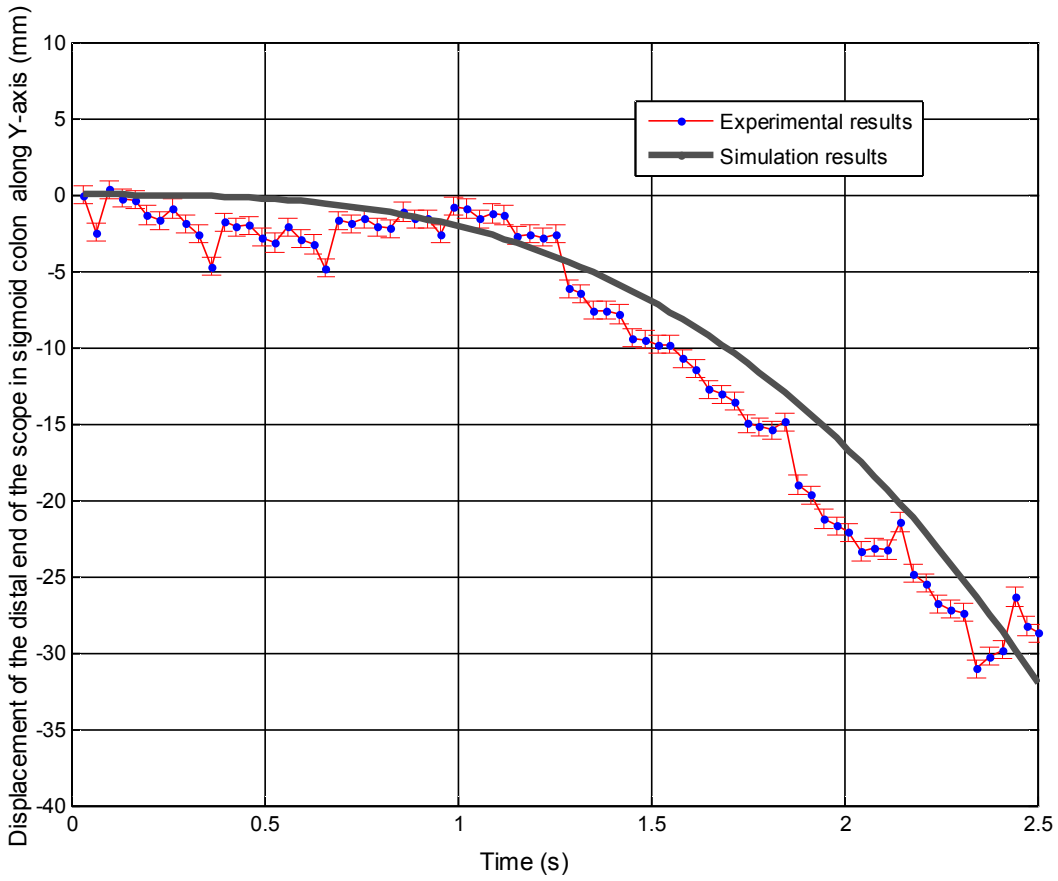

Figure 5.20 Comparison between simulation and experimental results of the displacement of the distal end of the scope along the Y-axis with scope in sigmoid colon

During the colonoscopy operation, the contact force between the distal end of scope and the colon was recorded by the flexiforce sensor. Figure 5.21 shows a comparison between simulation and experimental results of the contact force for the distal end of the scope on the colon wall when the scope was in the descending colon. RMSE of the contact force of the distal end of the scope in the descending colon was found to be about 0.0752 N.

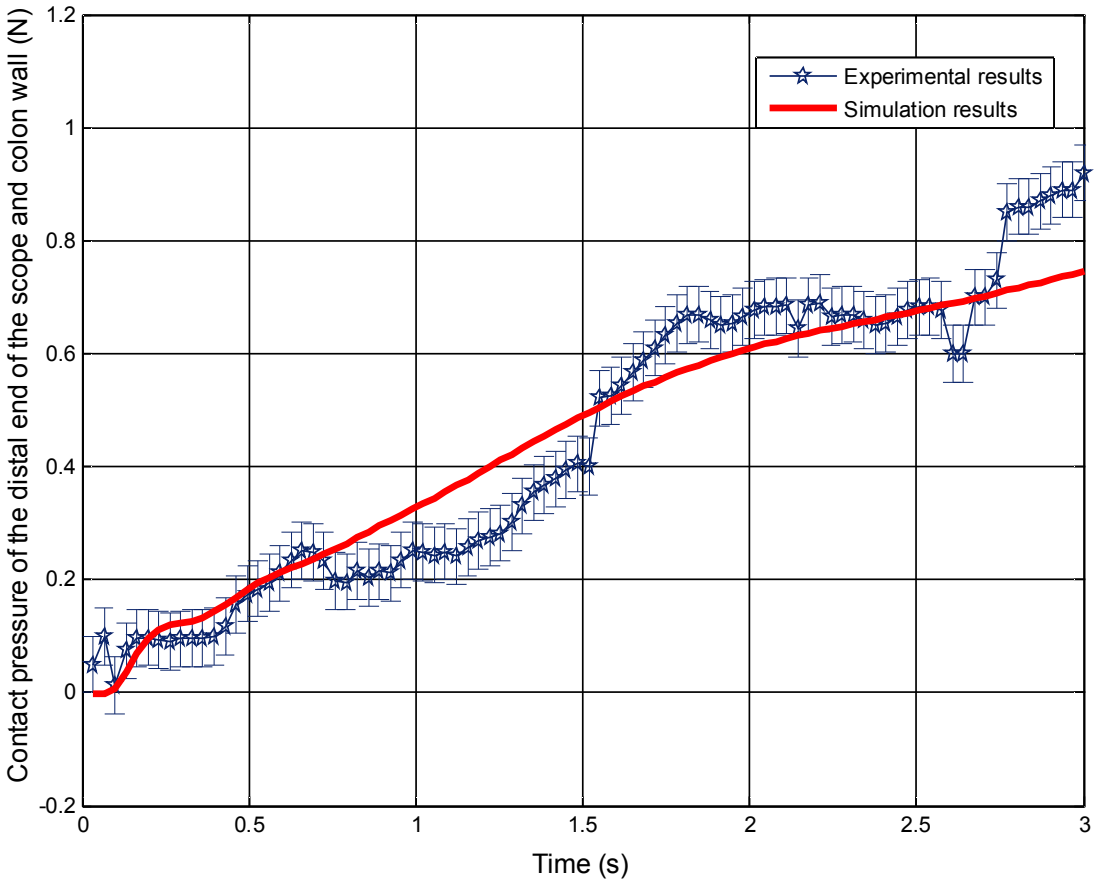

Figure 5.21 Comparison between simulation and experimental results of contact pressure of the distal end of the scope against the colon wall with scope in descending colon

Table 5.1 Summary of RMSE of the displacement of the distal end of the scope in different regions of the colon

Region of the colon	Colon Tissue 1		Colon Tissue 2		Colon Tissue 3	
	RMSE	A* (RMSE)	RMSE	A* (RMSE)	RMSE	A* (RMSE)
Sigmoid colon	4.982 (test 1) 2.059 (test 2) 3.504 (test 3)	3.514	2.109 (test 1) 2.890 (test 2) 5.462 (test 3)	4.231	2.952 (test 1) 3.450 (test 2) 2.086 (test 3)	2.829
Descending colon	1.597 (test 1) 1.834 (test 2) 2.503 (test 3)	1.978	2.546 (test 1) 1.351 (test 2) 2.905 (test 3)	2.264	2.896 (test 1) 3.846 (test 2) 4.717 (test 3)	3.819
Transverse colon	2.105 (test 1) 2.716 (test 2) 1.803 (test 3)	2.208	2.854 (test 1) 2.121 (test 2) 4.850 (test 3)	3.275	2.981 (test 1) 1.908 (test 2) 3.227 (test 3)	2.706
Ascending colon	0.961 (test 1) 2.245 (test 2) 4.470 (test 3)	2.558	3.229 (test 1) 4.576 (test 2) 3.194 (test 3)	3.663	3.692 (test 1) 2.058 (test 2) 2.438 (test 3)	2.724

A*: average

5.4 Discussion

In the comparison of experimental and simulation results, there was good agreement between the two. Probable reasons for the measured uncertainty error associated with Model-90 position sensors and the force sensor (the CFM and flexible force sensor) are discussed below. The major measurement error for the position sensors was due to jittery data. This measurement error was plotted as the error bar. The propagation error generated from the CFM should be considered because the CFM collected the external force/torque, and these values were applied to the mathematical model as the input force.

Furthermore, the errors generated from the model assumptions are inevitable such as the non-linear mechanical properties of the colon tissue and the viscous adhesive frictional force. Wang et al. [102] studied the frictional characteristics of porcine colon tissue. They found that the frictional force of porcine colon tissue is generally subject to Coulomb's law but also that the adhesive force generated by the viscoelastic intestine contributed to frictional resistance force; that is to say, frictional force consists of both nominal frictional force and viscoadhesive force. In this study, only the frictional force obtained from Coulomb's law was used.

For the FE model of the scope, the EI was assumed to be constant. In Chapter 4, three EIs were applied to the FE model of the scope to simulate the cantilever scope, and there were no significant differences found. Furthermore validation was made to see if there was significant difference in the motion of the scope between the simulation and experimental results. Two

different EIs of 300 N·cm^2 and700 N·cm^2 were given to the FE model of the scope, and the result of the comparison shows that there was no significant difference (P value = 0.58). Figure 5.22 shows a comparison between simulation results from using different EIs and experimental results of the displacement for the distal end of the scope along the X-axis when the scope was in the descending colon.

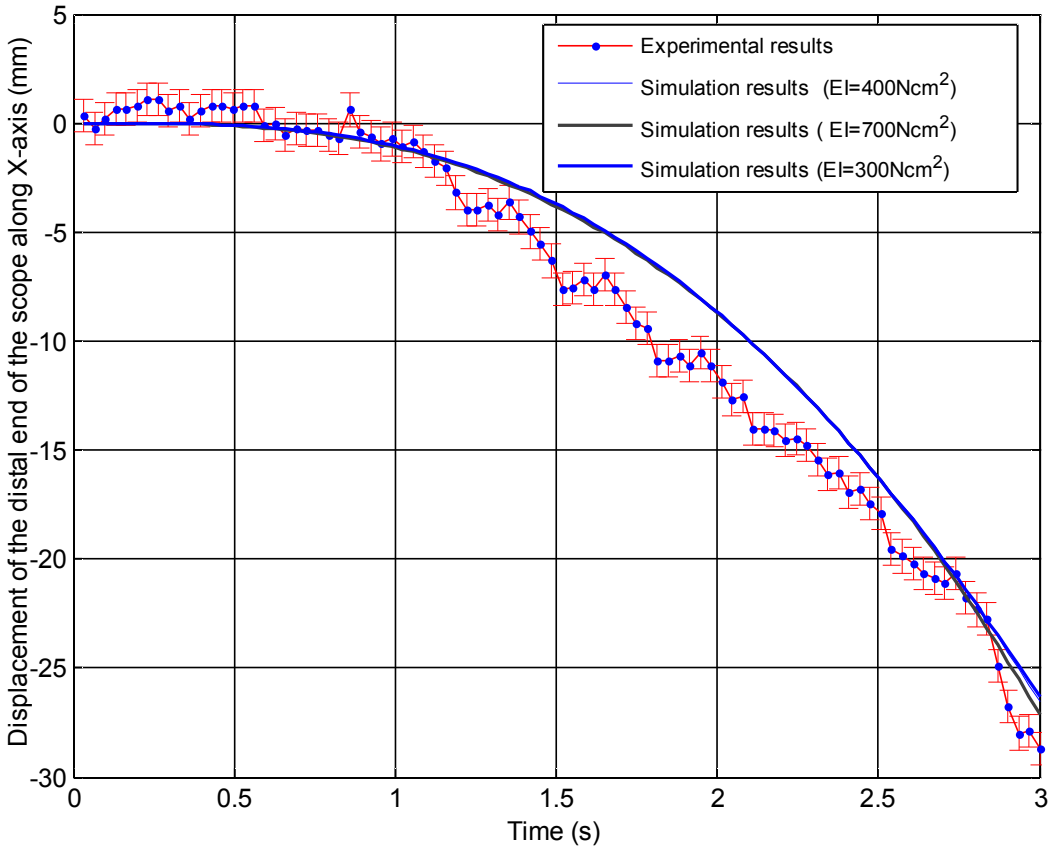

Figure 5.22 Comparison between simulation and experimental results of the displacement of the distal end of the scope along the X-axis with scope in descending colon

5.5 Conclusions

This chapter presented the mathematical model validation. An *ex-vivo* colonoscopy test-bed comprising a human-based colon tray and porcine colon tissue, and using an Ascension Trakstar-2 System, a CFM and an Olympus^{TM} CF-Q160L colonoscope was developed. Overall, there was good agreement between experimental and simulation results. The FE model of the colonoscope is reliable in terms of accuracy. The errors generated were analyzed based on the model assumptions, the measurement errors, and the parameters of the mathematical model.

In this study, only one model of a human-based colon tray was made for the experiments. However, a variety of human colons should be considered, for example those patients who have a redundant sigmoid colon (female gender, older age, and low BMI [body mass index]). Therefore, a model of a colon tray incorporated with this factor is necessary for further studies.

CHAPTER 6

CONCLUSION AND RECOMMENDATIONS

6.1 Overview and Conclusions

The colonoscope is an important tool in diagnosis and management of diseases of the colon. One of the ongoing challenges with this device is that a colonoscope may form a loop together with the colon during the procedure. The consequence of this loop is such that further insertion of the scope in the colon may be not possible, which means failure of the procedure. The loop also creates risks of perforation of the colon and pain in the patient.

There are currently several existing devices to overcome loop formation in colonoscopy which have been introduced in clinical work, including a variable stiffness colonoscope, an over-tube colonoscope, capsule endoscopy, a self-propelled endoscope, virtual colonoscopy, the Aer-O-Scope, the NES, and image-guided colonoscopy. However, the empirical assessment of these solutions in a clinic setting shows that they do not work very well. This was the motivation for the research presented in this thesis.

A preliminary analysis from the author has led him to believe that all the existing solutions to loop formation may have missed an important engineering concept called "self-locking" and its underlying principle governing the locking of relative motion (or "stick") between two objects (colon and scope, in this case). This observation, coupled with the author's belief that medical procedures and operations must be performed in interactive human/machine fashion (or, simply speaking, that a complete automation for this procedure is both undesirable and less if at all viable), led the author to propose a new paradigm of thinking for colonoscopy called "doctor-assisted colonoscopy". Under this new paradigm, the physician's role would be enhanced by new information involving the interaction between the scope and the colon such as their contact force, scope positions, and orientation of the scope's distal end within the colon. While this information can be acquired by assembling sensors on the scope especially on the distal end, this procedure would be quite intrusive and less reliable. The author's solution is to have sensors on a tube outside the human body and then to infer the information between the scope and colon with a kinetics model. Thus, it is clear that an accurate kinetic model is extremely important, and this thesis is devoted to the development of this kinetic model.

In Chapter 1, the research motivation and objectives were described. In particular, the research objectives are revisited here as follows:

(1) To analyze the existing devices and solutions that attempt to overcome loop formation in colonoscopy from an engineering design prospective, aiming to confirm the author's preliminary finding.

(2) To develop a kinetic model of the colonoscope that describes the motion of the colonoscope in the colon and also the contact force resulting from external force/torque

applied by the physician. Objective (2) can be further divided into three more specific objectives: (2a) to set up an experiment test-bed in order to identify and determine the parameters that should be included in the model; (2b) to set up a test-bed that can measure all the previously mentioned information that will serve as a means to validate the model; (2c) to establish the model from the first principle.

Chapter 2 presented an analysis of the causes for the looping including how existing devices and solutions are problematic from a systems design perspective. A well-proven design theory, the ADT, was employed for this analysis. The analysis confirmed the author's hypothesis that is implicitly behind the first objective of this study. This also indicated a green light for the development of a kinetic model for the dynamics of the scope-colon system in colonoscopy, i.e., the proposed second objective for this study.

Chapter 3 presented a literature review on modeling of deformable objects, providing the understanding of challenges of modeling and characteristics of the modeling problem. This chapter also elaborated on the suitability of using a finite element approach to the modeling problem.

In Chapter 4, the model for the colonoscope (i.e., a finite element model of the scope), and the model for the colon and the interaction between scope and colon were presented. The Timoshenko beam element was used for both the scope and the colon. The scope-colon interaction or contact model was formulated into a Linear Complementarity Problem (LCP) including consideration of frictional force (note: the viscous-adhesive frictional force of the porcine colon tissue was not considered in the friction model). For the scope, the stiffness,

inertial, and damping effects were considered. For the colon, only the stiffness effect was considered because both the inertial and damping effects are too small, they are ignored. All the parameters in these models were determined on the experiment test-bed. A particular scope, namely an Olympus^{TM} CF-Q160L colonoscope, and a particular pig model, namely Endo X Trainer^{TM} lower GI colon tray, were studied in great detail, without loss of the generality of the model.

In Chapter 5, the experimental validation of the model developed in Chapter 4 was presented. First, an experiment test-bed was built, which included the human-based "colon tray" with porcine colon tissue, position-tracking sensors, and the CFM on the proximal end of the colonoscope. Second, the validity and reliability of the model were discussed.

The following conclusions can be drawn from this study:

(1) Self-locking of the colonoscope is the most basic cause for the occurrence of looping, while structural instability of the colonsocope is dependent on the self-locking. The current literature asserting that structural instability of the scope is the main cause for looping is mistaken.

(2) Both the scope and the colon can be well represented with the Timoshenko beam elements, and the LCP formulation that considers frictional force to be the representation of interactions between the colon and scope is adequate.

(3) There are effects from the location, looping, and tip deflection of the scope on the flexural rigidity of the scope. Approximately, the EIs of the CF-Q160L colonoscope range from

300 to 650 $N \cdot cm^2$, and their accuracy is proven by a good agreement between the model predicted result and the experimental result.

(4) The Rayleigh damping of the CF-Q160L colonoscope depends more on the mass matrix [M] of the colonoscope than on the stiffness matrix [K], which is evident by the large coefficient value of "alpha" (0.3864) and the small coefficient value of "beta" (0.0164).

(5) A linear stress-strain relation can be used for the sigmoid colon for the strains ranging from 0 to 0.20, though each part of the colon may have different non-linear stress-strain relations.

6.2 Major Contributions of Thesis

This thesis research has generated several "firsts," implying a possible contribution to the field of biomedical engineering and particularly in biomechanics and bio-instrumentation. All contributions are summarized in the following:

(1) The finding that the main cause for the looping colonoscope is not the structural instability of the colonoscope but rather self-locking of the colonoscope, which will lead to the design of a "new-generation" colonoscope that avoids the looping.

(2) The systematic evaluation for the existing colonoscopy technologies based on the well-proven Axiomatic Design Theory (ADT) will serve as a guideline for future new colonoscope development.

(3) The approach to developing the kinetic model of the colonoscope is useful to modeling similar objects such as the catheter guide-wire.

(4) The novel ex-vivo colonoscopy test-bed with the kinetic and kinematic measurements is also useful for design validation in the colonoscopy technology, as well as for the training of physicians to perform the colonoscopy procedure.

(5) The new paradigm of thinking for colonoscopy, called "doctor-assisted" colonoscopy, has potential similar application to other medical procedures.

6.3 Future Work

Several future works are expected to improve this thesis work.

First, Wang et al. [102] found that frictional force of the porcine colon tissue was generally subject to the Coulomb's law but also to the adhesive force generated by the visco-elastic intestine. In this study, the adhesive force was not considered. The experimental study on frictional force between the colonoscope and the colon is expected to generate a comprehensive frictional model. (This model is expected to be incorporated into the contact model of the scope-colon system in order to further improve the accuracy of the model).

Second, a variety of human colons should be considered. For example, certain patients (female gender, older age, and low BMI [body mass index]) may have a redundant sigmoid colon. A model of a colon tray incorporated with this factor should be made for a further experimental study.

Third, considering the utility of the mathematical model of the colonoscope, a variety of colonoscope instruments with different physical properties are expected to test on this test-bed.

Finally, the kinetic model of the scope developed in this thesis will serve three proposed projects as future work. They are as follows:

(i) A New Approach of "Doctor-Assisted Colonoscopy" with Reduction of Loop Formation

The kinetic model of the scope will serve as a theoretical underpinning for the new approach of "doctor-assisted colonoscopy" for loop reduction as discussed in Chapter 1. The goal of this new approach is to predict loop formation and reduce loop formation in colonoscopy. For this approach, a sensor on the colonoscope tube outside human body and the kinetic model are required. The sensor reports the force and position information, and this information and the kinetic model are used to infer the information generated at the interaction between the scope and colon inside the body. Therefore, based on data generated by the CFM and the kinetic model, first, loop formation in colonoscopy is predicted; then a warning of loop initiation will be given to the physician if there is no relative motion between colonoscope and colon; next, the physician adjusts the operation in order to reduce the loop with the information given by the kinetic model, i.e., adjusts the distal end of the scope's orientation and direction by applying the proper force and torque to the proximal end of the colonoscope. This thesis has completed the development of the model, and future work will develop a procedure for this new approach.

(ii) Application of the Model of the Scope to Prevent Perforation of the Colon

Colonoscopy requires that pull and torque forces be applied to the instrument to advance it through the colon. The application of force to the colon and its anatomic attachments can be painful and excessive force can lead to perforation. Although sedation can reduce the pain, perforation is the most serious complication in colonoscopy. The reported rate of colonic perforations varies widely but is estimated to be about 0.5%. These perforations may then require open surgery for possible repair or removal of the damaged area. The perforation is particularly due to the occurrence of excessive contact pressure on colon tissue. The CFM is able to provide a physician with real-time feedback on the force and torque applied during colonoscopy, but it is not able to provide a reading of the contact pressure on the colon tissue. However, the kinetic model of the scope enables provision of information of the forces being exerted against colon tissue. Therefore, the kinetic model of the scope provides the best solution for overcoming perforation of the colon in colonoscopy; that is to say, physicians will receive a warning when the contact pressure on any particular section of colon tissue approaches the threshold of colon tissue perforation.

(iii) Application of the Model of the Scope to Design an Active Scope Device

The NES is an active scope that is described in Chapter 2. This system is a promising technology since it provides the full function of the conventional scope, such as biopsy. Unfortunately, the company stopped further development of the NES a few years ago. However, the NES remains

the design of the conventional colonoscope, including the long thin insertion tube. This insertion tube consists of 16 segments which are actuated by tendons. While the scope passes through the colon, each segment of the insertion tube is controlled to follow the first segment of the scope, i.e., the "head" of the scope. Segments following the "head" of the scope could be a promising approach in overcoming loop formation. However, with the proposed "active" colonoscope, a controller would accurately position each segment of the insertion tube of the scope and make sure that it is following the head of the scope. In order to design the controller and set its parameter, an accurate model of the scope is essential. Thus, this project is a typical application of the mathematical model of the scope.

REFERENCES

[1] Bell GD, Hancock J, Painter J, Rowland RS, Nylander D, Dogramadzi S, Allen C, Bladen JS, Atkin WS. Pain during flexible sigmoidoscopy and colonoscopy: When and why does it occur. *Gut* 2000; **46**: A30.

[2] Obstein KL, Valdastri P. Advanced endoscopic technologies for colorectal cancer screening. *World J Gastroenterol* 2013; **19**(4):431-39.

[3] Park HJ, Hong JH, Kim HS, Kim BR, Park SY, Jo KW, Kim JW. Predictive factors affecting cecal intubation failure in colonoscopy trainees. *BMC Med Educ* 2013; DOI:10.1186/1472-6920-13-5.

[4] Durdey P, Weston PMT, Williams NS. Colonoscopy or barium enema as initial investigation of colonic disease. *Lancet* 1987; **2**: 549-51.

[5] Wehrmeyer JA, Barthel JA, Roth JP. Colonoscope flexural rigidity measurement. *Med Biol Eng Comput* 1998; **36**: 475-79.

[6] American Accreditation HealthCare Commission. http://www.urac.org.

[7] Peter B. Cotton CBW, Robert HH, Brian P, Saunders ED. Practical gastrointestinal endoscopy: the fundamentals. the *6th Edition: John Wiley & Sons, Inc*. 2008.

[8] Messmann H. Atlas of colonoscopy: techniques, diagnosis, interventional procedures. *Thieme Medical Publishers*, 2006.

[9] Waye JD, Rex DK, Williams CB. Colonoscopy: principles and practice, the 1st Edition: Wiley-Blackwell, 2003.

[10] Cotton PB, Williams CB. Practical gastrointestinal endoscopy: the fundamentals, the 5th Edition: Wiley-Blackwell, 2003.

[11] Lee IL, Wu CS. Less patient discomfort by one-man colonoscopy examination. *Int J Clin Pract* 2006; **60**: 635-38.

[12] Church JM. Ancillary colonoscope insertion techniques - an evaluation. *Surg Endosc-ultras* 1993;**7**: 191-93.

[13] Saunders BP, Fukumoto M, Halligan S, Jobling C, Moussa ME, Bartram CI, Williams CB. Why is colonoscopy more difficult in women? *Gastrointest Endosc* 1996; **43**: 124-26.

[14] Shah SG, Brooker JC, Thapar C, Williams CB, Saunders BP. Patient pain during colonoscopy: an analysis using real-time magnetic endoscope imaging. *Endoscopy* 2002; **34**: 435-40.

[15] Shah SG, Pearson HJ, Moss S, Kweka E, Jalal PK, Saunders BP. Magnetic endoscope imaging: A new technique for localizing colonic lesions. *Endoscopy* 2002; **34**: 900-04.

[16] Saifuddin T, Trivedi M, King PD, Madsen R, Marshall JB. Usefulness of a pediatric colonoscope for colonoscopy in adults. *Gastrointest Endosc* 2000; **51**: 314-17.

[17] Brahmania M, Park J, Svarta S, Tong J, Kwok R, Enns R. Incomplete colonoscopy: maximizing completion rates of gastroenterologists. *Can J Gastroenterol* 2012; **26**: 589-92.

[18] American Accreditation HealthCare Commission. http://www.urac.org.

[19] Anderson JC, Messina CR, Cohn W, Gottfried E, Ingber S, Bernstein G, Coman E, Polito J. Factors predictive of difficult colonoscopy. *Gastrointest Endosc* 2001; **54**:558-62.

[20] Hawari R, Pasricha PJ. Going for the loop: A unique overtube for the difficult colonoscopy. *J Clin Gastroenterol* 2007; **41**:138-40.

[21] Marshall JB, Perez RA, Madsen RW. Usefulness of a pediatric colonoscope for routine colonoscopy in women who have undergone hysterectomy. *Gastrointest Endosc* 2002; **55**: 838-41.

[22] Shah SG, Saunders BP, Brooker JC, Williams CB. Magnetic imaging of colonoscopy: an audit of looping, accuracy and ancillary maneuvers. *Gastrointest Endosc* 2000; **52**:1-8.

[23] Cheng WB, Moser M, Kanagaratnam S, Zhang WJ. Overview of upcoming advances in colonoscopy. *Dig Endosc* 2012; **24**(1):1-6.

[24] Cheng WB, Moser M, Kanagaratnam S, Zhang WJ. Analysis of and mathematical model insight into loop formation in colonoscopy. *J Eng Med* 2012; **226**(11):858-67.

[25] Cheng WB, Di YY, Zhang EM, Moser MA, Kanagaratnam S, Korman LY, Sarvazyan N, Zhang WJ. Modeling and in-vitro experimental validation for kinetics of the colonoscope in colonoscopy. *Ann Biomed Eng* 2013; **41**(5):1084-93.

[26] Dequidt J, Duriez C, Cotin S, Kerrien E. Towards interactive planning of coil embolization in brain aneurysms. *Medical Image Computing and Computer-Assisted Intervention-MICCAI 2009* **5761**:377-85.

[27] Liu YZ. Stability of equilibrium of a helical rod under axial. *Acta Mechanica Solida Sinica* 2005 **26**(3): 256-60.

[28] Suh NP. Axiomatic design theory for systems. *Res Eng Des* 1998; 189-209.

[29] Rechtin E. The art of systems architecting. *IEEE Spectrum* 1992; **29**: 66-69.

[30] Suh NP. Design of systems. *CIRP Annals-Manufacturing Technology* 1997; **46**:75-80.

[31] Zhang W. Can design be more creative?. *Invited lecture, NJUST, China,* 2010.

[32] Suh NP. The principles of design. *New York: Oxford University Press.*1990.

[33] Suh NP. Axiomatic design: advances and applications. *New York: Oxford University Press.* 2001.

[34] Brooker JC, Saunders BP, Shah SG, Williams CB. A new variable stiffness colonoscope makes colonoscopy easier: a randomised controlled trial. *Gut* 2000; **46**:801-5.

[35] Töx U, Schumacher B, Toermer T, Terheggen G, Mertens J, Holzapfel B, Lehmacher W, Goeser T, Neuhaus H. Propofol sedation for colonoscopy with a new ultrathin or a standard endoscope: a prospective randomized controlled study. *Endoscopy* 2013 Mar 6. (Epub ahead of print)

[36] Sorbi D, Schleck CD, Zinsmeister AR, Gostout CJ. Clinical application of a new colonoscope with variable insertion tube rigidity: a pilot study. *Gastrointest Endosc* 2001; **53**:638-42.

[37] Yoshikawa I, Honda H, Nagata K, Kanda K, Yamasaki T, Kume K, Tabaru A, Otsuki M. Variable stiffness colonoscopes are associated with less pain during colonoscopy in unsedated patients. *Am J Gastroenterol* 2002; **97**:3052-5.

[38] Xie Q, Chen B, Liu L, Gan H. Does the variable-stiffness colonoscope makes colonoscopy easier? A meta-analysis of the efficacy of the variable stiffness colonoscope compared with the standard adult colonoscope. *BMC Gastroenterol* 2012; **12**:151-62.

[39] Odori T, Goto H, Arisawa T, Niwa Y, Ohimiya N, Hayakawa T. Clinical results and development of variable-stiffness video colonoscopes. *Endoscopy* 2001; **33**:65-69.

[40] Rex DK. Effect of variable stiffness colonoscopes on cecal intubation times for routine colonoscopy by an experienced examiner in sedated patients. *Endoscopy* 2001; **33**: 60-4.

[41] Kaffes AJ, Mishra A, Ding SL, Hope R, Williams SJ, Gillespie PE, Bourke MJ. A prospective trial of variable stiffness pediatric vs. standard instrument colonoscopy. *Gastrointest Endosc* 2003; **58**:685-89.

[42] Ginsberg GG. Colonoscopy with the variable stiffness colonoscope. *Gastrointest Endosc* 2003; **58**:579-84.

[43] Horiuchi A, Nakayama Y, Kajiyama M, Fujii H, Tanaka N. Usefulness of a small-caliber, variable-stiffness colonoscope as a backup in patients with difficult or incomplete colonoscopy. *American J Gastroenterology* 2004; **99**:1936-40.

[44] Sola-Vera J, Uceda F, Brotons A, Sáez J, Girona E, Pérez E, Picó MD, Grau C, Sillero C. Does the use of a variable stiffness colonoscope offer advantages during colonscopy under deep sedation? Results of arandomized trial. *Eur J Gastroenterol Hepatol* 2011; **23**(7): 593-97.

[45] Al−Shurieki SH, Marshall JB. Is the variable-stiffness paediatric colonoscopemore effective than a standard adult colonoscope for outpatient adult colonoscopy? A randomised controlled trial. *Dig Liver Dis* 2005; **37**:698-704.

[46] Lee DW, Li SAC, Ko CW, Chu DW, Chan KC, Poon CM, Sin KS, Leung KF, Sze TS, Chan AC, Chung SC. Use of a variable-stiffness colonoscope decreases the dose of patient-controlled sedation during colonoscopy: a randomized comparison of 3 colonoscopes. *Gastrointest Endosc* 2007; **65**:424-29.

[47] Shumaker DA, Zaman A, Katon RM. A randomized controlled trial in a training institution comparing a pediatric variable stiffness colonoscope, a pediatric colonoscope, and an adult colonoscope. *Gastrointest Endosc* 2002; **55**:112-79.

[48] Shah SG, Brooker JC, Williams CB, Thaper C, Suzuki N, Saunders BP. The variable stiffness colonoscope:assessment of efficacy by magnetic endoscope imaging. *Gastrointest Endosc* 2002; **56**:195-210.

[49] Rodriguez SA, Ormseth E, Tsuchida A. Bowel perforation with the variable stiffness colonoscope. *Gastrointest Endosc* 2003; **57**:271-73.

[50] Ruffolo TA, Lehman GA, Rex D. Colonscope damage from internal straightener use *Gastrointest Endosc* 1991; **37**:107-8.

[51] Raju GS, Rex DK, Kozarek RA, Ahmed L, Brining D, Pasricha PJ. A novel shape-locking guide for prevention of sigmoid looping during colonoscopy. *Gastrointest Endosc* 2004; **59**:416-9.

[52] Tierney WM, Adler DG, Conway JD, Diehl DL, Farraye FA, Kantsevoy SV, Kaul V, Kethu SR, Kwon RS, Mamula P, Pedrosa MC, Rodriguez SA. Overtube use in gastrointestinal endoscopy. *Gastrointest Endosc* 2009; **70**:828-34.

[53] Moglia A, Menciassi A, Dario P, Cuschieri A. Capsule endoscopy: progress update and challenges ahead. *Nat Rev Gastroenterol Hepatol* 2009; **6**:353-62.

[54] Moglia A, Menciassi A, Schurr MO, Dario P. Wireless capsule endoscopy: from diagnostic devices to multipurpose robotic systems. *Biomed Microdevices* 2007; **9**: 235-43.

[55] Mackay RS. Radio telemtering from within the human body. *Ire T Med Electron* 1959; **6**:100-5.

[56] Menciassi A, Quirini M, Dario P. Microrobotics for future gastrointestinal endoscopy. *Minim Invasive Ther Allied Tech* 2007; **16**:91-100.

[57] Iddan G, Meron G, Glukhovsky A, Swain P. Wireless capsule endoscopy. *Nature* 2000; **405**:417.

[58] Phee L, Accoto D, Menciassi A, Stefanini C, Carrozza MC, Dario P. Analysis and development of locomotion devices for the gastrointestinal tract. *IEEE T Bio-med Eng* 2002; **49**: 613-16.

[59] Shiba K, Morimasa A, Hirano H. Design and development of low-loss transformer for powering small implantable medical devices. *IEEE T Bio-med Circ Syst* 2010; **4**:77-85.

[60] Lenaerts B, Puers R. Inductive powering of a freely moving system. *Sensor Actuat A-phys* 2005; **123**:522-30.

[61] Lenaerts B, Puers R. An inductive power link for a wireless endoscope. *Biosens Bioelectron* 2007; **22**:1390-95.

[62] Ikuta K, Tsukamoto M, Hirose S. Shape memory alloy servo actuator system with electric resistance feedback and application for active endoscope. *IEEE International Conference on Robotics and Automation*, 24 Apr. 1998-29 Apr. 1998, Philadelphia, PA, USA.

[63] Kim B, Lee S, Park JH, Park JO. Design and fabrication of a locomotive mechanism for capsule-type endoscopes using shape memory alloys(SMAs). *IEEE-ASME T Mech* 2005; **10**:77-86.

[64] Hosokawa D, Ishikawa T, Morikawa H, Imai Y, Yamaguchi T. Development of a biologically inspired locomotion system for a capsule endoscope. *Int J Med Robotics Comput Assist Surg* 2009; **5**:471-8.

[65] Mavroidis C. Development of advanced actuators using shape memory alloys and electrorheological fluids. *Res Nondestruct Eval* 2002; **14**:1-32.

[66] Song G, Chaudhry V, Batur C. Precision tracking control of shape memory alloy actuators using neural networks and a sliding-mode based robust controller. *Smart Mater Struct* 2003; **12**: 223-31.

[67] Dario P, Carrozza MC, Pietrabissa A. Development and in vitro testing of a miniature robotic system for computer-assisted colonoscopy. *Comput Aid Surg* 1999; **4**:1-14.

[68] Goh P, Krishnan SM. Micromachines in endoscopy. *Best Pract Res Clin Gastroenterol* 1999; **13**:49-58.

[69] Phee L, Accoto D, Menciassi A, Stefanini C, Carrozza MC, Dario P. Analysis and development of locomotion devices for the gastrointestinal tract. *IEEE T Bio-med Eng* 2002; **49**:613-6.

[70] Phee L, Accoto D, Menciassi A, Stefanini C, Carrozza MC, Dario P. Analysis and development of locomotion devices for the gastrointestinal tract. *IEEE T Bio-med Eng* 2002; **49**:613-6.

[71] Kim B, Lim HY, Park JH, Park JO. Inchworm-like colonoscopic robot with hollow body and steering device. *JSME Int J C-mech Syst* 2006; **49**:205-12.

[72] Chen G, Pham MT, Redarce T. Sensor-based guidance control of a continuum robot for a semi-autonomous colonoscopy. *Robot Auton Syst* 2009; **57**:712-22.

[73] Goh P, Krishnan SM. Micromachines in endoscopy. *Best Pract Res Clin Gastroenterol* 1999; **13**:49-58.

[74] Kim YT, Kim DE. Novel propelling mechanisms based on frictional interaction for endoscope robot. *Tribol T* 2010; **53**:203-11.

[75] Park H, Park S, Yoon E, Kim B, Park J. Paddling based microrobot for capsule endoscopes. *IEEE Int Robotic Autom* 2007; 3377-82.

[76] Park S, Park H, Kim B. A paddling based locomotive mechanism for capsule endoscopes. *J Mech Sci Technol* 2006; **20**:1012-8.

[77] Stefanini C, Menciassi A, Dario P. Modeling and experiments on a legged microrobot locomoting in a tubular, compliant and slippery environment. *Int J Robot Res* 2006; **25**: 551-60.

[78] Quirini M, Menciassi A, Scapellato S, Stefanini C, Dario P. Design and fabrication of a motor legged capsule for the active exploration of the gastrointestinal tract. *IEEE-ASME T Mech* 2008; **13**:169-79.

[79] Valdastri P, Webster RJ, Quaglia C, Quirini M, Menciassi A, Dario P. A new mechanism for mesoscale legged locomotion in compliant tubular environments. *IEEE T Robotic Autom* 2009; **25**:1047-57.

[80] Wang KD, Yan GZ, Jiang PP, Ye DD. A wireless robotic endoscope for gastrointestine. *IEEE T Robotic Autom* 2008; **24:**206-10.

[81] Yamazaki A, Sendoh M, Ishiyama K, Hayase T, Arai KI. Three-dimensional analysis of swimming properties of a spiral-type magnetic micro-machine. *Sensor Actuat A-phys* 2003; **105**:103-8.

[82] Chiba A, Sendoh M, Ishiyama K, Arai KI. Moving of a magnetic actuator for a capsule endoscope in the intestine of a pig. *J Magn Soc Jpn* 2005; **29**:343-6.

[83] Chiba A, Sendoh M, Ishiyama K, Suda Y, Arai KI, Komaru T, Shirato K. Colon endoscope navigation by magnetic actuator and intestine observation. *J Magn Soc Jpn* 2004; **28**:433-36.

[84] Mosse CA, Mills TN, Appleyard MN, Kadirkamanathan SS, Swain CP. Electrical stimulation for propelling endoscopes. *Gastrointest Endosc* 2001; **54**:79-83.

[85] Carpi F, Galbiati S, Carpi A. Magnetic shells for gastrointestinal endoscopic capsules as a means to control their motion. *Biomed Pharmacother* 2006; **60**:370-74.

[86] Ciuti G, Valdastri P, Menclassi A, Dario P. Robotic magnetic steering and locomotion of capsule endoscope for diagnostic and surgical endoluminal procedures. *Robotica* 2010; **28**: 199-207.

[87] Lee JS, Kim B, Hong YS. A flexible chain-based screw propeller for capsule endoscopes. *Int J Precis Eng Manuf* 2009; **10**:27-34.

[88] Simi M, Valdastri P, Quaglia C, Menciassi A, Dario P. Design, fabrication, and testing of a capsule with hybrid locomotion for gastrointestinal tract exploration. *IEEE-ASME T Mech* 2010; **15**:170-80.

[89] Gao MY, Hu CZ, Chen ZZ, Zhang HH, Liu S. Design and fabrication of a magnetic propulsion system for self-propelled capsule endoscope. *Ieee T Bio-med Eng* 2010; **57**: 2891-902.

[90] Halligan S, Fenlon HM. Virtual colonoscopy. *BMJ* 1999; **319**:1249-52.

[91] Arber N, Grinshpon R, Pfeffer J, Maor L, Bar-Meir S, Rex D. Proof-of-concept study of the Aer-O-Scope (TM) omnidirectional colonoscopic viewing system in ex vivo and in vivo porcine models. *Endoscopy* 2007; **39**:412-7.

[92] Pfeffer J, Grinshpon R, Rex D, Levin B, Rösch T, Arber N, Halpern Z. The Aer-O-Scope: Proof of the concept of a pneumatic, skill-independent, self-propelling, self-navigating colonoscope in a pig model. *Endoscopy* 2006; **38**:144-8.

[93] Vucelic B, Rex D, Pulanic R, Pfefer J, Hrstic I, Levin B, Halpern Z, Arber N. The Aer-O-Scope: Proof of concept of a pneumatic, skill-independent, self-propelling, self-navigating colonoscope. *Gastroenterology* 2006; **130**: 672-7.

[94] Eickhoff A, Jakobs R, Kamal A, Mermash S, Riemann JF, van Dam J. In vitro evaluation of forces exerted by a new computer-assisted colonoscope (the NeoGuide Endoscopy System). *Endoscopy* 2006; **38**:1224-9.

[95] Van Dam J, Eickhoff A, Jakobs R, Kudis V, Hartmann D, Riemann JF. Computer-assisted colonoscopy (the NeoGuide System): results of the first human clinical trial. *Gastrointest Endosc* 2006; **63**:Ab100.

[96] Eickhoff A, Van Dam J, Jakobs R, Kudis V, Hartmann D, Damian U, Weickert U, Schilling D, Riemann JF. Computer-assisted colonoscopy (The NeoGuide Endoscopy System): Results of the first human clinical trial ("PACE study"). *Am J Gastroenterol* 2007; **102**: 261-66.

[97] Shah SG, Brooker JC, Williams CB, Thapar C, Saunders BP. Effect of magnetic endoscope imaging on colonoscopy performance: a randomised controlled trial. *Lancet* 2000; **356**: 1718-22.

[98] Saunders BP, Bell GD, Williams CB, Bladen JS, Anderson AP. First clinical-results with a real-time, electronic imager as an aid to colonoscopy. *Gut* 1995; **36**:913-7.

[99] Sato K, Fujinuma S, Sakai Y. Evaluation of the looping formation and pain during insertion into cecum in colonoscopy. *Dig Endosc* 2006; **18**:181-7.

[100] Mosse CA, Mills TN, Bell GD, Swain CP. Device for measuring the forces exerted on the shaft of an endoscope during colonoscopy. *Med Biol Eng Comput* 1998; **36**:186-90.

[101] Kim JS, Sung IH, Kim YT, Kim DE, Jang YH. Analytical model development for the prediction of the frictional resistance of a capsule endoscope inside an intestine. *J Eng Med* 2007; **221**:837-45.

[102] Wang KD, Yan GZ. Research on measurement and modeling of the gastro intestine's frictional characteristics. *Meas Sci Technol* 2009; **20**:1-6.

[103] Choi J. Design and development of a minimally invasive endoscope: highly flexible stem with large deflection and stiffenable.exoskeleton structure. *Ph.D Dissertation, Virgina Polytechnic Institute & State University,* 2006.

[104] Plaut RH, Mroz Z. Uni-directional buckling of a pinned elastica with external pressure. *Int J Solids Struct* 1992; **29**:2091-100.

[105] Plaut RH, Suherman S, Dillard DA, Williams BE, Watson LT. Deflections and buckling of a bent elastica in contact with a flat surface. *Int J Solids Struct* 1999; **36**:1209-29.

[105] Plaut RH, Williams NL, Dillard DA. Elastic Analysis of the loop tack test for pressure sensitive adhesives. *J Adhesin* 2001; **76**:37-53.

[107] Plaut RH, Taylor RR, Dillard DA. Postbuckling and vibration of a flexible strip clamped at its ends to a hinged substrate. *Int J Solids Struct* 2004; **41**:859-70.

[108] Cotin S, Duriez C, Lenoir J, Neumann P, Dawson S. New approaches to catheter navigation for interventional radiology simulation. *The 8th International Conference on Medical Image Computing and Computer-Assisted Intervention*, 26 Oct. 2005 to 30 Oct. 2005, Palm Springs, CA, USA.

[109] Kukuk M. A model-based approach to intraoperative guidance of flexible endoscopy. *PhD Thesis, Universität Dortmund***,** 2002.

[110] Shabana AA. Dynamcis of multibody systems. *John Wiley & Sons*, New York, 1989.

[111] Shabana AA. Flexible multibody dynamics: review of past and recent developments. *Multibody Syst Dyn* 1997; **1**: 189-222.

[112] Likins PW. Modal method for analysis of free rotations of spacecraft, *AIAA J* 1967; **5**(7):1304-08.

[113] Dawson SL, Cotin S, Meglan D, Shaffer DW, Ferrell MA. Designing a computer-based simulator for interventional cardiology training, *Catheter Cardio Inte* 2000; **51**: 522-27.

[114] Shabana AA. Computer implementation of the absolute nodal coordinate formulation for flexible multibody dynamics. *Nonlinear Dynamics* 1998; **16**:293-306.

[115] Shabana AA, Dynamics of Multibody Systems. *Cambridge University Press*, 1998.

[116] Terzopoulos D, Platt J, Barr A, Fleischer K. Elastically deformable models. *Computer Graphics* 1987; **21**(4):205-14.

[117] Qin H, Terzopoulos D. D-NURBS: A physics-based framework for geometric design. *IEEE T Vis Comput Gr* 1996; **2**(1): 85-96.

[118] Nocent O, R´emion Y. Continuous deformation energy for dynamic material splines subject to finite displacements. *Proceedings of the eurographic workshop on computer animation and simulation (ACM)*. New York (NY, USA) 2001; 88-97.

[119] Rem´ion Y, Nourrit JM, Gillard D. Dynamic animation of spline like objects. *J Visual Comp Animat* 1999*;* **11**(1): 17-26

[120] Lenoir J, Meseure P, Grisoni L, Chaillou C. Surgical thread simulation. *In MS4CMS* 2002; **12:**02-107.

[121] Lenoir J, Meseure P, Grisoni L, Chaillou C. A suture model for surgical simulation. *The 2nd international symposium on medical simulation* 2004;105-13.

[122] Lenoir J, Grisoni L, Meseure P, Chaillou C. Adaptive resolution of 1d mechanical B-spline. *Graphite*. Dunedin (New Zealand) 2005; 395-403.

[123] Walsum TV. Deformable B-splines for Catheter Simulation. *Computer Assisted Radiology and Surgery* (CARS'99), 1999.

[124] Theetten A, Grisoni L, Andriot C. Barsky B. Geometrically exact dynamic splines. *Comput Aided Des* 2008; **40**: 35-48.

[125] Valentini PP, Pennesti E. Modeling elastic beams using dynamic splines. *Multibody Syst Dyn* 2011; **25**: 271-84.

[126] Shinya M. Theories for mass-spring simulation in computer graphics: stability, costs and improvements. *Ieice T Inf Syst* 2005; **88**(4):767-74.

[127] Wasfy TM. A torsional spring-like beam element for the dynamic analysis of flexible multibody systems. *Int J Numer Meth Eng* 1996; **39**: 1079-96.

[128] Mollemans W, Schutyser F, Cleynenbreugel J, Suetens P. Fast soft tissue deformation with tetrahedral mass spring model for maxillofacial surgery planning systems. *Lecture Notes in Computer Science* (MICCAI) 2004; **3217**:371-79.

[129] Mollemans W, Schutyser F, Cleynenbreugel J, Suetens P. Tetrahedral mass spring model for fast soft tissue deformation. *Lecture Notes in Computer Science* (MICCAI) 2003; **2673**: 145-54.

[130] Mollemans W, Schutyser F, Cleynenbreugel J, Suetens P. Very fast soft tissue predictions with mass tensor model for maxillofacial surgery planning systems. *In: Proceedings of CARS* 2005; 491-96.

[131] Hong M, Jung S, Choi M, Welch SW. Fast volume preservation for a mass-spring system. *IEEE Comput Graph Appl* 2006; **26**(5):83-91.

[132] Raghupathi L, Grisoni L, Faure F, Marchal D, Cani M, Chaillou C. An intestinal surgery simulator: real-time collision processing and visualization. *IEEE Trans Visual Comput Graphics* 2004; **10**(6):708-718.

[133] France L, Lenoir J, Angelidis A, Meseure P, Cani M, Faure F, Chaillou C. A layered model of a virtual human intestine for surgery simulation. *Med Image Anal* 2005; **9**(2):123-32.

[134] Nealen A, Mu¨ ller M, Keiser R, Boxerman E, Carlson M. Physically Based Deformable Models in Computer Graphics. *Computer Graphics Forum* 2006; **25**(4):809-836.

[135] Phungpaingam B, Athisakul C, Chucheepsakul S, Large deflections of spatial variable-arc-length elastica under terminal forces, *Struct Eng Mech* 2009; **4**:501-16.

[136] Goyal S, Perkins NC, Lee CL, Nonlinear dynamics and loop formation in Kirchhoff rods with implications to the mechanics of DNA and calbes, *J Comput Phys* 2005; **209**:371-89.

[137] Klapper I. Biological applications of the dynamics of twisted elastic rods, *J Comput Phys* 1996; **125**: 325-37.

[138] Schlick T. Modeling superhelical DNA: recent analytical and dynamic approaches, *Curr Opin Struct Biol* 1995; **5**:245-62.

[139] Olson WK. Simulating DNA at low resolution, *Curr Opin Struct Biol* 1996; **6**: 242-56.

[140] Goyal S, Perkins NC, Lee CL, Torsional buckling and writhing dynamics of elastic cables and DNA, *Proceedings of ASME 2003 Design Engineering and Technical Conference*, 2002; Chicago, USA.

[141] Yin H, Wang MD, Svoboda K, Landick R, Block SM, Gelles J, Transcription against an applied force, *Science* 1995; **270**:1653-57.

[142] Finzi L, Gelles J, Measurement of lactose repressor-mediated loop formation and breakdown in single DNA molecules, *Science* 1995; **267**: 378-80.

[143] Mehta RA, Kahn JD, Designed hyperstable lac repressor DNA loop topologies suggest alternative loop geometries, *J Mol Biol* 1999; **294**:67-77.

[144] Smith SB, Cui YJ, Bustamante C, Overstretching B-DNA: the elastic response of individual double-stranded and singlestranded DNA molecules, *Science* 1996; **271**:795-98.

[145] Katopodes FV, Barber JR, Shan Y, Torsional deformation of an endoscope probe, *P Roy Soc London* 2001; **457**(2014): 2497-2506.

[146] Lu CL, Perkins NC, Complex spatial equilibria of U-joint supported cables under torque, thrust and self-weight, *Int J Non-Linear Mech* 1995; **30**: 271-85.

[147] Love AEH, A Treatise on the Mathematical Theory of Elasticity, *Dover Publications*, New York, 1927.

[148] Pai D. Strands: Interactive simulation of thin solids using cosserat models. *Eurographics* 2002; **21**(3):347-52.

[149] Spillmann J, Teschner M. CORDE: cosserat rod elements for the dynamic simulation of one-dimensional elastic objects. *Eurographics/ACM Siggraph Symposium on Computer Animation* 2007; 1-10.

[150] Chen HH, Lin WY, Hsiao KM. Co-rotational finite element formulation for thin-walled beams with generic open section. *Int J Numer Meth Eng* 2006; **195**:2334-70.

[151] Felippa CA. A systematic approach to the element-independent corotational dynamics of finite elements, *Report No. CU-CAS-00-03*, University of Colorado, 2000.

[162] Linn J, Stephan T, Carlsson J, Bohlin R. Fast simulation of quasistatic rod deformations for VR applications. *In: Progress in Industrial Mathematics at ECMI* 2007; 247-53.

[153] Bergou M, Wardetzky M, Robinson S, Audoly B, Grinspun, E. Discrete elastic rods. *ACM Transactions on Graphics (SIGGRAPH)* 2008; **27**:(3)1-63

[154] Chang J, Shepherd D, Zhang JJ. Cosserat-beam-based dynamic response modelling. *Comput Anim Virtual Worlds* 2007; **18**:(4-5) 429-36.

[155] Altenbach J, Altenbach H, Eremeyev VA. On generalized Cosserat-type theories of plates and shells: a short review and bibliography, *Arch Appl Mech* 2010; **80**:73-92.

[156] Manning RS, Maddocks JH, A continuum rod model of sequence dependent DNA structure. *J Chem Phys*1996; **105:**5626-46.

[157] Cosserat E, Cosserat F. Sur la théorie de l'elasticité. *Ann Toulouse* 1896; **10**:1-116.

[158] Cosserat E, Cosserat F. Théorie des corps déformables. *Herman et Fils*, Paris ,1909.

[159] Grégoire M, Schömer E. Interactive simulation of one-dimensional flexible parts. *Comput Aided Des* 2007; **39**(8): 694-707.

[160] Antman SS. Nonlinear Problems of Elasticity. *Springer Verlag*, 1995.

[161] Poon A. Real time simulation of colonoscopy using dynamic models, *Ph.D. dissertation*, Imperial College of Science, Technology and Medicine, 1991.

[162] Hellier D. Determination of colonoscope's structure properties for interactive simulation of colonoscopy. *Master Thesis*. The University of Queensland, 2010.

[163] Körner O. Development of a computer-based training simulator for colonoscopy with active force-feedback. *Ph.D. dissertation*, Universität Mannheim, Fakultät für Mathematik und Informatik, 2003.

[164] Körner O, Männer R. Implementation of a haptic interface for a virtual reality simulator for flexible endoscopy. *The 11th Symposium on Haptic Interfaces for Virtual Environment and Teleoperator Systems* (HAPTICS'03) 2003; 278-284.

[165] Konings MK, van de Kraats EB, Alderliesten T, Niessen WJ. Analytical guide wire motion algorithm for simulation of endovascular interventions. *Med Biol Eng Comput* 2003; **41**(6):689-700.

[166] Ikuta K. Virtual Endoscope System with Force Sensation. *IEEE International Conference on Robotics and Automation* 1999; **4**:1715-21.

[167] Ikuta K. Portable Virtual Endoscope System with Force and Visual Display for Insertion Training. *Medical Image Computing and Computer-Assisted Intervention- MICCAI* 2000 ; **1935**:907-20.

[168] Kukuk M, Geiger B. A real-time deformable model for flexible instruments inserted into tubular structures. *Medical Image Computingand Computer-Assisted Intervention* 2002; **2489**: 331-38.

[169] Kukuk M. A model-based approach to intraoperative guidance of flexible endoscopy. *Ph.D. dissertation*, Universität Dortmund, 2002.

[170] Przemieniecki JS. Theory of matrix structural analysis. *Dover Publications*, 1985.

[171] Bathe KJ. Finite element procedures. *Prentice-Hall: Englewood-Cliffs 1*996.

[172] Ghali B. Algorithms for nonlinear finite element-based modeling of soft-tissue deformation and cutting. *Master Thesis*, McMaster University, 2008.

[173] Nakao K, Kuroda T, Oyama H, Sakaguchi G, Komeda M. Physicsbased simulation of surgical fields for preoperative strategic planning. *J Med Syst* 2006; **30**: 371-380.

[174] Delingette H, Ayache N. Hepatic surgery simulation. *Communications of the ACM* 2005; **48**:31-36.

[175] Wang P, Becker A, Jones I, Glover A, Benford S, Greenhalgh C, Vloeberghs M. Virtual reality simulation of surgery with haptic feedback based on the boundary element method. *Comput & Struct* 2007; **85**:331-39.

[176] Hansen K, Brix L, Pedersen C, Haase J, Larsen O. Modelling of interaction between a spatula and a human brain. *Med Image Anal* 2004; **8**: 23-33.

[177] Cotin S, Delingette H, Ayache N. A hybrid elastic model for real-time cutting, deformations, and force feedback for surgery training and simulation. *The Visual Comput* 2000; **16**:437-52.

[178] Frank A, Twombly I, Barth T, Smith J. Finite element methods for real time haptic feedback of soft-tissue models in virtual reality simulators. *Proceedings of the Virtual Reality 2001 Conference (VR'01)* 2001; 257-63.

[179] Bro-Nielsen M. Finite element modeling in surgery simulation. *Proceedings of the IEEE: special issue on surgery simualtion*1998; **86**:490-503.

[180] Wu X, Downes M, Goktekin T, Tendick F. Adaptive nonlinear finite elements for deformable body simulation using dynamic progressive meshes. *Comput Graphics Forum* 2001; **20**: 349-58.

[181] Picinbono G, Delingette H, Ayache N. Non-linear anisotropic elasticity for real-time surgery simulation. *Graphical Models* 2003; **65**:305-21.

[182] Tillier Y, Paccinia A, Delottea J, Revillea MD, Chenota JL. Finite element modelling for soft tissues surgery based on nonlinear elasticity behaviour. *International Congress Series* 2004; **1268**: 384-89.

[183] Satava RM. Virtual reality surgical simulator. *Surg Endosc* 1993; **7:**203-05.

[184] Miller K, Chinzei K, Orssengo G, Bednarz P. Mechanical properties of brain tissue in-vivo: experiment and computer simulation. *J Biomech* 2000; **33**:1369-76.

[185] Miller K, Chinzei K. Constitutive modelling of brain tissue: experiment and theory. *J Biomech* 1997; **30**:1115-21.

[186] Miller K, Taylor Z, Wittek A. Mathematical models of brain deformation behavior for computer-integrated neurosurgery. *Research Report ISML*, The University of Western Australia, 2006.

[187] Miller K, Chinzei K. Mechanical properties of brain tissue in tension. *J Biomech* 2002; **35:** 483-90

[188] Wittek A, Laporte J, Miller K. Computing reaction forces on surgical tools for robotic neurosurgery and surgical simulation. *Proceedings of the Australasian Conference on Robotics and Automation* 2004; 1-8.

[189] Gao C, Tay FH, Nowinski WL. A finite element method based deformable brain atlas suited for surgery simulation," *Proceedings of the 2005 IEEE Engineering in Medicine and Biology 27th Annual Conference* 2005; 4337-40.

[190] Belytschko T. A survey of numerical methods and computer programs for dynamic structural analysis. *Nucl Eng Des* 1976; **37**:23-34.

[191] Wasfy TM, Noor AK. Computational strategies for flexible multibody systems. *Appl* Mech Rov 2003; **56**(6): 553-97.

[192] Fenner RT, Finite element methods for engineers, *Imperial College Press*, 1996.

[193] Zupan D, Saje M. The three-dimensional beam theory: finite element formulation based on curvature, *Computers & Structures* 2003; **81**:1875-88.

[194] Anderson JH, Raghavan R. A vascular catheterization simulator for training and treatment planning. *J Digit Imaging* 1998; **11**(1): 120-23.

[195] Chui CK, Nguyen HT, Wang YP, Mullick R, Raghavan R, Anderson JH. Potential field of vascular anatomy for realtime computation of catheter navigation. *First Visible Human Conference*, 1996; Bethesda, MD, USA.

[196] Cotin S, Duriez C. Lenoir J, Neumann P, Dawson S. New approaches to catheter navigation for interventional radiology simulation. *Med Image Comput Comput Assist Interv* 2005; **8**: 534-42.

[197] Lenoir J, Cotin S, Duriez C, Neumann P. Interactive physically-based simulation of catheter and guidewire, *Computers & Graphics* 2006; **30**: 416-22.

[198] Liu CH. A finite element based dynamic modeling method for design analysis of flexible multibody systems *Ph.D Dissertation*. Georgina Institute of Technology, 2010.

[199] Rao SS. The finite element method in engineering (4th edition). *Elsevier Butterworth-Heinemann*, 2005.

[200] Nemirovskii ME, Kuz´min AI. Investigation of the flexural and torsional rigidity of flexible elements of endoscopes. *Biomed Eng* 1984; **18**: 214-17.

[201] Nemirovskii ME. Torsional rigidity of outer sheaths of flexible medical endoscopes. Biomed Eng 1994; **28**:(5) 262-64.

[202] Nemirovskii ME. Bending rigidity testing of outer envelopes of flexible medical endoscopes. *Biomed Eng* 1993; **27**:(4) 224-28.

[203] Brooker JC, Saunders BP, Shah SG, Williams CB. A new variable stiffness colonoscope makes colonoscopy easier: a randomised controlled trial. *Gut* 2000; **46**: 801-05.

[204] Wehrmeyer JA, Barthel JA, Roth JP, Saifuddin T. Colonoscope flexural rigidity measurement, *Med and Biol Eng Comput* 1998; **36**:475-79.

[205] Bell GD, Burn K. Measurement of the stiffness of endoscopes a plea for commonality. *Gut* 2001; **49:**154.

[206] Dogramadzi S, Burn K, Bicker R, Bell GD. The effect of temperature on the flexural rigidity of various commercially available colonoscopes and gastroscopes. *Gut* 2002; **50**: a41.

[207] Burn K, Bicker R, Bell D. A novel system to rapidly analyse the flexural rigidity of endoscopes used in colonoscopy and flexible sigmoidoscopy. *Int J COMADEM* 2003; **6**:23-32.

[208] Hellier D, Albermni F, Evans B, Visser H, Adam C, Passeger J. Flexural and torsional rigidity of colonoscopes at room and body temperatures. *Proc. IMechE Part H: J Eng Med* 2011; **225:**389-99.

[209] Adhikari S. Damping models for structural vibration. *PhD dissertation, University of Cambridge*, 2000.

[210] Chowdhury I, Dasgupta SP. Computation of Rayleigh damping coefficients for large systems. *Electron J Geotech Eng* 2003; **8**:1-11.

[211] Ramamurti V, Mithun S, Prabhakar N, Sukumar T. Experimental determination of damping ratios at higher modes for use in modal superposition. *J Eng Tech Res* 2012; **4**(6):114-28.

[212] Ramamurti V. Finite Element Method in Machine Design. *Alpha Sciences International, London*; 2012.

[213] Ewins DJ. Modal Testing: Theory and Practice. *Research Studies Press Ltd*., 1984.

[214] Ehnes CW. Damping in stiffener welded structures. *Master Thesis, Naval Postgraduate School*, 2003.

[215] Ju SH, Ni SH. Determining Rayleigh damping parameters of soil for finite element analysis. *Int J Numer Anal Meth Geomech* 2007; **31**:1239-55.

[216] Sergio CG, Gregorio LB. Dynamic analysis of olive trees in intensive orchards under forced vibration. *Trees* 2008; **22**:795-802.

[217] Guo YF, Xu WC, Fu YF, Zhang W. Comparison studies on dynamic packaging properties of corrugated paperboard pads. *Engineering* 2010; **2**:378-86.

[218] Hatch MR. Virbration simulation using Matlab and analysis (1st edition). *Chapman and* Hall/CRC, 2000.

[219] Yamada H. Yamada Strength of Biological Materials (2nd edition), Williams and Watkins, Baltimore, 1972.

[220] Fung YC. Biomechanics: mechanical properties of living tissues, 2rd Ed. Springer-Verlag, New York, 278-79, 1993.

[221] Dario P, Ciarletta P, Menciassi A, Kim B. Modeling and experimental validation of the locomotion of endoscopic robots in the colon. *Int J Robot Res* 2009; **23**:5540-45.

[222] Shu Q, Freeman Q, Gill HS. Probiotic treatment using Bifidobacterium lactis HN019 reduces weanling diarrhea associated with rotavirus and Escherichia coli infection in a piglet model. *J Pediatr Gastr Nutr* 2001; **33**:171-77.

[223] Asrar FM, O'Connor DL. Bacterially synthesised folate and supplemental folic acid are absorbed across the large intestine of piglets. *J Nutr Biochem* 2005; **16**:587-93.

[224] Crump MH. A comparison of the structure and function of the large intestine in man (homo sapiens), dog (canis familiaris) and pig (susdomesticus). In: Stevens CE, Ed. Literature Reviews of Selected Topics in Comparative Gastroenterology. *New York: New York State Veterinary College*, 1-24, 1975.

[225] Gilardi G, Sharf I. Literature survey of contact dynamics modeling. *Mech Mach Theory* 2002; **37**: 1213-39.

[226] Modarres N, Kovecses SA, Angles J. A comparative study of approaches to dynamics modeling of contact transitions in multibody system. *2005 ASME International Design Engineering Technical Conferences*, *DETC2005-85418, Long Beach, California, USA*, 2005; 1-10.

[227] Duriez C, Dubois F, Kheddar A, Andriot C. Realistic haptic rendering of interacting deformable objects in virtual environments. *IEEE Trans Vis Comput Graph* 2006; **12**:(1) 36-47.

[228] Adachi Y, Kumano T, Ogino K. Intermediate representation for stiff virtual objects. *Proc Virtual Reality Ann Int'l Symp (VRAIS '95)* 1995; 203-210.

[229] Mark WR, Randolph SC, Finch M, Van Verth JM, Taylor II RM. Adding force feedback to graphics systems: issues and solutions. *Proc Conf Computer Graphics and Interactive Techniques*, 1996; 447-52.

[230] Garre C, Otaduy MA. Haptic rendering of complex deformations through handle-space force linearization. *Proc World Haptics Conf* 2009; 422-27.

[231] Forest C, Delingette H, Ayache N. Surface contact and reaction force models for laparoscopic simulation. *Medical Simulation, Lecture Notes in Computer Science* 2004; **3078**:168-76.

[232] Otaduy MA, Gross M. Transparent rendering of tool contact with compliant environments. *Proc Second Joint EuroHaptics Conf and Symp Haptic Interfaces for Virtual Environment and Teleoperator Systems*, 2007; 225-30.

[233] Garre C, Otaduy MA. Toward haptic rendering of full-hand touch. *Proc CEIG (Spanish Computer Graphics Conf)* 2009; 422-27.

[234] Saupin G, Duriez C, Cotin S. Contact model for haptic medical simulations. *ISBMS '08: Proc Fourth Int'l Symp Biomedical Simulation*, 2008;157-65.

[235] Lin MC, Otaduy MA. Haptic rendering foundations, algorithms, and application. *A K Peters Ltd. Wellesley*, Massachusetts, 2008.

[236] Moreau JJ, Jean M. Numerical treatment of contact and friction: the contact dynamics method. *Eng Systems Design and Analysis* 1996; **4**: 201-08.

[237] Mahvash M, Hayward V. High-fidelity haptic synthesis of contact with deformable bodies. *IEEE Comput Graph Appl* 2004; **24**: 48-55.

[238] Jourdan F, Alart P, Jean M. A gauss-seidel like algorithm to solve frictional contact problems. *Compute Method Appl Mech Eng* 1991; **92**: 353-75.

[239] Liu T, Wang MY. Computation of three-dimensional rigid-body dynamics of multiple contacts using time-stepping and gauss-seidel methods. *IEEE Trans Autom Sci Eng* 2005; **2**:(1)19-31.

[240] Alart P, Curnier A. A mixed formulation for frictional contact problems prone to Newton like solution method. *Compute Method Appl Mech Eng* 1998; **155**: 33-47.

[241] Louis Y, Korman LY, Egorov V, Tsuryupa S, Corbin B, Anderson M, Sarvazyan N, Sarvazyan A. Characterization of forces applied by endoscopists during colonoscopy by using a wireless colonoscopy force monitor. *Gastrointest Endosc* 2010; **71**(2): 327-34.

APPENDIX A

Calculation for the Critical Load of the Rod Model

The critical load of the rod model was adapted from Ref. [27]:

$$F_{cr} = \frac{4\pi^2 EI \cos^3 \vartheta}{L^2(1+3\cos^2 \vartheta)} \tag{A.1}$$

where

L : length of the rod;

ϑ : spiral angel; and

EI : flexural rigidity of the rod.

Based on the geometrical parameters of the scope in the sigmoid colon, given L = 35 cm, ϑ = 45^0, and the flexural rigidity EI = 400 N·cm^2 [100], the critical load of the scope is approximately equal to 1.82 N.

APPENDIX B

Normal Load to Overcome Frictional Force and Fluid Resistance

Friction force of the scope can be expressed as the sum of the components as shown in Eq. (B.1) [100]:

$$F = F_w + F_s + F_p \tag{B.1}$$

where

F_w: frictional force associated with weight of insertion tube;

F_s: frictional force induced by the stress due to the viscoleastic deformation of the intestine wall; and

F_p : frictional force induced by the stress due to fluid resistance.

The diameter of the insertion tube of the scope is about 13.6 mm, and site of the least diameter of the entire colon located at the junction site of the sigmoid-descending colon is about 25 mm; thus, there is no significant frictional force induced by stress due to the small viscoelastic deformation of the intestine. The friction component F_p is not considered because fluid resistance generated from inside the intestine is very small. Therefore, only the frictional force associated with the weight of the insertion tube of the scope is considered. The weight of a 35cm-length of insertion

tube is about 4 N, so the frictional force is $F_w \approx 1\,\mathrm{N}$. The load needed to overcome the friction and fluid resistance is about 1 N.

APPENDIX C

Quasi-Static Frictional Force from Colonoscope

The rectum-sigmoid and sigmoid-descending segments both have small curvatures with an "S"-shaped profile. A looped scope generates quasi-static forces against the intestinal wall. When the scope is advanced, this quasi-static force becomes the frictional force. Thus, the quasi-static force created by a looped scope should be considered.

Choi [103] analyzed an endoscope's elastics in an exoskeleton structure, and derived Eq. (C.1) with regard to distributed force along a segment of a stem based on Plaut's works [104-107].

$$D = EI\frac{d^3\theta}{dl^3} + N\frac{d\theta}{dl} + \frac{EI}{2}\left(\frac{d\theta}{dl}\right)^3 \tag{C.1}$$

where $N(l)$ is the normal force at position l, D is the distributed force on dl that is an infinitesimal length of the stem, $d\theta$ is an infinitesimal angle along dl at the center of radius or curvature, and EI is the flexural rigidity of the stem.

To simplify Eq. (C.1), a quadrant shape of a looped colonoscope is studied to obtain the quasi-static force along the colon as shown in Figure C.1. The corresponding boundary conditions are applied to Eq. (C.1). To solve for the quasi-static force along the looped colonoscope, the following parameters are defined:

Q: quasi-static force along the colonoscope;

S: given length of the colonoscope; and

r: radius of curvature of looped colonoscope.

Applying initial normal force $N = 0$ and $dl = rd\theta$ leads to

$$D = EI\left(\frac{d^3\theta}{dl^3} + \frac{1}{2r^3}\right) \tag{C.2}$$

Three boundary conditions were applied to integrate Eq. (C.2) based on the moment M and shear force τ at the free end of the scope, as shown in Eq. (C.3)

$$\begin{cases} M = EI\dfrac{d\theta}{dl} \\ \tau = EI\dfrac{d^2\theta}{dl^2} \end{cases} \tag{C.3}$$

At the free end of the scope (l_{end}), moment M and shear force τ are equal to zero, leading to

$$\begin{cases} \left.\dfrac{d\theta}{dl}\right|_{l=l_{end}} = 0 \\ \left.\dfrac{d^2\theta}{dl^2}\right|_{l=l_{end}} = 0 \end{cases} \tag{C.4}$$

At the clamped end of the scope, $l = 0$, so the third boundary condition is $\theta_{l=0} = 0$. Integrating Eq. (C.2) into the 2nd ordinary differential equation leads to

$$\frac{d^2\theta}{dl^2} = \left(\frac{D}{EI} - \frac{1}{2r^3}\right)l + c_1 \tag{C.5}$$

Using boundary condition Eq. (C.4) to find constant $c_1 = -l_{end}\left(\dfrac{D}{EI} - \dfrac{1}{2r^3}\right)$ leads to

$$\frac{d^2\theta}{dl^2} = \left(\frac{D}{EI} - \frac{1}{2r^3}\right)l - l_{end}\left(\frac{D}{EI} - \frac{1}{2r^3}\right) \tag{C.6}$$

Integrating Eq. (C.6) using the other boundary condition leads to

$$\theta(l) = \left(\frac{l^3}{6} - l_{end} \frac{l^2}{2} + l_{end}^2 \frac{l}{2} \right) \left(\frac{D}{EI} - \frac{1}{2r^3} \right) \tag{C.7}$$

Given length S to find the disturbed force along $l \in (0, S)$, let $l = S$. At the free end of the scope, l_{end} is the total length of the scope. Substituting $l = S$ and $l_{end} = S$ into Eq. (C.7) to find distributed force D along given length S of the scope leads to

$$D = EI \left(\frac{6\theta}{S^3} + \frac{1}{2r^3} \right) \tag{C.8}$$

The quasi-static force of the looped scope is obtained as

$$Q = EI \left(\frac{6\theta}{S^2} + \frac{S}{2r^3} \right) \tag{C.9}$$

$$S = r\theta \tag{C.10}$$

Therefore, the frictional force F_f induced by the quasi-static force is expressed by

$$F_f = \frac{\mu EI}{r^2} \left(\frac{12 + \theta^2}{2\theta} \right) \tag{C.11}$$

where μ is the dynamic frictional coefficient and θ is a function of length l.

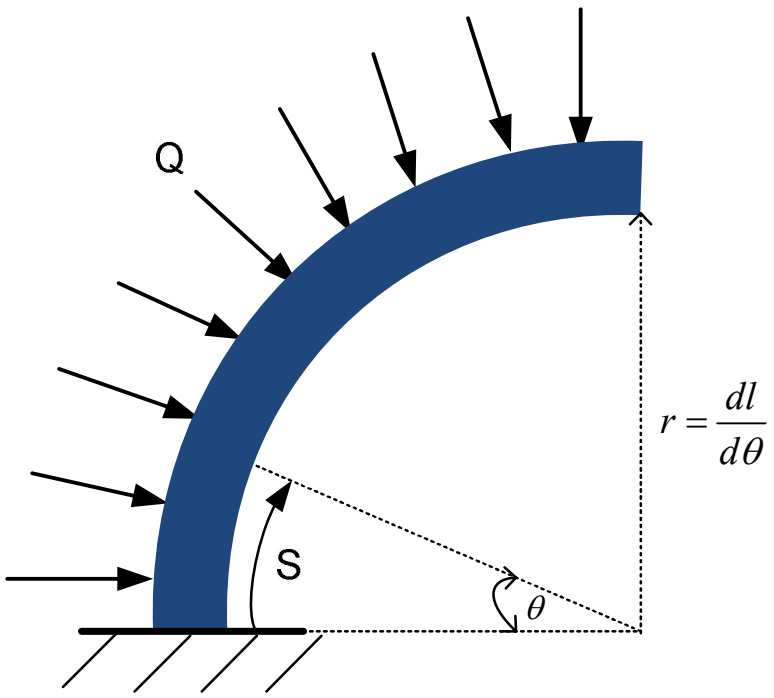

Figure C.1 Quasi-static force along a looped colonoscope with a quadrant

APPENDIX D

Elongation of Intestinal Wall

Capsular endoscope generates frictional force F_f on the intestinal wall that causes the elongation of the intestinal wall. As a matter of fact, both the intestinal wall and the mesentery have the same elongation; thus, the elongation of the mesentery is equivalent to that of the intestinal wall (see Figure D.1).

In the following, σ_{xc} is stress of the intestinal wall along the length of the capsular endoscope; σ_{xm} is stress of the mesentery along the length of the capsular endoscope, leading to

$$\sigma_{xc} \cdot t_c \cdot \pi \cdot d_c + \sigma_{xm} \cdot t_m \cdot h = F_f \tag{D.1}$$

where t_c and t_m are the thickness of intestine and mesentery, repectively, and h is the mesenteric transversal length.

Eq. (D.2) refers to Ref. [221], leading to

$$\begin{cases} \sigma_{xc} = b_{xc}\varepsilon^2_{xc} + d_{xc}\varepsilon_{xc} \\ \sigma_{xm} = b_{xm}\varepsilon^2_{xm} + d_{xm}\varepsilon_{xm} \end{cases} \tag{D.2}$$

Substituting Eq. (D.2) into Eq. (D.1) leads to

$$(b_{xc}\varepsilon^2_{xc} + d_{xc}\varepsilon_{xc}) \cdot t_c \cdot \pi \cdot d_c + (b_{xm}\varepsilon^2_{xm} + d_{xm}\varepsilon_{xm}) \cdot t_m \cdot h = F_f \tag{D.3}$$

$$\varepsilon_{xc} = \varepsilon_{xm} = \Delta l / L \tag{D.4}$$

where L is the length of capsular endoscope.

Substituting Eq. (D.4) into Eq. (D.3) leads to

$$\left\{ b_{xc} \left(\frac{\Delta l}{L} \right)^2 + d_{xc} \left(\frac{\Delta l}{L} \right) \cdot t_c \cdot \pi \cdot d_c + b_{xm} \left(\frac{\Delta l}{L} \right)^2 + d_{xm} \left(\frac{\Delta l}{L} \right) \cdot t_m \cdot h \right\} = F_f \tag{D.5}$$

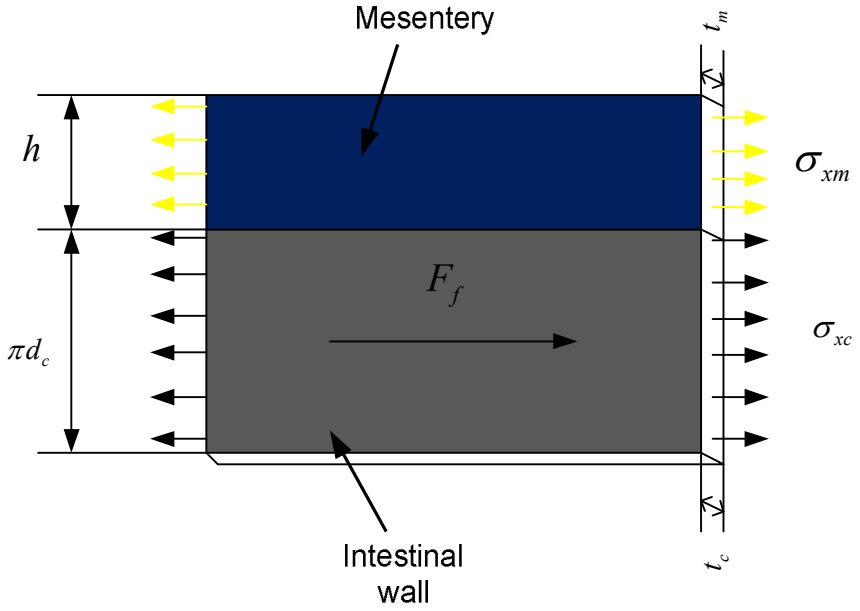

Figure D.1 Frictional force acting along the length of intestinal wall and its mesentery

APPENDIX E

Stiffness Matrix of a Beam Element

The derivation of the stiffness matrix k_e of the beam element is attributed in Ref. [170]. The beam element has axial forces S_1 and S_7, shearing forces S_2, S_3, S_8 and S_9, bending moments S_5, S_6, S_{11} and S_{12}, and twisting moments (torques) S_4 and S_{10} as shown in Figure E.1. The corresponding displacements $u_1,...,u_{12}$ are along with these forces and moments. Thus, the stiffness matrix of the beam element is on the order of 12×12.

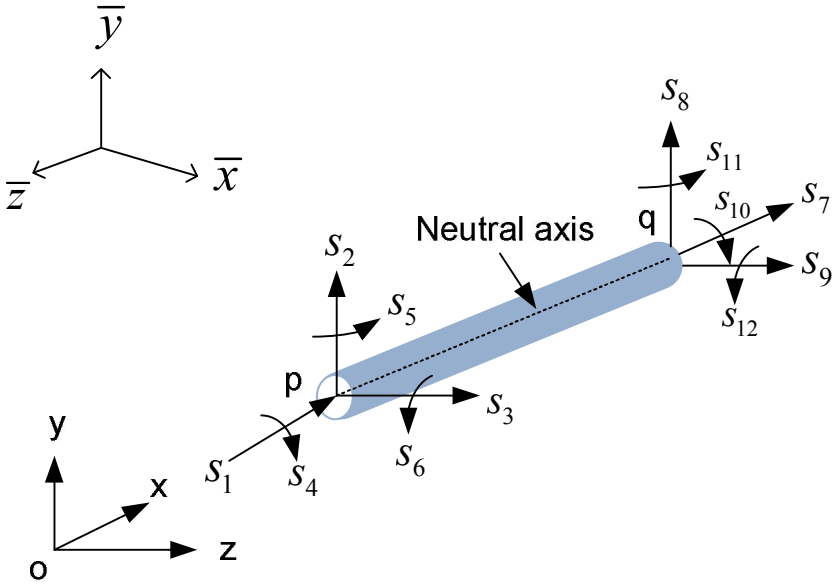

Figure E.1 Beam element

(i) For the Axial forces (S_1 and S_7)

The differential equation for the axial displacement u is shown in Figure E2 (a) is:

$$S_1 = -\left(\frac{du}{dx}\right)EA \tag{E.1}$$

Integrating Eq. (E.1) leads to

$$S_1 x = -uEA + C_1 \tag{E.2}$$

where C_1 is a constant.

The boundary conditions:

$$\begin{cases} u = u_1 \ \ at\ x = 0; \\ u = 0 \ \ at\ x = l. \end{cases} \tag{E.3}$$

Hence:

$$C_1 = S_1 l \tag{E.4}$$

Eqs. (E.2) and (E.4) and taking $x = 0$ lead to

$$S_1 = \frac{EA}{l} u_1 \tag{E.5}$$

$$S_1 = -S_7 \tag{E.5}$$

Hence:

$$\begin{cases} k_{11} = \dfrac{S_1}{u_1} = \dfrac{EA}{l} \\ k_{71} = \dfrac{S_7}{u_1} = \dfrac{-EA}{l} \end{cases} \tag{E.6}$$

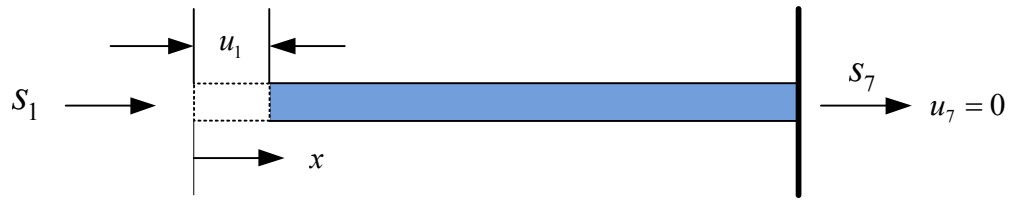

(a)

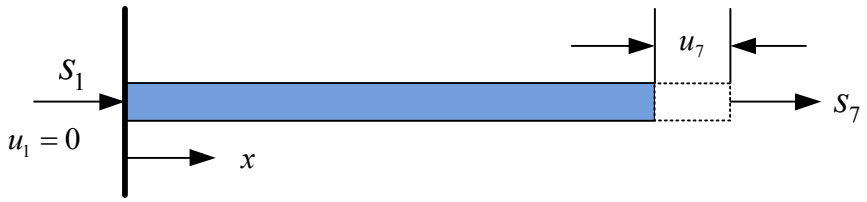

(b)

Figure E.2 Axial forces S_1 and S_7

(ii) For the Twisting moment (S_4 and S_{10})

The differential equation for the twist θ as shown in Figure E.3 (a)

$$S_4 = -GJ\frac{d\theta}{dx} \tag{E.7}$$

where GJ is the torsional stiffness of the cross section of the beam;

Integrating Eq. (E.9) leads to

$$S_4 x = -GJ\theta + C_1 \tag{E.8}$$

The boundary conditions: $\theta = 0$ at $x = l$; evaluating the boundary condition leads to

$$C_1 = S_4 l \tag{E.9}$$

The boundary conditions: $\theta = u_4$ at $x = 0$; evaluating the boundary condition leads to

$$S_4 = \frac{GJ}{l} u_4 \tag{E.10}$$

$$S_{10} = -S_4 \tag{E.11}$$

Further,

$$\begin{cases} k_{4,10} = \dfrac{S_4}{u_4} = \dfrac{GJ}{l} \\ k_{10,4} = \dfrac{S_{10}}{u_4} = \dfrac{-GJ}{l} \end{cases} \tag{E.12}$$

Let $u_4 = 0$ as shown in Figure E.3 (b), leading to

$$k_{10,10} = \frac{GJ}{l} \tag{E.13}$$

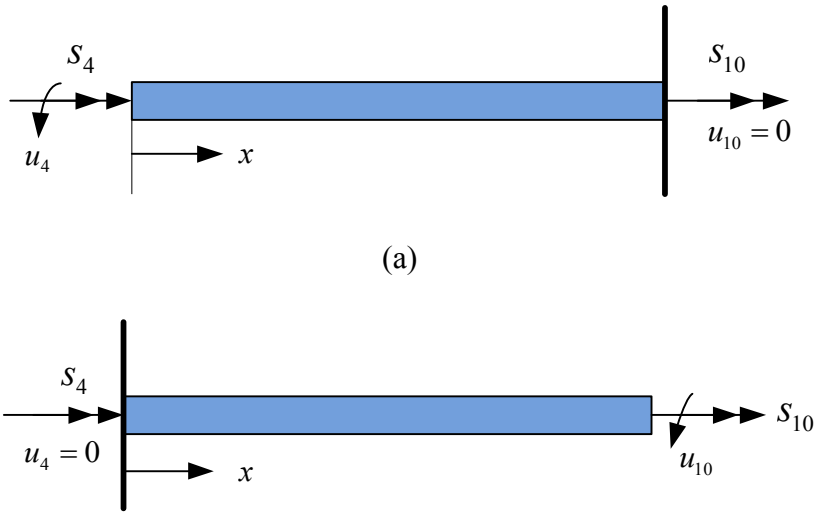

Figure E.3 Axial forces S_4 and S_{10}

(iii) Shearing Forces (S_2 and S_8)

The lateral deflection v subjected to shearing forces and moments, as shown in Figure E.4 (a), is expressed by

$$v = v_b + v_s \tag{E.14}$$

where v_b is the lateral deflection induced by bending strains and v_s is the additional deflection induced by shearing strains.

The v_s is expressed by

$$\frac{dv_s}{dx} = \frac{-S_2}{GA_s} \tag{E.15}$$

where A_s: the cross-sectional area of the beam.

The v_b is expressed by

$$EI_z \frac{d^2 v_b}{dx^2} = S_2 x - S_6 \tag{E.16}$$

Integrating of Eq. (E.15) and (E.16) leads to

$$EI_z v = \frac{S_2 x^3}{6} - \frac{S_6 x^2}{2} + \left(C_1 - \frac{S_2 EI_z}{GA_s} \right) x + C_2 \tag{E.17}$$

where C_1 and C_2 are the constants;

Evaluating the boundary condition in Figure E.4 (a) leads to

$$\begin{cases} \dfrac{dv}{dx} = \dfrac{dv_s}{dx} = \dfrac{-S_2}{GA_s} \ at \ x = 0, x = l \\ v = 0 \ at \ x = l \end{cases} \tag{E.18}$$

Eq. (E.17) leads to

$$\begin{cases} EI_z v = \dfrac{S_2 x^3}{6} - \dfrac{S_6 x^2}{2} - \dfrac{S_2 \phi x l^2}{12} + (1+\phi)\dfrac{l^3 S_2}{12} \\ S_6 = \dfrac{S_2 l}{2} \\ \phi = \dfrac{12EI_z}{GA_s l^2} \end{cases} \tag{E.19}$$

Similarly,

$$\begin{cases} S_8 = -S_2 \\ S_{12} = -S_6 + S_2 l \end{cases} \tag{E.20}$$

By noting $v = u_2$ at $x = 0$, it follows Eq. (E.19)

$$u_2 = (1+\phi)\frac{l^3 S_2}{12EI_z} \tag{E.21}$$

Eqs. (E.19), Eq. (E.20), and (E.21) lead to

$$\begin{cases} k_{2,2} = \dfrac{S_2}{u_2} = \dfrac{12EI_z}{(1+\phi)l^3} \\ k_{6,2} = \dfrac{S_6}{u_2} = \dfrac{S_2 l}{2u_2} = \dfrac{6EI_z}{(1+\phi)l^2} \\ k_{2,2} = \dfrac{S_8}{u_2} = \dfrac{-12EI_z}{(1+\phi)l^3} \\ k_{2,2} = \dfrac{S_{12}}{u_2} = \dfrac{-S_6 + S_2 l}{u_2} = \dfrac{6EI_z}{(1+\phi)l^2} \end{cases} \tag{E.22}$$

Similarly,

$$\begin{cases} k_{8,8} = k_{2,2} = \dfrac{12EI_z}{(1+\phi)l^3} \\ k_{12,8} = -k_{6,2} = \dfrac{-6EI_z}{(1+\phi)l^2} \end{cases} \tag{E.23}$$

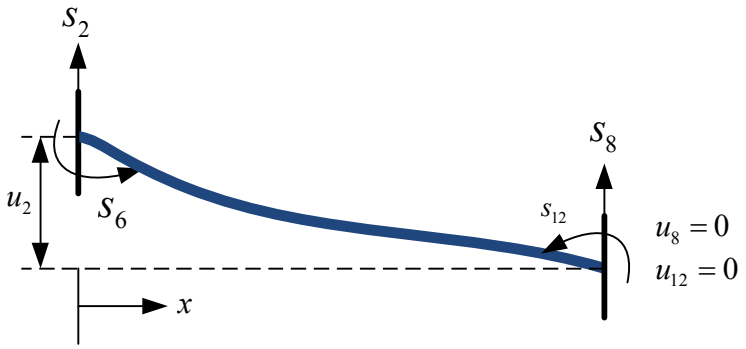

(a)

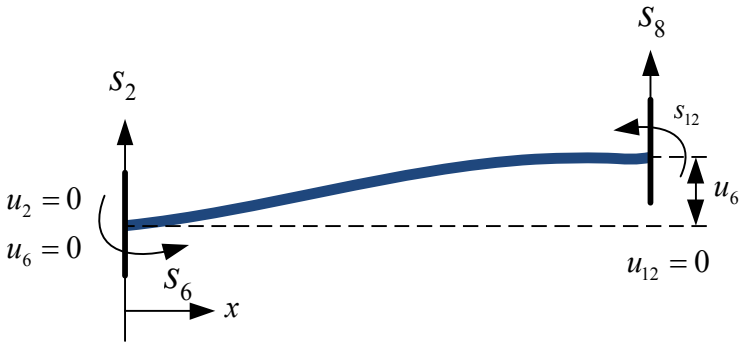

(b)

Figure E.4 Shear forces S_2 and S_8

(iv) Bending Moments (S_6 and S_{12})

The beam is subjected to bending moments and the associated shears, as shown in Figure E.5 (a) and (b). Evaluating the boundary conditions as shown in Figure E.5 (a) lead to

$$\begin{cases} v = 0 \ \ at \ \ x = 0, \ x = l \\ \dfrac{dv}{dx} = \dfrac{dv_s}{dx} = \dfrac{-S_2}{GA_s} \ \ at \ x = l \end{cases} \tag{E.24}$$

Eq. (E.17) becomes:

$$\begin{cases} EI_z v = \dfrac{S_2}{6}(x^3 - l^2 x) + \dfrac{S_6}{2}(lx - x^2) \\ S_2 = \dfrac{6S_6}{(4+\phi)l} \end{cases} \tag{E.25}$$

At $x = 0$, leading to

$$\frac{dv_b}{dx} = \frac{dv}{dx} - \frac{dv_s}{dx} = u_6 \tag{E.26}$$

$$u_6 = \frac{S_6(1+\phi)l}{EI_z(4+\phi)} \tag{E.27}$$

Eq. (E.20), (E.26) and (E.27) lead to

$$\begin{cases} k_{6,6} = \dfrac{S_6}{u_6} = \dfrac{(4+\phi)EI_z}{(1+\phi)l} \\ k_{8,6} = \dfrac{S_8}{u_6} = \dfrac{-S_2}{u_6} = -\dfrac{6EI_z}{(1+\phi)l^2} \\ k_{12,6} = \dfrac{S_{12}}{u_6} = \dfrac{-S_6 + S_2 l}{u_6} == \dfrac{(2-\phi)EI_z}{(1+\phi)l} \end{cases} \tag{E.28}$$

Evaluating the boundary conditions as shown in Figure E.5 (b) lead to

$$k_{12,12} = k_{6,6} = \frac{(4+\phi)EI_z}{(1+\phi)l} \tag{E.29}$$

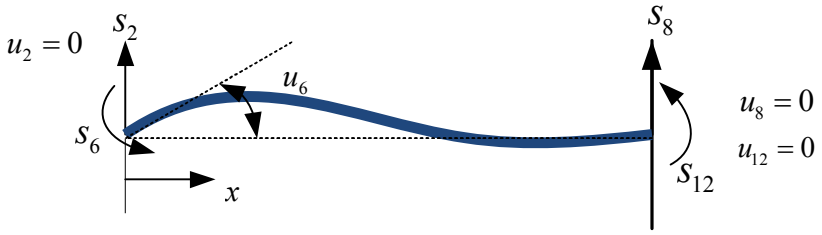

(a)

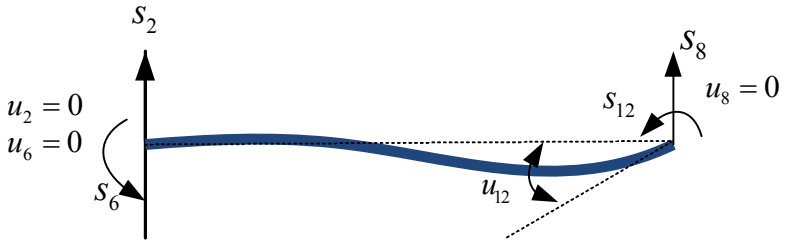

(b)

Figure E.5 Bending moments S_6 and S_{12}

(v) Shearing Forces (S_3 and S_9)

Positive direction of the bending moments S_5, S_{11}, S_6 and S_{12} are shown in Figure E.6.

Similarly,

$$\begin{cases} k_{3,3} = -k_{2,2} \\ k_{5,3} = -k_{6,2} \\ k_{9,3} = k_{8,2} \\ k_{11,3} = -k_{12,2} \\ k_{9,9} = k_{8,8} \\ k_{11,9} = -k_{12,8} \end{cases} \tag{E.30}$$

(a)

(b)

Figure E.6 Sign convention for shear forces and bending moments

(vi) Bending Moments (S_5 and S_{11})

Similar to the derivation of previous section,

$$\begin{cases} k_{5,5} = k_{6,6} \\ k_{9,5} = -k_{8,6} \\ k_{11,5} = k_{12,6} \end{cases} \tag{E.31}$$

Thus, the elementary stiffness matrix $[K_e]$ for the beam is shown in Figure E.7.

$$[K_e]=\frac{E}{l}\left[\begin{array}{cccccc|cccccc}
A & & & & & & & & & & & \\
0 & \frac{12I_z}{l^2(1+\phi_y)} & & & & & & & & & & \\
0 & 0 & \frac{12I_y}{l^2(1+\phi_z)} & & & & & & \textit{symmetric} & & & \\
0 & 0 & 0 & \frac{GJ}{E} & & & & & & & & \\
0 & 0 & \frac{-6I_y}{l(1+\phi_z)} & 0 & \frac{(4+\phi_z)I_y}{1+\phi_z} & & & & & & & \\
0 & \frac{6I_z}{l(1+\phi_y)} & 0 & 0 & 0 & \frac{(4+\phi_z)I_y}{1+\phi_y} & & & & & & \\
\hline
-A & 0 & 0 & 0 & 0 & 0 & A & & & & & \\
0 & \frac{-12I_z}{l^2(1+\phi_y)} & 0 & 0 & 0 & \frac{-6I_z}{l(1+\phi_y)} & 0 & \frac{12I_z}{l^2(1+\phi_y)} & & & & \\
0 & 0 & \frac{-12I_y}{l^2(1+\phi_z)} & 0 & \frac{6I_y}{l(1+\phi_z)} & 0 & 0 & 0 & \frac{12I_y}{l^2(1+\phi_z)} & & & \\
0 & 0 & 0 & \frac{-GJ}{l} & 0 & 0 & 0 & 0 & 0 & \frac{GJ}{E} & & \\
0 & 0 & \frac{6I_y}{l(1+\phi_z)} & 0 & \frac{(2-\phi_z)I_y}{1+\phi_z} & 0 & 0 & 0 & \frac{6I_y}{l(1+\phi_z)} & 0 & \frac{(4+\phi_z)I_y}{1+\phi_z} & \\
0 & \frac{6I_z}{l(1+\phi_y)} & 0 & 0 & 0 & \frac{(2-\phi_y)I_z}{1+\phi_y} & 0 & \frac{-6I_z}{l(1+\phi_y)} & 0 & 0 & 0 & \frac{(4+\phi_z)I_y}{1+\phi_z}
\end{array}\right]$$

Figure E.7 A stiffness matrix of the beam element

where

E : Young's modulus;

ν : Possion's ratio;

A : cross-sectional area of the beam and l is the length of the beam;

I_y : cross-section moments of inertia along y axis;

I_z : cross-section moments of inertia along z axis;

ϕ_y : shear deformation parameters, defined as $\phi_y = \frac{12EI_z}{GA_{sy}l^2}$ with A_{sy} the shear area along y axis; and

ϕ_z : shear deformation parameters, defined as $\phi_z = \frac{12EI_y}{GA_{sz}l^2}$ with A_{sz} the shear area along z axis.

APPENDIX F

Stiffness Matrix [K] of the Colonoscope

```
function [stiffness]=
formStiffnessK3D(GDof,numberElements,elementNodes,numberNodes,nodeCoordinates
);
stiffness=zeros(GDof);
% computation of the system stiffness matrix
for e=1:numberElements;
    % elementDof: element degrees of freedom (Dof)
    indice=elementNodes(e,:) ;
    elementDof=[6*indice(1)-5 6*indice(1)-4 6*indice(1)-3 6*indice(1)-2
6*indice(1)-1 6*indice(1) 6*indice(2)-5 6*indice(2)-4 6*indice(2)-3
6*indice(2)-2 6*indice(2)-1 6*indice(2)] ;
    x1=nodeCoordinates(indice(1),1);
    y1=nodeCoordinates(indice(1),2);
    z1=nodeCoordinates(indice(1),3);
    x2=nodeCoordinates(indice(2),1);
    y2=nodeCoordinates(indice(2),2);
    z2=nodeCoordinates(indice(2),3);
    L = sqrt((x2-x1)*(x2-x1) + (y2-y1)*(y2-y1) + (z2-z1)*(z2-z1));
    r = 6.65;                   % radius of colonoscope (mm)
    A = pi*(r^2);               % cross-sectional area (mm^2)
    I = pi*r^4/4;               % moment of inertia
    Iy = I;                     % second moment of area
    Iz = I;                     % second moment of area
    % Input parameters
    GJ = 7000;                  % torsional rigidity (N*mm^2)
    EI = 40000;                 % flexural stiffness (N*mm^2)
    % end input
    E = EI/I;                   % modulus of elasticity (N/mm^2 or Mpsi)
    k1 = E*A/L;
    k2 = 12*E*Iz/(L*L*L);
```

```
    k3 = 6*E*Iz/(L*L);
    k4 = 4*E*Iz/L;
    k5 = 2*E*Iz/L;
    k6 = 12*E*Iy/(L*L*L);
    k7 = 6*E*Iy/(L*L);
    k8 = 4*E*Iy/L;
    k9 = 2*E*Iy/L;
    k10 = GJ/L;
    a=[k1 0 0; 0 k2 0; 0 0 k6];
    b=[ 0 0 0; 0 0 k3; 0 -k7 0];
    c=[k10 0 0; 0 k8 0; 0 0 k4];
    d=[-k10 0 0; 0 k9 0; 0 0 k5];
    k = [a b -a b; b' c b d; (-a)' b' a -b; b' d' (-b)' c] ;
    if x1 == x2 & y1 == y2
       if z2 > z1
          Lambda = [0 0 1 ; 0 1 0 ; -1 0 0];
       else
          Lambda = [0 0 -1 ; 0 1 0 ; 1 0 0];
       end
    else
    CXx = (x2-x1)/L;
    CYx = (y2-y1)/L;
    CZx = (z2-z1)/L;
    D = sqrt(CXx*CXx + CYx*CYx);
    CXy = -CYx/D;
    CYy = CXx/D;
    CZy = 0;
    CXz = -CXx*CZx/D;
    CYz = -CYx*CZx/D;
    CZz = D;
    Lambda = [CXx CYx CZx; CXy CYy CZy; CXz CYz CZz];
    end
    R = [Lambda zeros(3,9); zeros(3) Lambda zeros(3,6); zeros(3,6) Lambda
zeros(3);zeros(3,9) Lambda];
    stiffness(elementDof,elementDof)=
stiffness(elementDof,elementDof)+R'*k*R;
end
```

APPENDIX G

Mass Matrix of a Beam Element

The derivation of the mass matrix k_e of the beam element is attributed in Ref. [170]. A local coordinate system for a beam element was shown in Figure E.1. The displacement matrix [U] for a beam element has 12 displacements: 6 deflections and 6 rotations, as shown in Eq. (G.1).

$$[U] = \begin{bmatrix} U_1 \\ U_2 \\ U_3 \\ U_4 \\ U_5 \\ U_6 \\ U_7 \\ U_8 \\ U_9 \\ U_{10} \\ U_{11} \\ U_{12} \end{bmatrix} \tag{G.1}$$

For static problem, displacement u in a continuous structure can be related to a finite number of displacements be selected at some arbitrary points on the structure, this relationship is expressed by

$$u = [A]U \tag{G.2}$$

where

$u = [u_x \; u_y \; u_z]$ and $[A] = A(x, y, z)$.

Based on the engineering theory of bending and torsion, the matrix $[A]$ in Eq. (G.2) is given by

$$[A]^T=\begin{bmatrix} 1-\xi & 0 & 0 & \\ 6(1-\xi^2)\eta & 1-3\xi^2+2\xi^3 & 0 & \\ 6(1-\xi^2)\xi & 0 & 1-3\xi^2+2\xi^3 & \\ 0 & -(1-\xi)l\xi & -(1-\xi)l\eta & \\ (1-4\xi+3\xi^2)l\eta & 0 & (-\xi+2\xi^2-\xi^3)l & \\ (-1+4\xi-3\xi^2)l\eta & (-\xi-2\xi^2+\xi^3)l & 0 & (\xi^2-\xi^3)l \\ \xi & 0 & 0 & \\ 6(-\xi+\xi^2)\eta & 3\xi^2-2\xi^3 & 0 & \\ 6(-\xi+\xi^2)\xi & 0 & 3\xi^2-2\xi^3 & \\ 0 & -l\xi\zeta & -l\xi\eta & \\ (-2\xi+3\xi^2)l\zeta & 0 & (\xi^2-\xi^3)l & \\ (2\xi-3\xi^2)l\eta & (-\xi^2+\xi^3)l & 0 & \end{bmatrix} \tag{G.3}$$

The non-dimensional parameters in Eq. (G.3) are defined as:

$$\begin{cases} \xi=\dfrac{x}{l} \\ \eta=\dfrac{y}{l} \\ \zeta=\dfrac{z}{l} \end{cases} \tag{G.4}$$

where l is the length of the beam element.

The element mass matrix is calculated by Eq. (G.5) (see Section 10.5 in Ref. [170])

$$m=\int \rho A^T A dv \tag{G.5}$$

where ρ is the density; v is the volume of element; and the matrix $[A]$ must refer to all nodal displacement in local coordinate system.

The matrix $[A]$ in Eq. (G.3) is substituted to Eq. (G.5), and integration of Eq. (G.5) is performed over the whole volume v of the element, leading to Eq. (G.6) (as shown in the next page).

where

I_y : rotatory inertia also called the moments of inertia along y axis;

I_z : rotatory inertia also called the moments of inertia along z axis;

J_x : torsional inertia also called the polar moment of inertia along x axis;

A : cross-sectional area of the beam; and

l : length of the beam.

$$
m=\rho Al\left[\begin{array}{cccccc|cccccc}
\frac{1}{3} & & & & & & & & & & & \\
0 & \frac{13}{35}+\frac{6I_z}{5Al^2} & & & & & & & & & & \\
0 & 0 & \frac{13}{35}+\frac{6I_z}{5Al^2} & & & & & & \textit{symmetric} & & & \\
0 & 0 & 0 & \frac{J_x}{3A} & & & & & & & & \\
0 & 0 & -\frac{11l}{201}-\frac{I_y}{10Al} & 0 & \frac{l^2}{105}+\frac{2I_y}{15A} & & & & & & & \\
0 & \frac{11l}{201}+\frac{I_z}{10Al} & 0 & 0 & 0 & \frac{l^2}{105}+\frac{2I_y}{15A} & & & & & & \\
\hline
\frac{1}{6} & 0 & 0 & 0 & 0 & 0 & \frac{1}{3} & & & & & \\
0 & \frac{9}{70}-\frac{6I_z}{5Al^2} & 0 & 0 & 0 & \frac{13l}{420}-\frac{I_z}{10Al} & 0 & \frac{13}{35}+\frac{6I_z}{5Al^2} & & & & \\
0 & 0 & \frac{9}{70}-\frac{6I_y}{5Al^2} & 0 & -\frac{13l}{420}+\frac{I_y}{10Al} & 0 & 0 & 0 & \frac{13}{35}+\frac{6I_y}{5Al^2} & & & \\
0 & 0 & 0 & \frac{J_x}{3A} & 0 & 0 & 0 & 0 & 0 & \frac{J_x}{3A} & & \\
0 & 0 & \frac{13l}{420}-\frac{I_y}{10Al} & 0 & -\frac{l^2}{140}-\frac{I_y}{30A} & 0 & 0 & 0 & \frac{11l}{201}+\frac{I_y}{10Al} & 0 & \frac{l^2}{105}+\frac{2I_y}{15A} & \\
0 & -\frac{13l}{420}+\frac{I_z}{10Al} & 0 & 0 & 0 & -\frac{l^2}{140}-\frac{I_z}{30A} & 0 & -\frac{11l}{201}-\frac{I_z}{10Al} & 0 & 0 & 0 & \frac{l^2}{105}+\frac{2I_z}{15A}
\end{array}\right] \qquad (G.6)
$$

APPENDIX H

Mass Matrix [M] of the Colonoscope

```
function
[massmatrix]=formMassmatrix(GDof,numberElements,elementNodes,numberNodes,node
Coordinates,A,Iz,Iy,Jx);
massmatrix=zeros(GDof);
% computation of the system mass matrix
for e=1:numberElements;
    % elementDof: element degrees of freedom (Dof)
    indice=elementNodes(e,:) ;
    elementDof=[6*indice(1)-5 6*indice(1)-4 6*indice(1)-3 6*indice(1)-2
6*indice(1)-1 6*indice(1) 6*indice(2)-5 6*indice(2)-4 6*indice(2)-3
6*indice(2)-2 6*indice(2)-1 6*indice(2)] ;
    x1=nodeCoordinates(indice(1),1);
    y1=nodeCoordinates(indice(1),2);
    z1=nodeCoordinates(indice(1),3);
    x2=nodeCoordinates(indice(2),1);
    y2=nodeCoordinates(indice(2),2);
    z2=nodeCoordinates(indice(2),3);
    L = sqrt((x2-x1)*(x2-x1) + (y2-y1)*(y2-y1) + (z2-z1)*(z2-z1));
    k = [1/3 0 0 0 0 0 1/6 0 0 0 0 0;
        0 13/35+6*Iz/(5*A*L*L) 0 0 0 (11*L)/210+Iz/(10*A*L) 0 9/70-
6*Iz/(5*A*L*L) 0 0 0 (-13*L)/420+Iz/(10*A*L);
        0 0 13/35+6*Iy/(5*A*L*L) 0 (-11*L)/210-Iz/(10*A*L) 0 0 0 9/70-
6*Iy/(5*A*L*L) 0 13*L/420-Iy/(10*A*L) 0;
        0 0 0 Jx/(3*A) 0 0 0 0 0 Jx/(6*A) 0 0;
        0 0 (-11*L)/210-Iy/(10*A*L) 0 (L*L)/105+(2*Iy)/(15*A) 0 0 0 (-
13*L)/420+Iy/(10*A*L) 0 (-L*L)/140-Iy/(30*A) 0;
        0 (11*L)/210+Iz/(10*A*L) 0 0 0 (L*L)/105+(2*Iz)/(15*A) 0 (13*L)/420-
Iz/(10*A*L) 0 0 0 (-L*L)/140-Iz/(30*A);
        1/6 0 0 0 0 0 1/3 0 0 0 0 0;
```

```
        0 9/70-6*Iz/(5*A*L*L) 0 0 0 13*L/420-Iz/(10*A*L) 0
13/35+6*Iz/(5*A*L*L) 0 0 0 (-11*L)/210-Iz/(10*A*L);
        0 0 9/70-6*Iy/(5*A*L*L) 0 (-13*L)/420+Iy/(10*A*L) 0 0 0
13/35+6*Iy/(5*A*L*L) 0 (11*L)/210+Iy/(10*A*L) 0;
        0 0 0 Jx/(6*A) 0 0 0 0 0 Jx/(6*A) 0 0;
        0 0 (13*L)/420-Iy/(10*A*L) 0 (-L*L)/140-Iy/(30*A) 0 0 0
(11*L)/210+Iy/(10*A*L) 0 (L*L)/105+(2*Iy)/(15*A) 0;
        0 (-13*L)/420+Iz/(10*A*L) 0 0 0 (-L*L)/140-Iz/(30*A) 0 (-11*L)/210-
Iz/(10*A*L) 0 0 0 (L*L)/105+(2*Iz)/(15*A)];
    if x1 == x2 & y1 == y2
       if z2 > z1
          Lambda = [0 0 1 ; 0 1 0 ; -1 0 0];
       else
          Lambda = [0 0 -1 ; 0 1 0 ; 1 0 0];
       end
    else
    CXx = (x2-x1)/L;
    CYx = (y2-y1)/L;
    CZx = (z2-z1)/L;
    D = sqrt(CXx*CXx + CYx*CYx);
    CXy = -CYx/D;
    CYy = CXx/D;
    CZy = 0;
    CXz = -CXx*CZx/D;
    CYz = -CYx*CZx/D;
    CZz = D;
    Lambda = [CXx CYx CZx; CXy CYy CZy; CXz CYz CZz];
    end
    R = [Lambda zeros(3,9); zeros(3) Lambda zeros(3,6); zeros(3,6) Lambda
zeros(3);zeros(3,9) Lambda];
    massmatrix(elementDof,elementDof)=
massmatrix(elementDof,elementDof)+R'*k*R;
end
```

APPENDIX I

Natural Frequency of the Colonoscope

```
%  input: size of beam and material
    r = 6.65;                    % radius of colonoscope(mm)
    I = pi*r^4/4;                % moment of inertia
    A = pi*(r^2);                % cross-sectional A (mm^2)
    lbeam = 200;                 % length of the colonoscope unit: (mm)
    EI = 40000;                  % flexural stiffness (N*mm^2 )
    E = 1000*EI/I;               % modulus of elasticity (mN/mm^2=1000Mpa)
    mass = 0.4;                  % mass of colonoscope (kg): 300 mm length
    density = mass/(lbeam*A);    % unit: (kg/mm^3)
    num_elements = 8;
%   define length of each element, uniform lengths
    l = lbeam/num_elements;
%   define whether or not to do Guyan Reduction
```

The following codes refer to Ref. [217].

```
    guyan = input('enter "1" to do Guyan elimination of rotations, "enter" to
not do Guyan ...  ');
    if (isempty(guyan))
        guyan = 0;
    else
    end
     if  guyan == 0
        num_plot_max = 2*num_elements;
        num_plot_default = num_elements;
    else
        num_plot_max = num_elements;
        num_plot_default = num_elements;
    end
    num_plot = input(['enter the number of modes to plot, max
',num2str(num_plot_max),', default ',num2str(num_plot_default),' ...  ']);
    if (isempty(num_plot))
```

```
        num_plot = 9;
    else
    end
%   define length of each element, uniform lengths
    l = lbeam/num_elements;
%   define length vector for plotting, right-to-left numbering
    lvec = 0:l:lbeam;
%   define the node numbers
    n = 1:num_elements+1;
%   number the nodes for the elements
    node1 = 1:num_elements;
    node2 = 2:num_elements+1;
%   size the stiffness and mass matrices to have 2 times the number of nodes
%   to allow for translation and rotation dof's for each node, including
built-
%   in end
    max_node1 = max(node1);
    max_node2 = max(node2);
    max_node_used = max([max_node1 max_node2]);
    mnu = max_node_used;
    k = zeros(2*mnu);
    m = zeros(2*mnu);
%   now build up the global stiffness and consistent mass matrices, element
by element
    mpl = density*A;
    for  i = 1:num_elements
        dof1 = 2*node1(i)-1;
        dof2 = 2*node1(i);
        dof3 = 2*node2(i)-1;
        dof4 = 2*node2(i);
        k(dof1,dof1) = k(dof1,dof1)+(12*E*I/l^3);
        k(dof2,dof1) = k(dof2,dof1)+(6*E*I/l^2);
        k(dof3,dof1) = k(dof3,dof1)+(-12*E*I/l^3);
        k(dof4,dof1) = k(dof4,dof1)+(6*E*I/l^2);
        k(dof1,dof2) = k(dof1,dof2)+(6*E*I/l^2);
        k(dof2,dof2) = k(dof2,dof2)+(4*E*I/l);
        k(dof3,dof2) = k(dof3,dof2)+(-6*E*I/l^2);
        k(dof4,dof2) = k(dof4,dof2)+(2*E*I/l);
```

```
        k(dof1,dof3) = k(dof1,dof3)+(-12*E*I/l^3);
        k(dof2,dof3) = k(dof2,dof3)+(-6*E*I/l^2);
        k(dof3,dof3) = k(dof3,dof3)+(12*E*I/l^3);
        k(dof4,dof3) = k(dof4,dof3)+(-6*E*I/l^2);
        k(dof1,dof4) = k(dof1,dof4)+(6*E*I/l^2);
        k(dof2,dof4) = k(dof2,dof4)+(2*E*I/l);
        k(dof3,dof4) = k(dof3,dof4)+(-6*E*I/l^2);
        k(dof4,dof4) = k(dof4,dof4)+(4*E*I/l);
        m(dof1,dof1) = m(dof1,dof1)+(mpl/420)*(156*l);
        m(dof2,dof1) = m(dof2,dof1)+(mpl/420)*(22*l^2);
        m(dof3,dof1) = m(dof3,dof1)+(mpl/420)*(54*l);
        m(dof4,dof1) = m(dof4,dof1)+(mpl/420)*(-13*l^2);
        m(dof1,dof2) = m(dof1,dof2)+(mpl/420)*(22*l^2);
        m(dof2,dof2) = m(dof2,dof2)+(mpl/420)*(4*l^3);
        m(dof3,dof2) = m(dof3,dof2)+(mpl/420)*(13*l^2);
        m(dof4,dof2) = m(dof4,dof2)+(mpl/420)*(-3*l^3);
        m(dof1,dof3) = m(dof1,dof3)+(mpl/420)*(54*l);
        m(dof2,dof3) = m(dof2,dof3)+(mpl/420)*(13*l^2);
        m(dof3,dof3) = m(dof3,dof3)+(mpl/420)*(156*l);
        m(dof4,dof3) = m(dof4,dof3)+(mpl/420)*(-22*l^2);
        m(dof1,dof4) = m(dof1,dof4)+(mpl/420)*(-13*l^2);
        m(dof2,dof4) = m(dof2,dof4)+(mpl/420)*(-3*l^3);
        m(dof3,dof4) = m(dof3,dof4)+(mpl/420)*(-22*l^2);
        m(dof4,dof4) = m(dof4,dof4)+(mpl/420)*(4*l^3);
    end
%   now that stiffness and mass matrices are defined for all dof's, including
%   constrained dof's, need to delete rows and columns of the matrices that
%   correspond to constrained dof's, in the left-to-right case, the first two
%   rows and columns
    k(1:2,:) = [];  % translation/rotation of node 1
    k(:,1:2) = [];
    m(1:2,:) = [];
    m(:,1:2) = [];
    if  guyan == 1
 %   Guyan Reduction - reduce out the rotation dof's, leaving displacement
dof's
%   re-order the matrices
%   re-order the columns of k
```

```
    kr = zeros(2*(mnu-1));
    krr = zeros(2*(mnu-1));
%    rearrange columns, rotation and then displacement dof's
     mkrcolcnt = 0;
     for  mkcolcnt = 2:2:2*(mnu-1)
         mkrcolcnt = mkrcolcnt + 1;
         kr(:,mkrcolcnt) = k(:,mkcolcnt);
         mr(:,mkrcolcnt) = m(:,mkcolcnt);
     end
     mkrcolcnt = num_elements;
     for  mkcolcnt = 1:2:2*(mnu-1)
         mkrcolcnt = mkrcolcnt + 1;
         kr(:,mkrcolcnt) = k(:,mkcolcnt);
         mr(:,mkrcolcnt) = m(:,mkcolcnt);
     end

%   rearrange rows, rotation and then displacement dof's
     mkrrowcnt = 0;
     for  mkrowcnt = 2:2:2*(mnu-1)
         mkrrowcnt = mkrrowcnt + 1;
         krr(mkrrowcnt,:) = kr(mkrowcnt,:);
         mrr(mkrrowcnt,:) = mr(mkrowcnt,:);
     end
     mkrrowcnt = num_elements;
     for  mkrowcnt = 1:2:2*(mnu-1)
         mkrrowcnt = mkrrowcnt + 1;
         krr(mkrrowcnt,:) = kr(mkrowcnt,:);
         mrr(mkrrowcnt,:) = mr(mkrowcnt,:);
     end
%    define sub-matrices and transformation matrix T
     kaa = krr(1:num_elements,1:num_elements);
     kab = krr(1:num_elements,num_elements+1:2*num_elements);
     T = [-inv(kaa)*kab
            eye(num_elements,num_elements)]
%    calculate reduced mass and stiffness matrices
     kbb = T'*krr*T
      mbb = T'*mrr*T
```

```
     else
     kbb = k;
     mbb = m;
     end
%    define the number of dof for state-space version, 2 times dof left after
%    removing constrained dof's
     [dof,dof] = size(kbb);
%    define the sizes of mass and stiffness matrices for state-space
     ssdof = 2*dof;
    aud = zeros(ssdof);     % creates a ssdof x ssdof null matrix
%    divide the negative of the stiffness matrix by the mass matrix
    ksm = inv(mbb)*(-kbb);
%    now expand to state space size
%    fill out unit values in mass and stiffness matrices
    for  row = 1:2:ssdof
        aud(row,row+1) = 1;
    end
%    fill out mass and stiffness terms from m and k
    for  row = 2:2:ssdof
        for  col = 2:2:ssdof
           aud(row,col-1) = ksm(row/2,col/2);
         end
     end
%    calculate the eigenvalues/eigenvectors of the undamped matrix for
plotting
%    and for calculating the damping matrix c
    [evec1,evalu] = eig(aud);
     evalud = diag(evalu);
     evaludhz = evalud/(2*pi);
     num_modes = length(evalud)/2;
%    now reorder the eigenvalues and eigenvectors from low to high freq
     [evalorder,indexhz] = sort(abs((evalud)));
     for  cnt = 1:length(evalud)
         eval(cnt,1) = evalud(indexhz(cnt));
         evalhzr(cnt,1) = round(evaludhz(indexhz(cnt)));
        evec(:,cnt) = evec1(:,indexhz(cnt));
    end
%    now check for any imaginary eigenvectors and convert to real
```

```
    for  cnt = 1:length(evalud)
        if  (imag(evec(1,cnt)) & imag(evec(3,cnt)) & imag(evec(5,cnt))) ~= 0
            evec(:,cnt) = imag(evec(:,cnt));
         else
        end
     end
     if  guyan == 0
%   now separates the displacement and rotations in the eigenvectors
%   for plotting mode shapes
    evec_disp = zeros(ceil(dof/2),ssdof);
      rownew = 0;
     for  row = 1:4:ssdof
         rownew = rownew+1;
         evec_disp(rownew,:) = evec(row,:);
        end
     evec_rotation = zeros(ceil(dof/2),ssdof);
     rownew = 0;
    for row = 3:4:ssdof
        rownew = rownew+1;
        evec_rotation(rownew,:) = evec(row,:);
     end
     else
     evec_disp = zeros(ceil(dof/4),ssdof);
       rownew = 0;
     for  row = 1:2:ssdof
         rownew = rownew+1;
         evec_disp(rownew,:) = evec(row,:);
     end
    end
 %   normalize the displacement eigenvectors wrt one for plotting
     for  col = 1:ssdof
         evec_disp(:,col) =
evec_disp(:,col)/max(abs(real(evec_disp(:,col))));
         if  evec_disp(floor(dof/2),col) >= 0
             evec_disp(:,col) = -evec_disp(:,col);
         else
        end
     end
```

```
 %   list eigenvalues, hz
     format long e
     evaludhz_list = sort(evaludhz(1:2:2*num_modes))
     format short
 %   list displacement (not velocity) eigenvectors
     evec_disp(:,1:2:2*num_plot)
    if  guyan == 0
%   plot mode shapes
     for  mode_cnt = 1:num_plot
         evec_cnt = 2*mode_cnt -1;
         plot(lvec,[0; evec_disp(:,evec_cnt)],'ko-')
        title(['Cantilever Beam, Mode ', ...
            num2str(mode_cnt),': ',num2str(abs(evalhzr(evec_cnt))),' hz']);
        xlabel('Distance From Built-In End')
        ylabel('Normalized Y-Displacement')
        axis([0 lbeam -1.5 1.5])
        grid on
       disp('execution paused to display figure, "enter" to continue'); pause
    end
    else
%   plot mode shapes, Guyan Reduced
    for  mode_cnt = 1:num_plot
        evec_cnt = 2*mode_cnt -1;
         plot(lvec,[0; evec_disp(:,evec_cnt)],'ko-')
        title(['Cantilever Beam, Mode ', ...
            num2str(mode_cnt),': ',num2str(abs(evalhzr(evec_cnt))),' hz']);
        xlabel('Distance From Built-In End')
        ylabel('Normalized Y-Displacement')
        axis([0 lbeam -1.5 1.5])
        grid on
       disp('execution paused to display figure, "enter" to continue'); pause
    end
    end
%   normalization with respect to mass on a filled (not diagonal) mass matrix
%   calculate the displacement (displacement and rotation) eigenvectors
%   to be used for the modal model eigenvectors
     xm = zeros(dof);
    col = 0;
```

```
for  mode = 1:2:ssdof
     col = col + 1;
     row = 0;
     for  ndof = 1:2:ssdof
         row = row + 1;
         xm(row,col) = evec(ndof,mode);
     end
 end
%  normalize with respect to mass
for  mode = 1:dof
     xn(:,mode) = xm(:,mode)/sqrt(xm(:,mode)'*mbb*xm(:,mode));
 end
%  calculate the normalized mass and stiffness matrices for checking
mm = xn'*mbb*xn;
km = xn'*kbb*xn;
%  check that the sqrt of diagonal elements of km are eigenvalues
p = (diag(km)).^0.5;
row = 0;
for cnt = 1:2:ssdof
    row = row + 1;
    evalrad(row) = abs((eval(cnt)));
end
[p evalrad']/(2*pi)
evalhz = evalrad/(2*pi);
semilogy(evalhz)
xlabel('Mode Number')
ylabel('Frequency, hz')
grid
disp('execution paused to display figure, "enter" to continue'); pause
```

APPENDIX J

Permission to Use Figures

Figure 2.3

License Number	3115731348608
License date	Mar 25, 2013
Licensed content publisher	Elsevier
Licensed content publication	Gastrointestinal Endoscopy
Licensed content title	A novel shape-locking guide for prevention of sigmoid looping during colonoscopy
Licensed content author	Gottumukkala S Raju,Douglas K Rex,Richard A Kozarek,Ijaz Ahmed,Douglas Brining,Pankaj Jay Pasricha
Licensed content date	March 2004
Licensed content volume number	59
Licensed content issue number	3
Number of pages	4
Type of Use	reuse in a thesis/dissertation
Portion	figures/tables/illustrations
Number of figures/tables/illustrations	1
Format	both print and electronic
Are you the author of this Elsevier article?	No
Will you be translating?	No
Order reference number	
Title of your thesis/dissertation	DEVELOPMENT OF A KINETIC MODEL FOR LOOP-FREE COLONOSCOPY TECHNOLOGY
Expected completion date	Apr 2013
Estimated size (number of pages)	150
Elsevier VAT number	GB 494 6272 12

Permissions price	0.00 USD
VAT/Local Sales Tax	0.00 USD
Total	0.00 USD

Figure 2.4 and Figure 2.5

Thesis / Dissertation Reuse

The IEEE does not require individuals working on a thesis to obtain a formal reuse license, however, you may print out this statement to be used as a permission grant:

Requirements to be followed when using any portion (e.g., figure, graph, table, or textual material) of an IEEE copyrighted paper in a thesis:

1) In the case of textual material (e.g., using short quotes or referring to the work within these papers) users must give full credit to the original source (author, paper, publication) followed by the IEEE copyright line © 2011 IEEE.
2) In the case of illustrations or tabular material, we require that the copyright line © [Year of original publication] IEEE appear prominently with each reprinted figure and/or table.
3) If a substantial portion of the original paper is to be used, and if you are not the senior author, also obtain the senior author's approval.

Requirements to be followed when using an entire IEEE copyrighted paper in a thesis:

1) The following IEEE copyright/ credit notice should be placed prominently in the references: © [year of original publication] IEEE. Reprinted, with permission, from [author names, paper title, IEEE publication title, and month/year of publication]
2) Only the accepted version of an IEEE copyrighted paper can be used when posting the paper or your thesis on-line.
3) In placing the thesis on the author's university website, please display the following message in a prominent place on the website: In reference to IEEE copyrighted material which is used with permission in this thesis, the IEEE does not endorse any of [university/educational entity's name goes here]'s products or services. Internal or personal use of this material is permitted. If interested in reprinting/republishing IEEE copyrighted material for advertising or promotional purposes or for creating new collective works for resale or redistribution, please go tohttp://www.ieee.org/publications_standards/publications/rights/rights_link.html to learn how to obtain a License from RightsLink.

If applicable, University Microfilms and/or ProQuest Library, or the Archives of Canada may supply single copies of the dissertation.

Figure 2.6

License Number 3115740867689

License date	Mar 25, 2013
Licensed content publisher	Springer
Licensed content publication	International Journal of Precision Engineering and Manufacturing
Licensed content title	A flexible chain-based screw propeller for capsule endoscopes
Licensed content author	Ju-Sung Lee
Licensed content date	Jan 1, 2009
Volume number	10
Issue number	4
Type of Use	Thesis/Dissertation
Portion	Figures
Author of this Springer article	No
Country of republication	other
Title of your thesis / dissertation	DEVELOPMENT OF A KINETIC MODEL FOR LOOP-FREE COLONOSCOPY TECHNOLOGY
Expected completion date	Apr 2013
Estimated size(pages)	150
Total	0.00 USD

Figure 2.7

License Number	3115750482347
License date	Mar 25, 2013
Licensed content publisher	Elsevier
Licensed content publication	Gastroenterology
Licensed content title	The Aer-O-Scope: Proof of Concept of a Pneumatic, Skill-Independent, Self-Propelling, Self-Navigating Colonoscope
Licensed content author	Boris Vucelic,Douglas Rex,Roland Pulanic,Jorge Pfefer,Irena Hrstic,Bernard Levin,Zamir Halpern,Nadir Arber

Licensed content date	March 2006
Licensed content volume number	130
Licensed content issue number	3
Number of pages	6
Type of Use	reuse in a thesis/dissertation
Portion	figures/tables/illustrations
Number of figures/tables/illustrations	1
Format	both print and electronic
Are you the author of this Elsevier article?	No
Will you be translating?	No
Order reference number	
Title of your thesis/dissertation	DEVELOPMENT OF A KINETIC MODEL FOR LOOP-FREE COLONOSCOPY TECHNOLOGY
Expected completion date	Apr 2013
Estimated size (number of pages)	150
Elsevier VAT number	GB 494 6272 12
Permissions price	0.00 USD
VAT/Local Sales Tax	0.00 USD
Total	0.00 USD

Figure 2.8 and Figure 2.9

License Number	3115750886659
License date	Mar 25, 2013
Licensed content publisher	Nature Publishing Group
Licensed content publication	The American Journal of Gastroenterology
Licensed content title	Computer-Assisted Colonoscopy (The NeoGuide Endoscopy System): Results of the First Human Clinical Trial ([ldquo]PACE Study[rdquo])
Licensed content author	Axel Eickhoff, Jacques Van Dam, Ralf Jakobs, Valerie Kudis, Dirk Hartmann et al.
Licensed content date	Feb 1, 2007
Type of Use	reuse in a thesis/dissertation

Volume number	102
Issue number	2
Requestor type	academic/educational
Format	print and electronic
Portion	figures/tables/illustrations
Number of figures/tables/illustrations	1
High-res required	no
Figures	Figure 1 and Figure 2
Author of this NPG article	no
Your reference number	
Title of your thesis / dissertation	DEVELOPMENT OF A KINETIC MODEL FOR LOOP-FREE COLONOSCOPY TECHNOLOGY
Expected completion date	Apr 2013
Estimated size (number of pages)	150
Total	0.00 USD

Figure 3.1

License Number	3115751417593
License date	Mar 25, 2013
Licensed content publisher	John Wiley and Sons
Licensed content publication	Computer Graphics Forum
Licensed content title	Physically Based Deformable Models in Computer Graphics
Licensed copyright line	Copyright © 2006, John Wiley and Sons
Licensed content author	Andrew Nealen,Matthias Müller,Richard Keiser,Eddy Boxerman,Mark Carlson
Licensed content date	Dec 7, 2006
Start page	809

End page	836
Type of use	Dissertation/Thesis
Requestor type	University/Academic
Format	Print and electronic
Portion	Figure/table
Number of figures/tables	1
Original Wiley figure/table number(s)	Figure 5
Will you be translating?	No
Total	0.00 USD